NUREG/CR-4379
Vol. 1

Long-Term Performance of Materials Used for High-Level Waste Packaging

First Quarterly Report, Year Four
April - June 1985

Compiled by D. Stahl, N. E. Miller

Battelle's Columbus Laboratories

**Prepared for
U.S. Nuclear Regulatory
Commission**

NOTICE

This report was prepared as an account of work sponsored by an agency of the United States Government. Neither the United States Government nor any agency thereof, or any of their employees, makes any warranty, expressed or implied, or assumes any legal liability of responsibility for any third party's use, or the results of such use, of any information, apparatus, product or process disclosed in this report, or represents that its use by such third party would not infringe privately owned rights.

NOTICE

Availability of Reference Materials Cited in NRC Publications

Most documents cited in NRC publications will be available from one of the following sources:

1. The NRC Public Document Room, 1717 H Street, N.W.
   Washington, DC 20555
2. The Superintendent of Documents, U.S. Government Printing Office, Post Office Box 37082, Washington, DC 20013-7082
3. The National Technical Information Service, Springfield, VA 22161

Although the listing that follows represents the majority of documents cited in NRC publications, it is not intended to be exhaustive.

Referenced documents available for inspection and copying for a fee from the NRC Public Document Room include NRC correspondence and internal NRC memoranda; NRC Office of Inspection and Enforcement bulletins, circulars, information notices, inspection and investigation notices; Licensee Event Reports; vendor reports and correspondence; Commission papers; and applicant and licensee documents and correspondence.

The following documents in the NUREG series are available for purchase from the GPO Sales Program: formal NRC staff and contractor reports, NRC-sponsored conference proceedings, and NRC booklets and brochures. Also available are Regulatory Guides, NRC regulations in the *Code of Federal Regulations*, and *Nuclear Regulatory Commission Issuances*.

Documents available from the National Technical Information Service include NUREG series reports and technical reports prepared by other federal agencies and reports prepared by the Atomic Energy Commission, forerunner agency to the Nuclear Regulatory Commission.

Documents available from public and special technical libraries include all open literature items, such as books, journal and periodical articles, and transactions. *Federal Register* notices, federal and state legislation, and congressional reports can usually be obtained from these libraries.

Documents such as theses, dissertations, foreign reports and translations, and non-NRC conference proceedings are available for purchase from the organization sponsoring the publication cited.

Single copies of NRC draft reports are available free, to the extent of supply, upon written request to the Division of Technical Information and Document Control, U.S. Nuclear Regulatory Commission, Washington, DC 20555.

Copies of industry codes and standards used in a substantive manner in the NRC regulatory process are maintained at the NRC Library, 7920 Norfolk Avenue, Bethesda, Maryland, and are available there for reference use by the public. Codes and standards are usually copyrighted and may be purchased from the originating organization or, if they are American National Standards, from the American National Standards Institute, 1430 Broadway, New York, NY 10018.

NUREG/CR-4379
Vol. 1

Long-Term Performance of Materials Used for High-Level Waste Packaging

First Quarterly Report, Year Four
April - June 1985

Manuscript Completed: August 1985
Date Published: September 1985

Compiled by
D. Stahl, N. E. Miller

Battelle's Columbus Laboratories
505 King Avenue
Columbus, OH 43201-2693

Prepared for
Division of Radiation Programs and Earth Sciences
Office of Nuclear Regulatory Research
U.S. Nuclear Regulatory Commission
Washington, D.C. 20555
NRC FIN B6764
Under Contract No. NRC-04-82-015

CONTRIBUTORS

J. A. Beavers
H. J. Cialone
R. Kohli
A. J. Markworth
J. K. McCoy
J. L. Means
S. L. Nicolosi
R. Ramgta
S. W. Rust
E. D. Spinosa
N. G. Thompson

ABSTRACT

As part of the Nuclear Regulatory Commission's requirement to assess the Department of Energy's application to construct geologic repositories for high-level radioactive waste, Battelle's Columbus Division is investigating the long-term performance of materials used for high-level waste packages. High-level waste glass studies are being concluded and efforts are being directed toward studying spent-fuel performance. The effects of devitrification on glass leach rates are being investigated, and silica dissolution was studied to provide data for the glass dissolution model. Preliminary data support this model. A glass leach test using organic acids was conducted, and leaching trends were observed. Real and simulated spent fuels are being incorporated in integral tests using simulated groundwater in a prototypic repository environment. The reactions of groundwater species with steels are being analyzed to evaluate susceptability to pitting and stress-corrosion cracking. Potential cracking agents are being investigated by slow strain rate experiments. General and pitting corrosion models were further developed, based on known principles of mass transport and radiolytic production. A simplified groundwater-radiolysis model, developed for use with the corrosion models, was compared with other mechanisms for species concentration predictions.

This report documents investigations performed during the period April, 1985 through June, 1985.

TABLE OF CONTENTS

TABLE OF CONTENTS
(Continued)

LIST OF FIGURES

LIST OF FIGURES
(Continued)

LIST OF FIGURES
(Continued)

LIST OF FIGURES
(Continued)

LIST OF TABLES

LIST OF TABLES
(Continued)

PREVIOUS REPORTS IN SERIES

NUREG/CR-3405, Volume 1: "Long-Term Performance of Materials Used for High-Level Waste Packaging: Annual Report, March 1982-April 1983."

NUREG/CR-3427, Volume 1: "Long-Term Performance of Materials Used for High-Level Waste Packaging: Quarterly Report, April-June 1983."

NUREG/CR-3427, Volume 2: "Long-Term Performance of Materials Used for High-Level Waste Packaging: Quarterly Report, July-September 1983."

NUREG/CR-3427, Volume 3: "Long-Term Performance of Materials Used for High-Level Waste Packaging: Quarterly Report, October-December 1983."

NUREG/CR-3427, Volume 4: "Long-Term Performance of Materials Used for High-Level Waste Packaging: Annual Report, April 1983-April 1984."

NUREG/CR-3900, Volume 1: "Long-Term Performance of Materials Used for High-Level Waste Packaging: Quarterly Report, April-June 1984."

NUREG/CR-3900, Volume 2: "Long-Term Performance of Materials Used for High-Level Waste Packaging: Quarterly Report, July-September 1984."

NUREG/CR-3900, Volume 3: "Long-Term Performance of Materials Used for High-Level Waste Packaging: Quarterly Report, October-December 1984."

NUREG/CR-3900, Volume 4: "Long-Term Performance of Materials Used for High-Level Waste Packaging: Annual Report, April 1984-April 1985.

1. INTRODUCTION: PROJECT OBJECTIVES AND APPROACH

The Waste Policy Act of 1982 delegates to the Department of Energy (DOE) the authority for siting, construction, and operation of deep-mined geologic repositories for the disposal of high-level waste and spent fuel. The Nuclear Regulatory Commission (NRC) has the responsibility to regulate the activities of DOE to assure that the health and safety of the repository workers and of the public are adequately protected. Prior to construction, the DOE will submit a license application to the NRC describing in detail the proposed repository. The DOE has been directed to take a multiple barrier approach to the isolation of radioactive wastes with the waste package, the engineered facility, and the natural geohydrologic features of the site being the major barriers. Since NRC's compliance assessment requires the technical capability to understand relevant phenomena and processes relating to the long-term performance of the multiple barriers, the NRC's Office of Nuclear Regulatory Research (RES) has established this waste-package performance program at Battelle's Columbus Division to provide that part of the input to the assessment. As an important aid to this understanding, Battelle is evaluating total system performance by integrating combined-effects processes pertaining to the long-term performance of waste-package materials. This systems approach also serves to identify and evaluate research needs.

After the repository is closed, the dominant mechanism to cause the release of radionuclides from the repository is assumed to be groundwater transport. The generally accepted approach to minimizing the release is to provide a number of different barriers to the dissolution and transport of radionuclides by the groundwater. For a deep-mined repository, the geohydrologic features of the earth itself are expected to be a major barrier to the release of radionuclides. The repository site will be selected so that radionuclides will be isolated for very long times. In addition, engineered features of the repository will act as a barrier to the release of radionuclides. The repository will be constructed so as to minimize disturbing the adjacent rock and to accommodate the thermomechanical effects of the emplaced wastes with a minimum of degradation to its geohydrologic properties. Upon closure, the underground openings and shafts to the surface will be backfilled and sealed to minimize groundwater flow paths.

The waste package--which is the center of this study--will be constructed to provide essentially complete containment of the radionuclides through the period of time in which the repository is heated significantly by decaying fission products. After the container is eventually breached by some process, the waste form must remain sufficiently resistant to groundwater attack to provide high retention of the radionuclides and, together with the repository, to control the release of radionuclides for thousands of years. The objective of our research is to provide an improved understanding of the long-term performance of

the materials used for the high-level waste package. More specifically, we are identifying those processes that tend to degrade the performance of the waste-package materials, performing experiments to produce data where data are otherwise lacking on material performance, and analytically modeling the processes to utilize the data to better understand how the processes will affect material's future performance. In addition, we are identifying areas of work that should be performed by DOE to provide missing data which are beyond the resources of the NRC.

1.1 Individual Program Tasks

The program is being conducted in three parallel efforts: waste-form studies, container studies, and integrated system performance studies. A more detailed summary of achievements can be found in the second annual report for this program (NUREG/CR-2127, Volume 4, July 1985, Section 1).

1.1.1 Waste Forms

The waste-form studies are aimed at first describing and modeling those mechanisms that will alter or "age" the waste form during the containment period, and second, identifying and describing those processes that will influence waste-form dissolution after it is exposed to groundwater. The waste-form studies have been largely centered on borosilicate glasses for both defense and commercial high-level wastes. However, effort now is being directed toward evaluating spent fuel as a waste form. Spent-fuel-water reactions and the leach/dissolution of spent fuel and cladding will be studied.

In borosilicate glasses, the glass-forming agents can be selected to optimize the waste-form properties for each type of high-level waste. After the waste forms are produced, particularly during the very long period of time after disposal while sealed in their containers, they will experience processes that will cause structural changes. One detrimental effect is devitrification of the glass, which can lead both to new phases with increased solubility and to cracking of the glass (which is detrimental because it allows a greater surface area of the glass to be contacted by the groundwater). A model has been developed to predict the degree of devitrification that will occur from subsequent reheating in the repository after disposal. Another detrimental effect is cracking, which could be induced by the effects of radiation on glass. A study of the radiation effects on glass has revealed no new approach to evaluating this phenomenon experimentally, so we are largely dependent on the existing literature which indicates that radiation produces only a small effect on glass performance.

1.1.2 Overpack Corrosion

The overpack corrosion studies focus on processes that can degrade the metallic waste-package overpack. The objective is to collect data on the parameters that influence the degradation processes, to identify the

controlling parameters, and ultimately to model the degradation processes that determine the long-term performance of the overpack. The material under study is cast low-carbon steel. This material is currently favored by DOE for use in a basalt repository.

The dominant degradation processes that affect the outside of the overpack are general corrosion, stress-corrosion cracking, pitting, crevice corrosion, hydrogen attack, and mechanical stress. These processes may occur individually or in combination. The parameters that affect these processes include chemical composition and physical state of the steel, groundwater composition and flow rate, temperature, radiation intensity, availability of air, lithostatic forces, redox state, alkalinity/acidity, and availability of hydrogen. These can produce general corrosion, in which the rate of general corrosion will determine the necessary wall thickness, or localized corrosion (such as pitting or crevice corrosion), in which the rate of the localized attack and the container life must be used to establish the wall thickness.

If the steel is susceptible to cracking in the expected environment, the rate of cracking is so rapid relative to required container life that the corrosion-allowance approach cannot be used to achieve acceptable performance. What is important is the susceptibility of the metal to crack initiation. Cracking may result from stress-corrosion cracking or from reduction in fracture toughness from hydrogen attack. Both of these processes are under investigation.

In addition, a comprehensive mathematical model is under development for use in understanding the corrosion processes associated with the waste-container materials in a repository environment. The model computes the fluxes of corrosive species to the overpack surface, taking into account the fact that certain corrosive species may be generated by radiolysis, and also accounts for diffusion and convective flow to transport the species. The modeling effort is also being applied to pitting attack and considers three different aspects of the overall pitting process: pit-initiation kinetics, pit-growth kinetics, and the evolution of the pit-depth distribution. These analytical efforts are well integrated with the experimental efforts and are directed to providing an understanding of the long-term performance of the overpack materials, with emphasis on those processes that can lead to poor performance.

1.1.3 Integrated System Performance

The waste-package system studies are an interface between the waste-form studies and the container-material studies to provide an improved understanding of the performance of the total waste-package system. The current emphasis is on the processes involved in waste-package system degradation. One aspect of the total system under study is the production of radiolysis products in the groundwater by gamma radiation from the waste. This is of major importance in modeling the corrosion of the

overpack and in planning experiments to determine the effects of radiolysis. Our radiolysis model is based on existing codes and sets of chemical reactions combined to provide the best description of experimental data found in the literature. The output of the radiolysis model calculations provides input to the water-chemistry model, which is a fundamental part of the glass-dissolution model and the general-corrosion model.

The water-chemistry model which we initially developed for our use with our glass-dissolution and corrosion models has intentionally been kept simple. Simplifying assumptions were made and only a limited set of chemical species was used. This model calculates the concentration and activity of each of the water species.

Integral tests have been designed and will be performed using spent-fuel specimens. The tests will use real and simulated spent fuel with flowing simulated groundwater in a prototypic repository environment. These tests will aid in identifying combined-effects processes that will affect waste-package performance and will explore the role of the cladding in overall performance as well.

1.2 Overall Program Objectives

In all the program tasks, the ultimate objective is to develop a base of information to assist the NRC in evaluating the performance of the waste package proposed in DOE's license application. A near-term objective is to provide information to allow the NRC to prepare position papers on the information required of DOE for evaluation of their waste package. Of significance here is identifying sensitive parameters affecting the performance of materials and identifying data requirements.

To achieve the above objectives, the waste-form task is providing information to give a better understanding of the release of radionuclides from the waste form, beginning at the time it is first contacted by groundwater, through the 10,000-year period defined in the draft EPA Standard. This includes an understanding of the probable physiochemical condition of the waste form when it is contacted by groundwater, as well as the parameters of waste-form composition and environmental conditions which will cause changes from its state at the time of disposal. In addition, we are producing experimental data on the parameters that affect dissolution of the waste form, including composition of the groundwater and environmental conditions. The waste-form dissolution process is also being mathematically modeled to allow analysis of the performance of the waste form under specific input conditions.

The information on the performance of the overpack materials relates to the required containment period of 300 to 1000 years. Overpack performance is expected to be most affected by corrosion and hydrogen-attack processes. We are attempting to provide information on the parameters of overpack-material composition, groundwater composition, and environmental conditions that are most significant in these processes. Our

preliminary study of the titanium alloy in brine did not reveal any conditions that would cause general corrosion, pitting, crevice corrosion, or stress-corrosion cracking to affect the good performance of the material as claimed in the literature. However, vapor-phase attack was identified; this could degrade the material and should be more thoroughly investigated if the DOE selects the material for use.

Our studies of cast low-carbon steel in a basalt environment are currently focused on the susceptibility of the metal to stress-corrosion cracking under repository conditions, because steel is known to fail by this process in some environments. We are studying the chemical species and environmental conditions that cause cracking to determine whether this mode of failure is expected under credible repository conditions. Our experimental studies on general and localized corrosion, together with our comprehensive general-corrosion model, will assist in evaluating the corrosion-allowance approach for the use of steel as a long-life container.

Although the development of an integrated waste-package system model is no longer included in the scope of this project, modeling efforts in the integrated system-performance task are contributing significant information to studies of general corrosion and glass dissolution. These studies require knowledge of the amount and kind of chemical species that may be produced by radiolysis of the groundwater near the waste package as a result of gamma radiation from the enclosed waste. To obtain this information, energy deposition and radiolysis codes are used. To determine how these radiolysis products may affect the performance of the canister and waste form, it is necessary to determine their chemical activities. These are calculated by the water-chemistry model, using as input data from experiments and from the groundwater-radiolysis model. The output from the water-chemistry model is the concentration and activity of each chemical species in the groundwater near the waste package. This information is used not only as input to the general-corrosion and glass-dissolution models but also as a point of reference in directing the experimental efforts in corrosion and dissolution. Some effects of radiolysis may be observed in the integral experiments to be conducted during the fourth year of the program. The primary objectives of the integral experiments is to identify combined effects, possibly synergistic in nature, that affect the performance of the overpack and waste form, and to provide some insight into the role of cladding in the release of radionuclides from spent fuel.

2. WASTE FORMS

Glass leaching experimentation is being concluded so that more emphasis can be given to evaluating the leaching/dissolution behavior of spent fuel. During the past quarter, additional data were accumulated on the glass-dissolution-rate model-verification experiments. A number of glass samples were devitrified using RuO_2 nuclei in preparation for an experiment that is addressing the effect of devitrification on glass leach rates. A 28-day leach test of MCC 76-68 using solutions of fulvic and acetic acids was conducted. A significant amount of effort was devoted to preparing for and attending the 2nd NRC-JAERI (Japanese Atomic Energy Research Institute) Technical Group Meeting, which was held in Japan from June 17 to 21, 1985. Most of the work conducted this reporting period in regards to spent-fuel studies was directed to preparing plans for experiments and designing experimental apparatus.

2.1 Glass Experiments

2.1.1 Glass Dissolution Model Verification

An experiment was designed to verify a numerical model for the long-term dissolution and precipitation behavior of a simulated waste glass in water. In this on-going experiment, specimens of MCC 76-68 simulated waste glass are being exposed to distilled-water leachate at 90 C for durations ranging from 1 to 224 days. As of mid-June, the experiment is in its 140th day. The experimental procedure used is MCC-1P, which has been modified to isolate the glass specimen and leachate during cooling. Experimental surface-area-to-volume (SA/V) ratios have been adjusted to 10 $meter^{-1}$.

At the conclusion of each experiment, glass specimens are removed and glass surface layers are examined by scanning electron microscopy and energy dispersive X-ray (SEM-EDX) analysis for silica-bearing crystals that have formed in the alteration layer. Leachates are digested in high-purity Na_2CO_3 and then analyzed for silica using an ammonium molybdate colorimetric procedure.

This model predicts that SiO_2 is the glass component that controls glass dissolution and that amorphous silica from the glass dissolves in the leachate and later reprecipitates in the alteration layer as a crystalline phase (such as quartz or a silicate) having a lower solubility than amorphous silica. The overall kinetics of the glass dissolution are therefore determined by the time dependency of the rate constants for the dissolution and reprecipitation reactions and can be expressed as follows:

$$\frac{dC}{dt} = \frac{KS}{V}(C_o - C) + K'(C_o' - C) \qquad (2\text{-}1)$$

where

K = Reaction rate constant of the dissolution reaction

K' = Reaction rate constant of the precipitation reaction

S = Surface area of glass

V = Volume of leachate

C_o = Saturation concentration of silica with respect to glass

C_o' = Saturation concentration of silica with respect to precipitate

C = Instantaneous concentration of silica in leachate

t = Time.

The rate constant of the precipitation reaction, K', may be zero, a constant, or may increase with time, depending on the specific geochemical processes occurring. Figure 2.1 illustrates the theoretical dependence of C(t) on the magnitude of K'. In our experiment, C(t) is the concentration of dissolved silica in the leachate as a function of time. The results of the silica analyses through day 140 of the experiment are plotted in Figure 2.2. This figure shows that, as of day 140, the silica concentrations in the leachates are steadily increasing and have not yet approached equilibrium or steady-state values.

The precipitation of secondary silica-bearing crystals in the glass alteration layers was first observed at day 70. Typical crystals are shown in Figure 2.3. The crystals appear to be growing from cracks or other imperfections in the glass surfaces. EDX analysis shows that the crystals are composed primarily of zinc silicate, possibly with small amounts of sodium. From days 70 to 140, zinc silicate crystal density has increased with time, as shown for the 84- and 112-day samples in Figure 2.4.

In conclusion, our experimental observations qualitatively confirm the numerical model for glass dissolution and reprecipitation; however, data collected thus far are insufficient to calculate the rate constants in Equation 2-1. This experiment is currently scheduled to continue through day 224. It is hoped that the data collected during the later stages of the experiment will permit quantification of the various rate constants for the dissolution and reprecipitation of MCC 76-68.

2.1.2 Crystallinity Influences

Experimental work has continued in an effort to assess the influence of crystal size and volume fraction on glass waste-form leaching. Data and analyses from previous efforts in this program indicate that crystals

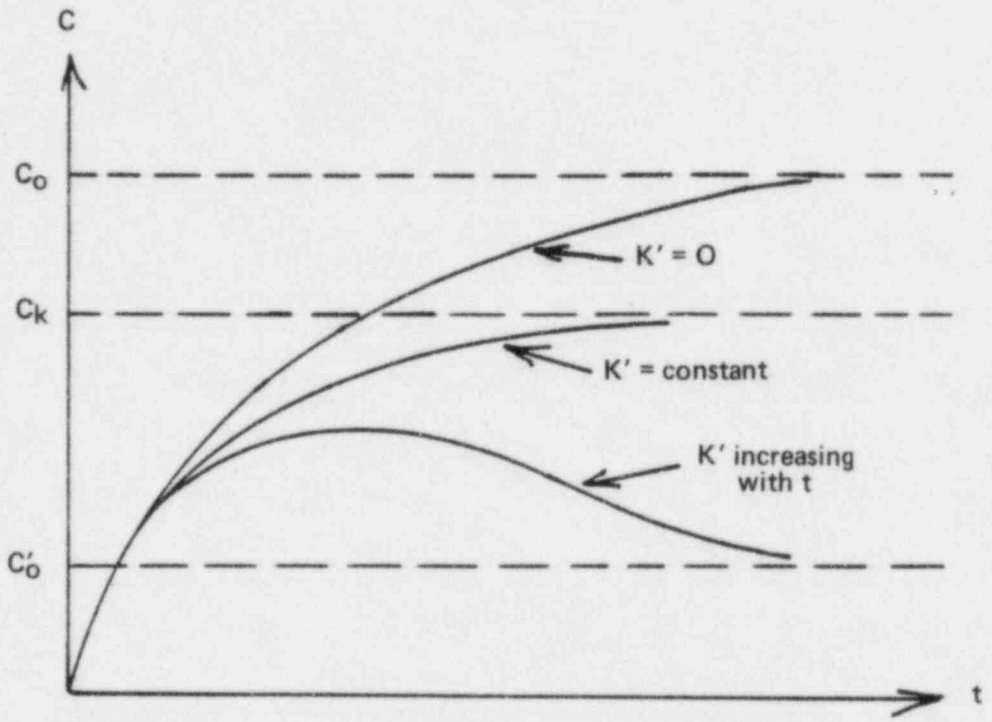

Figure 2.1. Dependence of C(t) on the magnitude of the reprecipitation rate constant, K'.

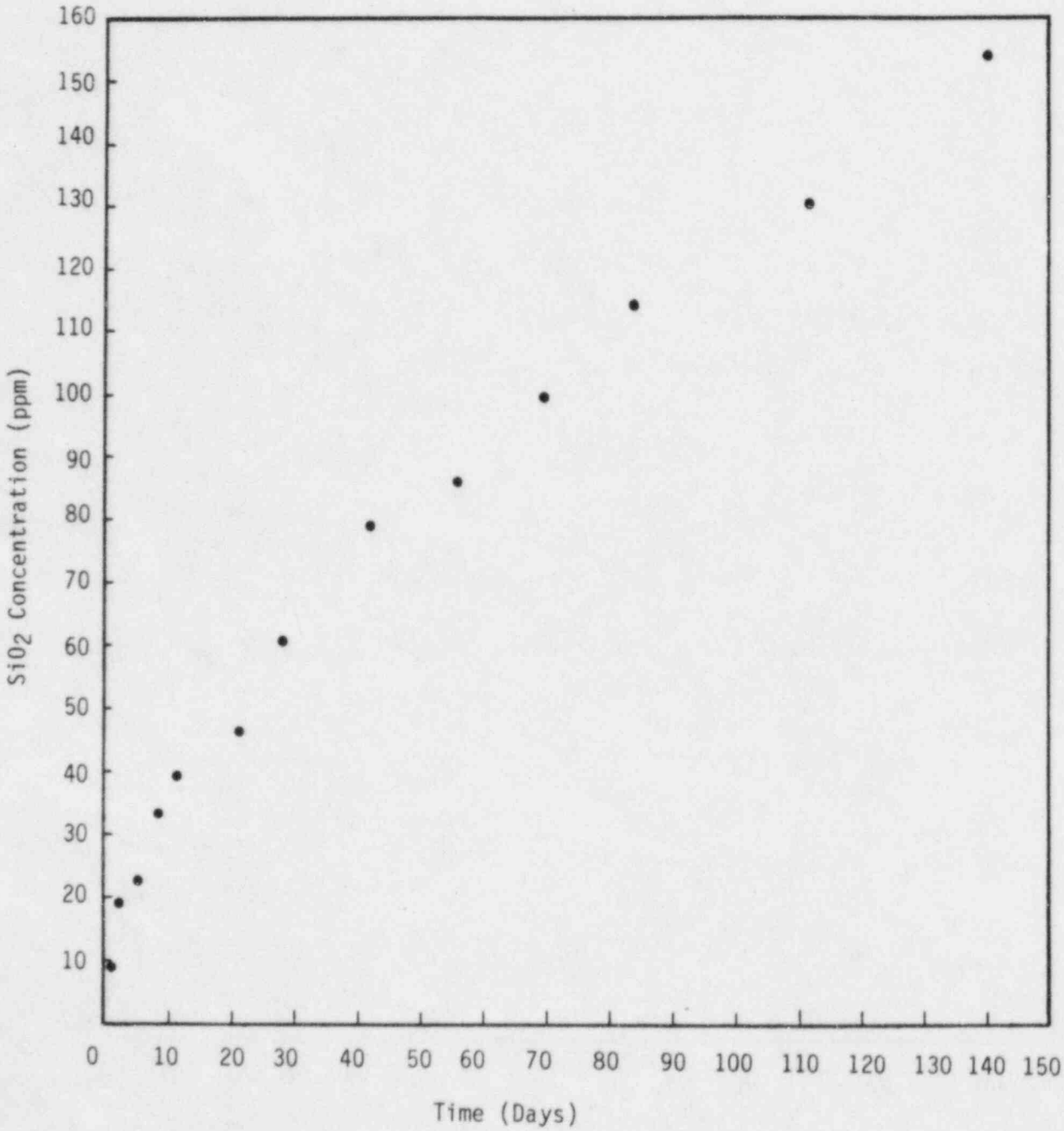

Figure 2.2 Dissolved SiO_2 concentration as a function of time.

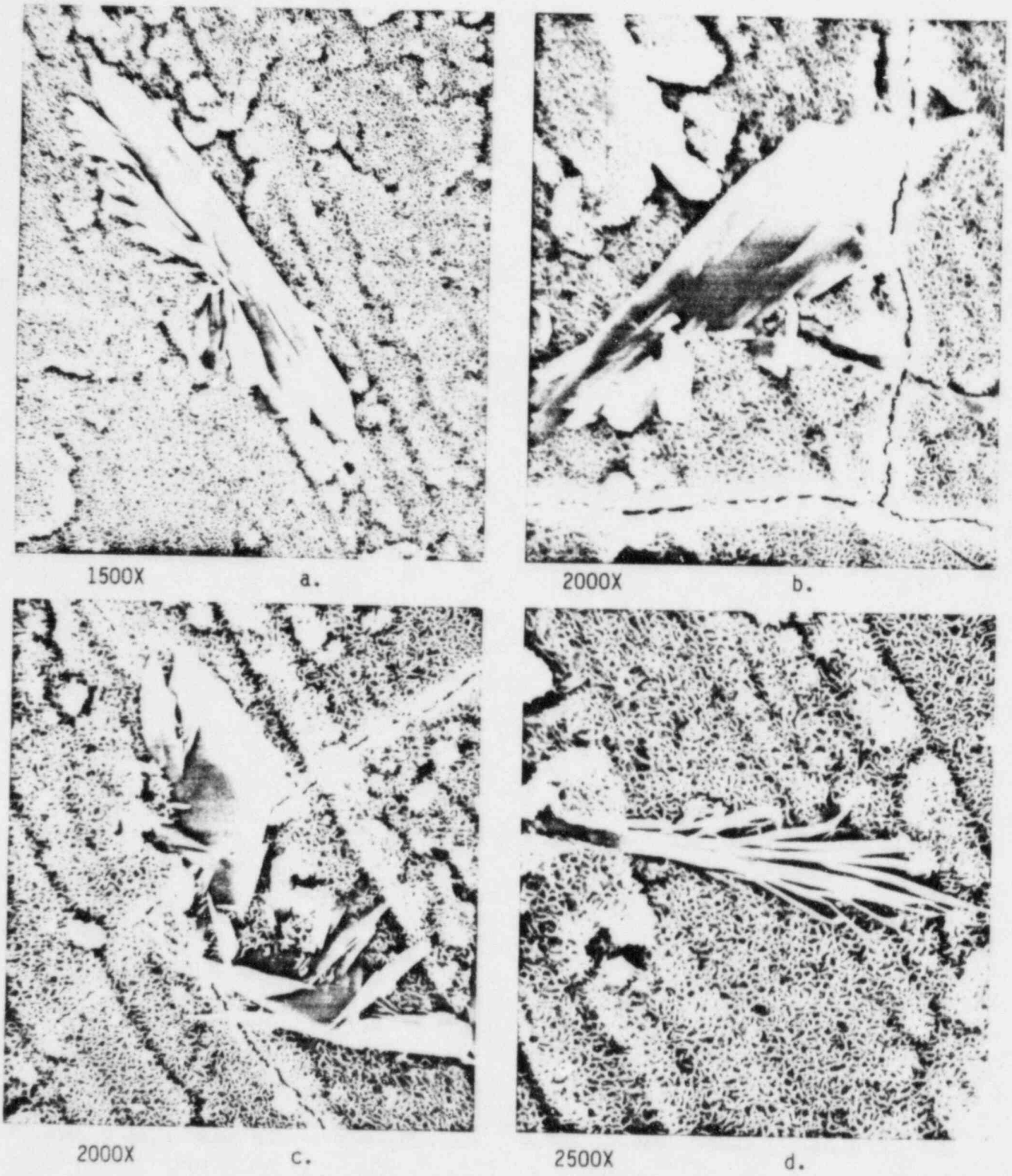

Figure 2.3. SEM micrographs of zinc silicate crystals in alteration layers of 84-day glass samples.

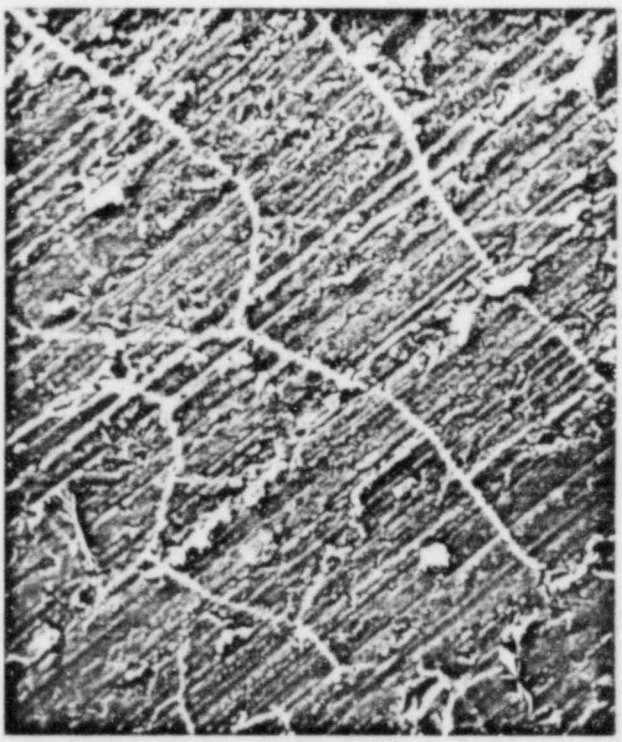

200X a. 84-day sample

200X b. 112-day sample

Figure 2.4. SEM micrographs showing zinc silicate crystal distribution increasing with leach time.

may develop as a result of heterogeneous nucleation and growth during cooling of the waste form. The present experiment is designed to develop volume fractions crystallized at two different crystal sizes. The volume fraction (V_C) targets are 15 percent and 80 percent, and the crystal size targets are 1 μm and 10 μm mean diameter (d-bar). These values are expected to bracket the effects of crystallinity on waste-form performance.

The primary variables in heterogeneous nucleation, i.e., temperature, exposure time, and concentration of nuclei, were studied experimentally and reported on in the Year Three Annual Report. In summary, these variables were found to be influential, but the ranges explored for each variable did not yield the target values of V_C or d-bar.

To better define the conditions that lead to target values of V_C and d-bar, the experimental work has been extended using higher temperatures and longer exposure times for two MCC 76-68 glasses with different concentrations of heterogeneous nuclei (N_p). The results of this testing are presented in Table 2.1. In this table, V_C and d-bar values are listed for two specific values of log N_p at various exposure times. The data show that higher temperatures and longer exposure times can generate V_C and d-bar values in the lower end of the target range. Furthermore, lower values of N_p seem to be more influential in altering V_C and d-bar than higher values.

Table 2.1. V_C and d-bar values for crystallization experiments conducted at 930 C for MCC 76-68 glass.

Exposure	log N_p = 6		log N_p = 9	
(hours)	V_C (%)	d-bar (μm)	V_C (%)	d-bar (μm)
24	5.49	4.07	3.88	2.34
48	6.67	4.75	3.39	2.23
72	8.33	5.19	3.34	2.31
96	9.56	4.94	3.17	2.28
120	13.45	9.63	4.47	2.47

Note: N_p = number of heterogeneous nuclei per cc
V_C = volume fraction crystals expressed as a percentage
d-bar = mean crystal diameter.

These data are being statistically evaluated. Present indications are that further experimentation is needed to clearly define the influence of the primary variables on crystal nucleation and growth. However, because the program direction is moving away from glass waste-form evaluation in favor of spent-fuel evaluation, further testing will not be conducted. The existing data base will be used to select glass specimens with two V_C and d-bar conditions for leach testing. This experiment to explore the effects of devitrification on glass dissolution should be completed during the next quarter.

2.1.3 Organic Acid Experiment

The objective of this experiment is to evaluate the effects of natural organic acids in groundwater on the leach rates of selected components of MCC 76-68 simulated waste glass. Natural organic acids in deep groundwaters may include compounds with a wide range of compositions. We have chosen to evaluate two species that typify two groups of organic acids frequently encountered in the natural environment: acetic acid and fulvic acid. Acetic acid is one of the principal anaerobic microbiological breakdown products of numerous natural organic compounds. It occurs widely in oil-field waters[2.1] and has been identified in deep groundwaters from the Palo Duro Basin, Texas--one of the sites recently selected as a potential high-level nuclear waste repository. Humic substances form mainly in soils and swamps and occur widely in surface waters and shallow groundwaters and occasionally in deep groundwaters. Fulvic acid (a slightly more oxygenated form of humic acid) has been identified in deep groundwaters from the Finnsjon and Sterno areas of Sweden--both of which are prospective waste disposal sites in granitic media.[2.2] Also, acetic and fulvic acids were found to be appropriate selections for testing because they represent limiting ranges of metal-complexing capacities for natural organic ligands, fulvic acid being a strong complexing agent and acetic acid being rather weak.

During this past quarter, a 28-day leach test at 90 C was conducted. MCC 76-68 was exposed to simulated Grande Ronde basalt groundwater[2.3] which was doped with either 200, 632, or 2,000 ppm acetic acid or 20, 63.2, or 200 ppm fulvic acid (reference Suwannee Stream Fulvic Acid was obtained from the International Humic Substance Society). Duplicate tests were conducted using vessels containing solutions with an organic-ligand acid concentration along with two blanks (no glass or acid solution), resulting in 14 different reaction vessels. The basic experimental design used was the MCC-1P procedure modified for isolating the glass sample and leachate during cooling. SA/V ratios were uniformly maintained at 10 m^{-1}. At the conclusion of the 28-day test, the leachate was digested with ultrapure HNO_3 at 95 C and then analyzed by inductively coupled argon-plasma (ICAP) spectroscopy.

The results of the ICAP spectroscopic analyses are presented in Table 2.2. Several trends are apparent. Sodium was selectively leached by acetic acid; nickel, zinc, and lanthanum--and to a lesser extent magnesium, barium, and aluminum--were selectively leached by fulvic acid.

Table 2.2. Results of ICAP spectroscopic analyses showing element concentrations in leachates.

Sample	Concentrations (mg/liter)								
	Al	Ba	Ca	Fe	Ni	Mg	Na	Zn	La
200 ppm AA*	0.2	0.05	0.8	0.2	<0.05	0.08	390	0.1	<0.05
200 ppm AA	0.1	0.04	1.5	0.1	<0.05	0.04	340	0.1	<0.05
632 ppm AA	0.2	0.04	0.9	0.04	<0.05	0.04	640	0.1	<0.05
632 ppm AA	0.1	0.05	0.9	0.2	<0.05	0.04	660	<0.1	<0.05
2,000 ppm AA	<0.1	0.06	2.0	0.07	<0.05	0.03	1,060	<0.1	<0.05
2,000 ppm AA	0.2	0.05	1.0	0.2	<0.05	0.05	1,150	0.1	<0.05
20 ppm FA**	0.2	0.06	1.3	0.3	0.07	0.08	360	0.6	<0.05
20 ppm FA	<0.1	0.12	5.8	0.3	0.05	0.08	300	0.9	<0.05
63.2 ppm FA	0.2	0.05	0.9	0.2	0.07	0.05	350	0.3	<0.05
63.2 ppm FA	0.2	0.15	5.3	0.3	0.1	0.14	330	1.7	0.05
200 ppm FA	0.7	0.21	2.9	0.1	2.7	0.14	350	9.7	0.08
200 ppm FA	0.3	0.17	3.3	0.1	1.2	0.11	310	2.6	0.53
Blank	0.2	0.03	0.6	0.2	<0.05	0.04	320	0.2	<0.05
Blank	<0.1	0.03	1.1	0.2	<0.05	0.03	290	0.1	<0.05

*AA = Acetic Acid.
**FA = Fulvic Acid.

At present, the data are being statistically analyzed; the results of these analyses will be described in the next Quarterly Report.

In conclusion, this experiment was intended to be an initial screening test and was to have been followed by a series of long-term tests that would have quantitatively evaluated organo-glass interactions. This effort, however, has been terminated so that our experimental activities can focus on the leaching of spent fuel.

2.1.4 Second JAERI/NRC Technical Group Meeting

Two Battelle staff members attended the 2nd JAERI (Japan Atomic Energy Research Institute)/NRC Technical Group meeting which was held in Japan from June 17 to 21, 1985. The objectives of the meeting were as follows:

(1) Exchange information on waste management research programs conducted by NRC and JAERI.

(2) Develop experimental plans for the following three experiments to be conducted by JAERI under the JAERI/NRC Cooperative Agreement:

   a) Flow-through test of high-level waste glass--prepare detailed experimental plan

   b) Radiation effect on the corrosion of high-level waste overpack material--prepare proposed experimental plan

   c) Radionuclide migration in soils--provide proposed modifications to JAERI experimental plan.

(3) Future meetings--discuss content and scope.

(4) Personnel exchange--NRC to JAERI, JAERI to NRC.

The Battelle participants presented pertinent aspects of their NRC-sponsored research relating to waste-package performance and also proposed experiments for JAERI to conduct for NRC under the Cooperative Agreement. JAERI agreed to conduct several experiments over the next two to three years in the areas of glass leaching, overpack corrosion, and radionuclide migration in soils. The next formal JAERI/NRC Technical Group Meeting is scheduled for the fall of 1986. JAERI intends to send several representatives to Battelle for informal technical discussions in November, 1985.

2.2 Spent-Fuel Experiments

2.2.1 Experimental Leach-Rate Studies

Most effort during this past quarter was devoted to developing test plans for spent-fuel leaching experiments and assembling and purchasing experimental apparatus. A comprehensive review of the literature on spent-fuel leaching experiments was also conducted. This literature survey showed that most of the previous studies on uranium dioxide (UO_2) and spent-fuel leaching have been conducted under oxidizing conditions that are not representative of expected long-term repository conditions. Also, most of the previous work in this subject has not included precise experimental redox measurement and control. As a result, there is considerable variation in existing UO_2 and spent-fuel leach-rate data, and it is difficult to assess the applicability of existing data to predicting spent-fuel performance in a deep geologic repository.

Therefore, the objective of the spent-fuel leaching tests conducted under this program will be to generate high-quality data on fuel leach rates under expected repository (i.e., anoxic) conditions. Spent fuel will be leached in flow-through systems using simulated basalt and tuff groundwaters as leachates. Anoxic conditions will be established using the methods of Jantzen[2.4], who produced low redox potentials (i.e., -0.15 to -0.45 volts) in simulated basalt groundwaters by contact with high SA/V-ratio basalt and ductile iron. The experimental leachate/fuel contact time (as a function of flow rate) and SA/V ratio will be varied to assess the importance of these variables on fuel leach rates.

Studies carried out on actual spent-fuel samples will be preceded by several short-term flow-through tests on unirradiated UO_2 fuel, so that any problems associated with experimental design and apparatus can be readily identified and rectified prior to proceeding with the hot (spent fuel) tests. The unirradiated-fuel experiments will be conducted both in the presence and absence of a radiation field. These experiments will provide data on UO_2 solubility and leach rates for both conditions and will serve as a valuable comparison to the spent-fuel data.

Depending on the progress of unirradiated-fuel testing in Year Four, the testing of irradiated fuel will commence either late in Year Four or early in Year Five of this program. This experimental plan, taken as a whole, is intended to be the definitive study for comparing the leach behaviors of unirradiated and irradiated fuel in repository-relevant chemical environments. This two-year study should also show whether spent fuel is as insoluble as unirradiated UO_2 under anoxic conditions.

2.2.2 Distribution of Radionuclides in Spent Fuel

Spent fuel is a complex mixture of numerous radionuclides that are unevenly distributed between the UO_2 matrix and grain boundaries. When exposed to water, radionuclides in grain boundaries will dissolve at different rates than radionuclides dispersed in the UO_2 matrix. Thus,

it is important to have quantitative information on the types, amounts, and chemical forms of radionuclides present in spent fuel and on how they are partitioned among grains and grain boundaries. The objective of this task, which will commence during the next quarter, will be to evaluate and summarize existing literature on the physical distribution of radionuclides in spent fuel. Emphasis will be placed on identifying long-half-life radionuclides that will be present in grain boundaries hundreds or thousands of years after fuel is discharged from a reactor. Uncertainties or gaps in the existing data base will also be identified.

2.3 Waste-Form Dissolution Modeling

The Battelle water-chemistry model was used during the past quarter to calculate dissolution rates for several waste glasses. The results of these calculations, summarized below, cast doubt on certain commonly held assumptions concerning glass dissolution.

2.3.1 Glass Compositions

The compositions of the waste glasses used in the model were based on glass types SRL 131 and 165 and PNL 76-68 and 77-260. However, even in their waste-free or "unloaded" form, these glasses contain some components that are not included in the Battelle water-chemistry program. Most of these species (ZnO, SrO, BaO, CuO, TiO_2, La_2O_3) were simply neglected, but Li_2O was assumed to be chemically similar to Na_2O. In general, the concentrations of the neglected species were small, and it is expected that their effects on glass durability would also be small. If reprecipitation were included in the model, some of these species, i.e., ZnO, might be more important and would be considered. With these modifications, the compositions of the glasses, expressed in molar ratios, are:

SRL 131: Si:Na:B:Mg = 1.0:0.988636:0.438235:0.051494

SRL 165: Si:Na:B:Mg = 1.0:0.784673:0.253840:0.021923

PNL 76-68: Si:Na:B:Ca = 1.0:0.363537:0.409951:0.053571

PNL 77-260: Si:Na:B:K:Ca:Al =

1.0:0.430858:0.431527:0.070874:0.029762:0.065476

It should be noted that the chemistry of these glasses would be significantly changed when high-level waste is added to them. Therefore, the results presented here should not be taken as an indication of the relative stability of the loaded waste glasses.

2.3.2 Glass Dissolution Calculations

Following our standard practice for modeling waste-form dissolution, it was assumed that silicon is solubility-limiting and that the glass

dissolves congruently; that is, the release rate of each component is proportional to its concentration in the glass. It was also assumed that all the oxides go into solution. This assumption might be questioned for Al_2O_3, which is the least soluble of the oxides treated. However, the calculated compositions of the glass solutions were always found to lie below the saturation limit for Al_2O_3 as calculated from data presented by Stumm and Morgan[2.5].

Dissolution of silicon was assumed to obey the following linear rate law:

$$\frac{dC}{dt} = \frac{KS}{V}(C_o - C) - \frac{\dot{v}}{V}(C - C_i) \qquad (2\text{-}2)$$

where

C = total concentration of silicon in the solution

t = time

K = kinetic constant

S = surface area of the glass

V = volume of water in contact with the glass

C_o = concentration of silicon at saturation

$\dot{v}$ = flow rate of the water

C_i = total concentration of silicon in the unaltered groundwater.

The value of K will depend on temperature and on the composition of the waste form, but it is expected that K will be roughly constant for isothermal dissolution of a given waste form. Physically, the first term of Equation 2-2 describes the removal of matter from the waste form, while the second term describes the transport into or out of the water volume by flow under conditions of perfect mixing.

An important feature of this calculation is that, unlike most glass-dissolution calculations, C_o is not assumed to be constant. Instead, it is assumed that the activity of unionized silicic acid (H_4SiO_4) is independent of pH and that the increase in silica solubility at high pH is due to ionization. This assumption is in good agreement with experimental data on silica solubility[2.6]. For any groundwater composition, the value of C_o is the saturation concentration of silicon calculated from the current activity coefficients for the silicon species and the current activities for all other species.

Two water types were used for our calculations: pure water and synthetic Grande Ronde basalt groundwater as described by Jones[2.3]. All the elements present in the synthetic groundwater composition are included in the water-chemistry model.

Glass dissolution rates were calculated for two important conditions. The first of these was the case of zero flow of water, or $\dot{v} = 0$, while the second is that of steady state, or $dC/dt = 0$. For both cases, we have expressed the dissolution rate as a dimensionless, normalized quantity, which is defined as follows:

$$\text{Normalized Dissolution Rate} \equiv \frac{\dot{v}(C - C_i)}{KSM} + \frac{dC}{dt}\frac{V}{KSM} \quad .$$

Here, M is the concentration of a 1-molar solution. The first term of the normalized dissolution rate gives the rate of transport out of the repository by water flow and is zero in the case zero flow of water. The second term gives the rate of accumulation in the water within the repository, so it is zero in the case of steady state.

In the case for which there is no flow of water, the differential equation for glass dissolution may be solved by the following process. The initial composition of the water is chosen. In our calculations, this would normally be either pure water or synthetic Grande Ronde groundwater. A water-chemistry code is used to calculate the pH and speciation, and these results are used to calculate C_o. The initial rate of dissolution can now be calculated from Equation 2-2. The waste form is allowed to dissolve congruently for a short period of time, thus changing the composition of the water. This process is then repeated with the altered water composition. In general, it is to be expected that C_o will change with time and that the dissolution rate will not follow a simple exponential curve. This is indeed the case, as is shown in Figures 2.5 and 2.6. In these curves, the normalized dissolution rate is plotted as a function of normalized time, which is defined as follows:

$$\text{Normalized Time} \equiv \frac{tKS}{V} \quad .$$

Note that the normalization of the dissolution rate and time removes any explicit dependence upon the kinetic constant, K. Since the actual, unnormalized dissolution rates reflect the effects of K, the data shown in the figures should not be used to compare the durabilities of the glasses.

In the case of pure water, The dissolution rates for all glasses go through a maximum before they begin to drop, and the rates are always greater than that calculated by assuming an exponential decay from the initial value, as would be the case if C_o were held constant. For the synthetic basalt groundwater, the dissolution rates drop monotonically from their initial value. However, the rates may decrease more or less rapidly than if they had simply decayed exponentially. The reason for these different effects is shown in Figures 2.7 and 2.8. As the waste

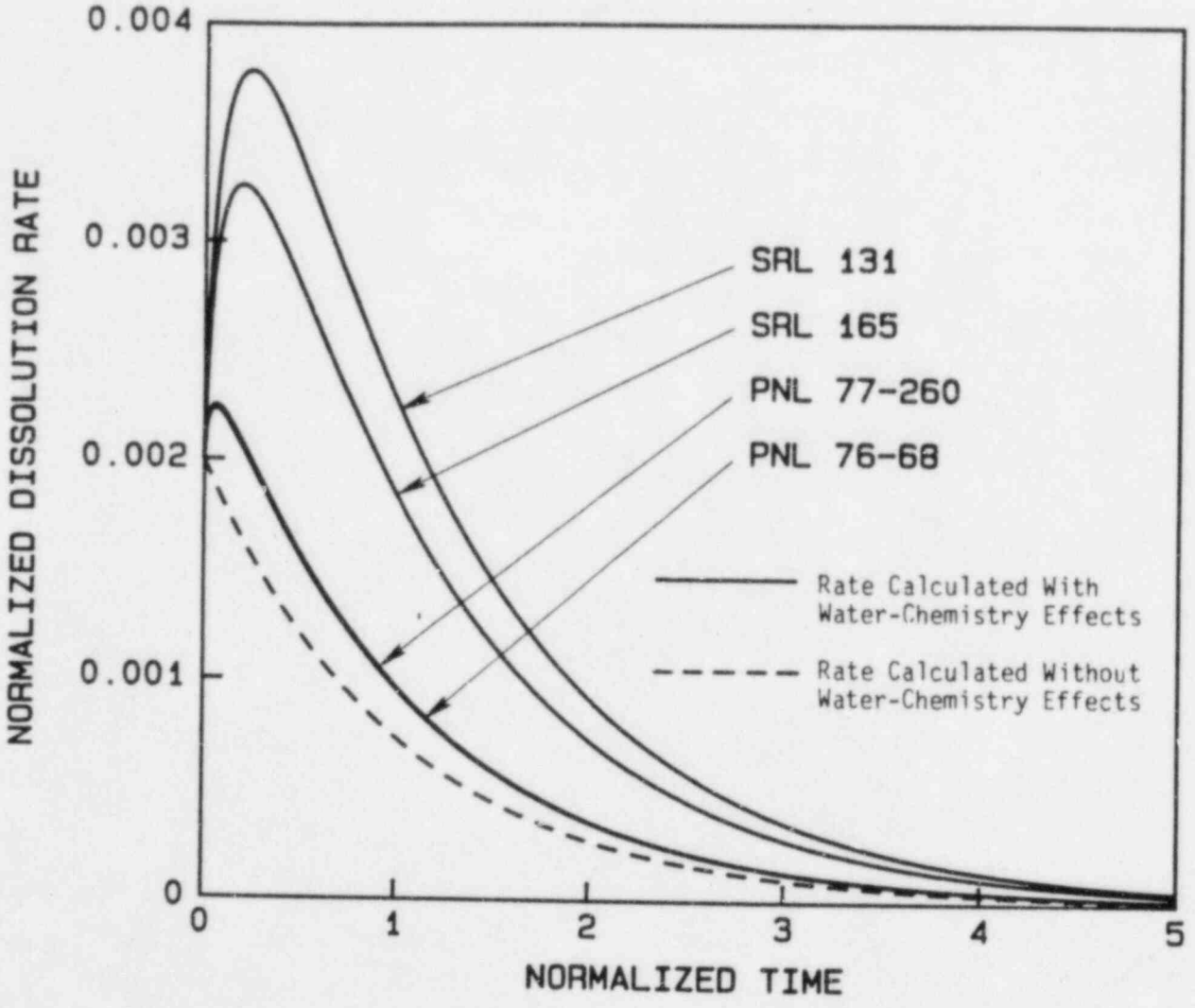

Figure 2.5. Dissolution rates as functions of time for four waste glasses in pure water.

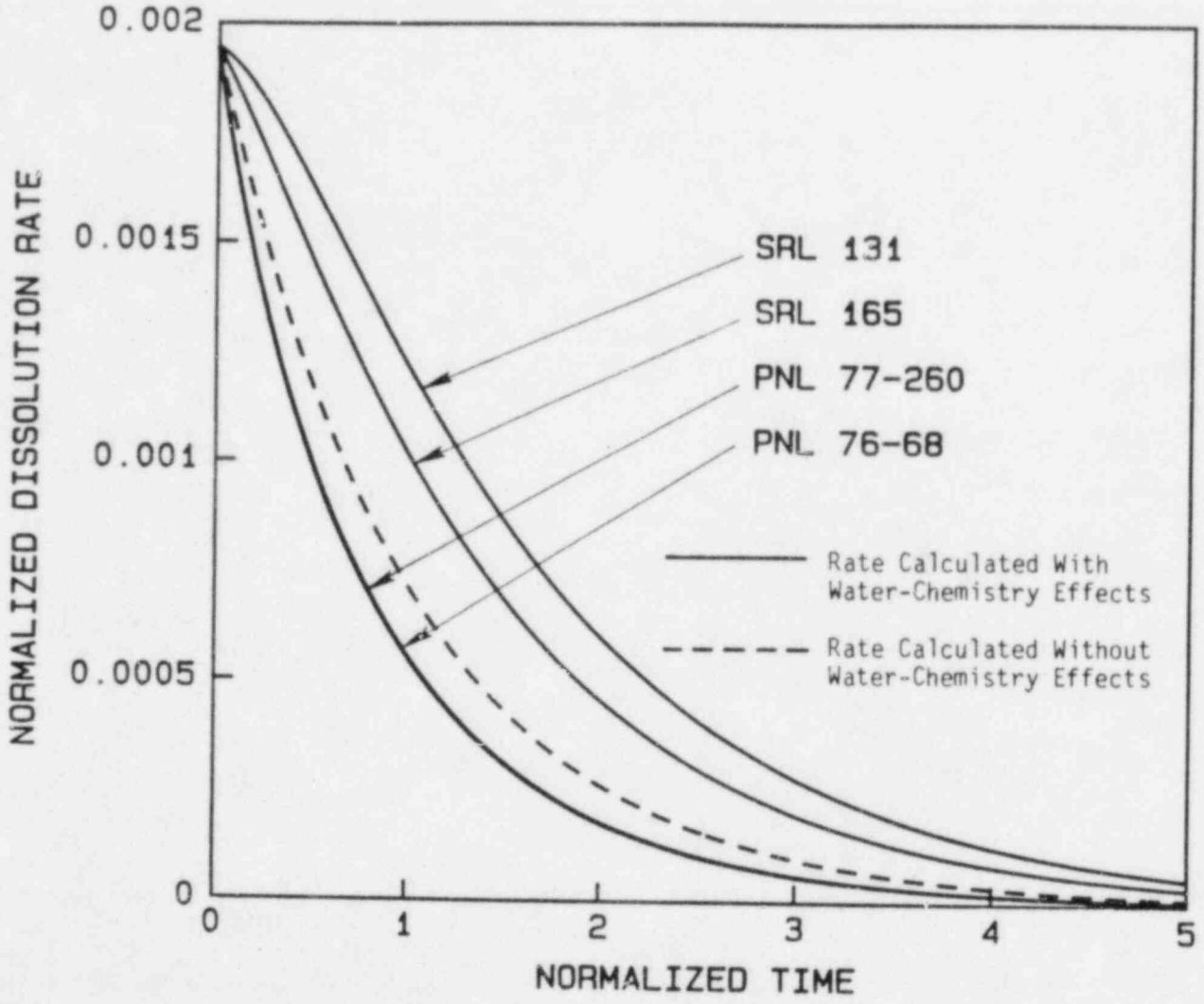

Figure 2.6. Dissolution rates as functions of time for four waste glasses in synthetic Grande Ronde basalt groundwater.

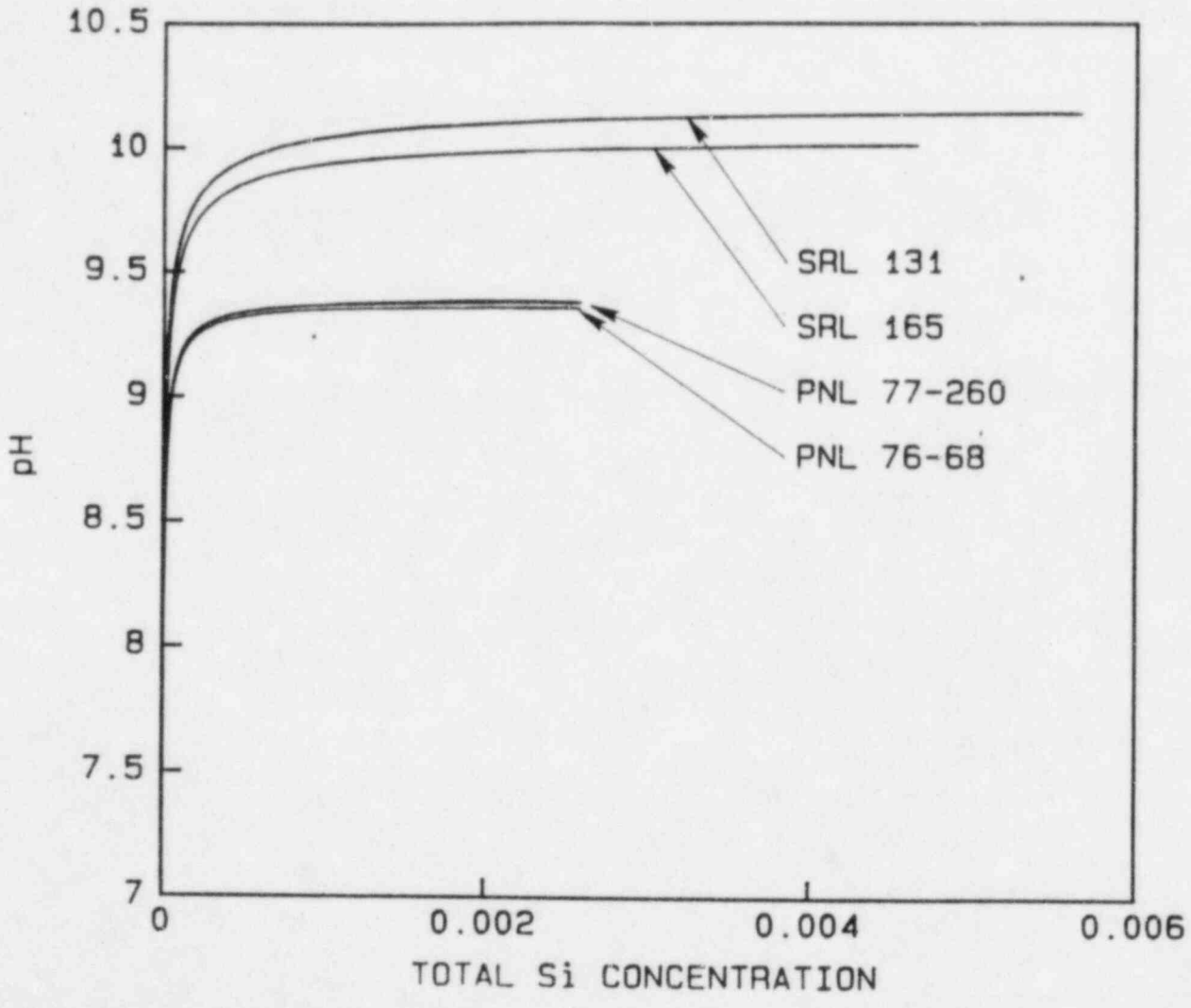

Figure 2.7. pH as a function of total molarity of dissolved silicon for four waste glasses in pure water.

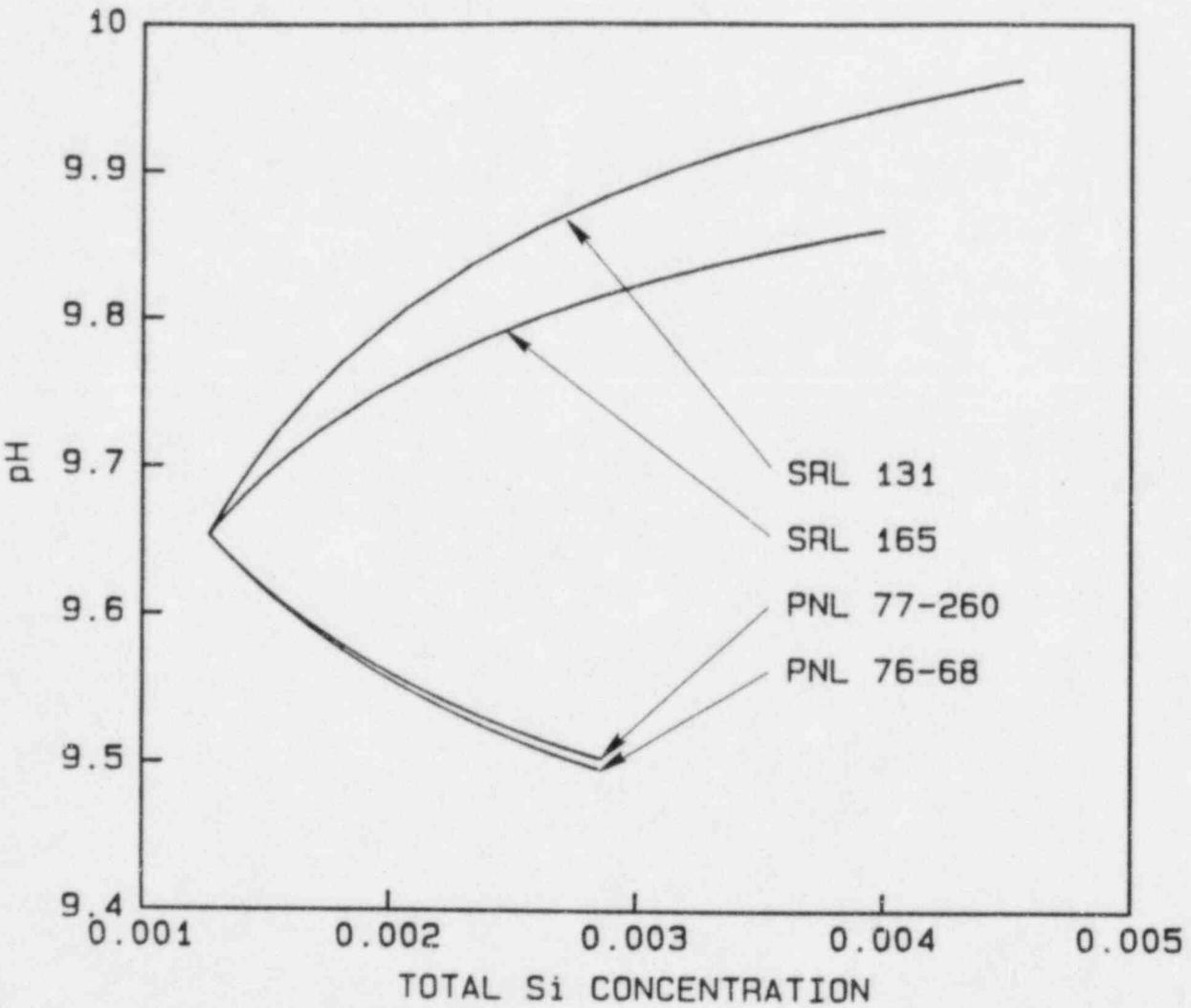

Figure 2.8. pH as a function of total molarity of dissolved silicon for four waste glasses in synthetic Grande Ronde basalt groundwater.

form dissolves in pure water, the pH of the water rapidly increases from an initial value of 7.0, and the total concentration of silicon at saturation, C_0, also increases, raising the dissolution rate. This occurs for all four glasses. In contrast, the pH of the synthetic basalt groundwater may either increase or decrease as the waste form dissolves. These changes in pH are reflected in a higher or lower dissolution rate.

From these results, it is apparent that short-term glass-degradation data must be interpreted with caution. In the case of pure water, the theory predicts that the dissolution rate will increase with time, at least for short times. Such experimental data might be incorrectly interpreted as suggesting that the waste form is undergoing catastrophic degradation. In the case of synthetic basalt groundwater, short-term data could be misinterpreted as suggesting that the glass is less stable than it actually is, as with the SRL glasses, or as being more stable than it is, as with the PNL glasses.

The second condition for which Equation 2-2 was solved is that of steady state, or $dC/dt = 0$. In Figures 2.9 and 2.10, normalized dissolution rate is plotted as a function of normalized flow rate for steady state conditions, where

$$\text{Normalized Flow Rate} \equiv \frac{\dot{v}}{KS} \quad .$$

Since the dissolution rate is normalized as for Figures 2.5 and 2.6, the steady-state dissolution rate at high flow rates is the same as the initial dissolution rate with no flow of water. Most discussions of the steady-state dissolution rate assume that C_0 is constant. Under this assumption, the solution to Equation 2-2 gives the following:

$$\text{Normalized Dissolution Rate (steady state, constant } C_0) = \frac{(C_0 - C_i)\,\frac{\dot{v}}{KS}}{1 + \frac{\dot{v}}{KS}} \quad .$$

In Figures 2.9 and 2.10 we show such a curve, taking C_0 to be the saturation concentration corresponding to the composition of the unaltered groundwater. In these figures, the solid lines represent the dissolution rates calculated with water-chemistry effects included. The dotted lines represent rates calculated without these effects added. It is clear that the curves deviate from the idealized behavior due to the variation of C_0 with composition. For the results shown in Figure 2.10, reasonable agreement with the standard equation can be obtained by adjusting the value of KS. For the results shown in Figure 2.9, however, we see that the dissolution rate in pure water does not increase monotonically with flow rate, but goes through a maximum. Therefore, the standard equation cannot adequately describe the kinetics

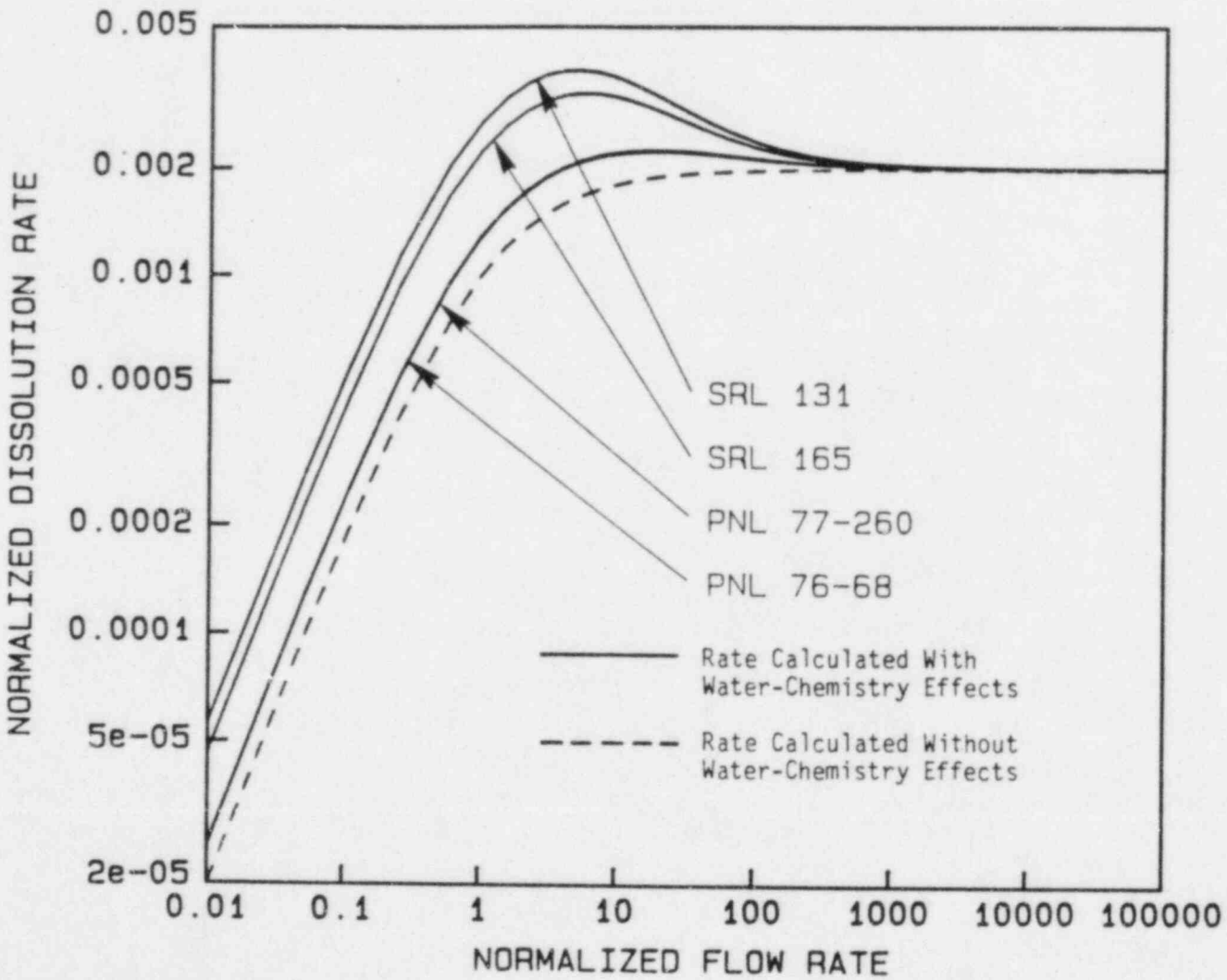

Figure 2.9. Dissolution rates as functions of flow rate for four waste glasses in pure water under steady-state conditions.

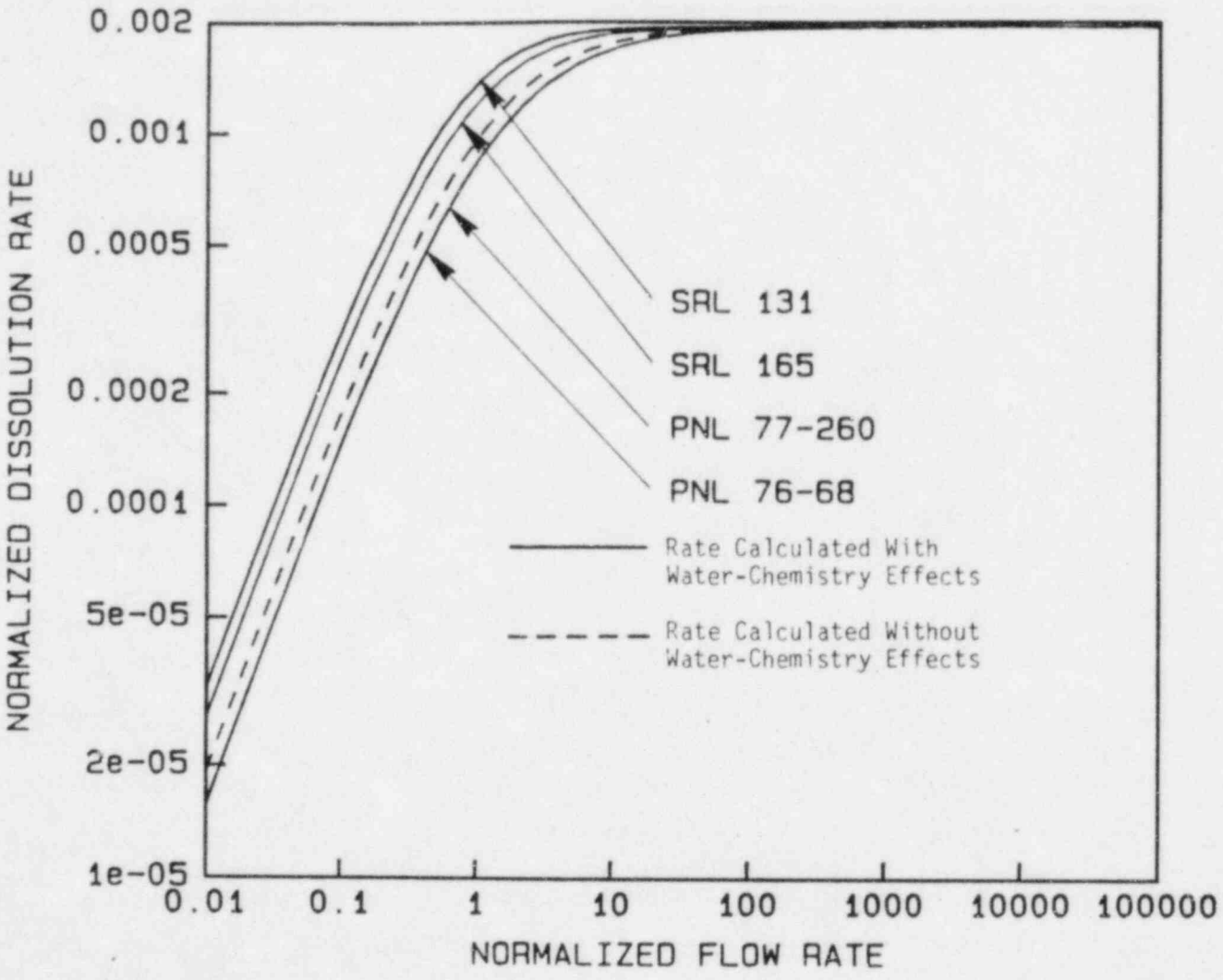

Figure 2.10. Dissolution rates as functions of flow rate for four waste glasses in synthetic Grande Ronde basalt groundwater under steady-state conditions.

of dissolution. This effect is particularly pronounced in the case of the SRL glasses. Effects of this type have been noted experimentally by Barkatt et al.(2.7)

In light of these results, caution should be taken in using the results of short-term static leach tests to predict long-term static leaching behavior or in using high-flow-rate steady-state results to predict low-flow-rate performance.

2.4 References for Section 2

(2.1) W. W. Carothers and Y. K. Kharaka, "Aliphatic Acid Anions in Oil-Field Waters--Implications for Origin of Natural Gas", American Association of Petroleum Geologists Bulletin, Vol. 62, No. 12, (1978), 2441-2453.

(2.2) J. L. Means, "The Organic Geochemistry of Deep Ground Waters", ONWI-268, prepared by Battelle's Columbus Laboratories for the Office of Nuclear Waste Isolation, Battelle Memorial Institute, Columbus, Ohio (1982).

(2.3) T. E. Jones, "Reference Material Chemistry--Synthetic Groundwater Formulation", RHO-BW-ST-37P (April, 1982).

(2.4) C. M. Jantzen, "Methods of Simulating Low Redox Potential (Eh) for a Basalt Repository", DP-M5-83-59, prepared by Savanna River Laboratory for the U.S. Department of Energy (1983).

(2.5) W. Stumm and J. J. Morgan, Aquatic Chemistry: An Introduction Emphasizing Chemical Equilibria in Natural Waters, 2nd. ed., pp. 241-247, Wiley and Sons, Inc., New York, 1981.

(2.6) G. B. Alexander, W. M. Heston, and R. K. Iler, "The Solubility of Amorphous Silica in Water", J. Chem. Phys., 58, 453 (1954).

(2.7) A. Barkatt, et al., "The Use of a Flow Test and a Flow Model in Evaluating the Durability of Various Nuclear Waste-Form Materials", Nucl. Chem. Waste Man., 4, 153 (1983).

3. OVERPACK CORROSION

Studies of overpack corrosion have focused this year on three areas: potentiodynamic polarization studies, slow strain rate studies, and pitting kinetics studies. All of the studies have examined the carbon steel - basalt rock system interactions. The objective of the potentiodynamic polarization studies is to evaluate the influence of metallurgy and groundwater chemistry on the tendency for stress-corrosion cracking (SCC) and pitting. The objective of the slow strain rate studies is to confirm the results of the electrochemical studies with regard to SCC and to investigate the effects of electrochemical potential, temperature, and environment composition in detail for the identified cracking agents. The objective of the pitting-kinetics studies is to investigate the effects of geometrical and environmental variables on pit propagation.

Corrosion correlation studies have continued. A basic model of the radiolysis process has been described and is being evaluated as part of the general-corrosion modeling effort. Studies of pit-generation kinetics have focused on deducing pit-generation and nucleation rates from pit-distribution data. Also, the mechanical aspects of overpack degradation are being evaluated.

3.1 Potentiodynamic Polarization Studies

In this task, potentiodynamic polarization techniques are being used to evaluate the influence of metallurgical and environmental variables on the electrochemical behavior of carbon steels in simulated repository environments. The results of these analyses are then used to assess the tendency for stress-corrosion cracking and pitting.

As explained in the Year Three Annual Report,(3.1) in the potentiodynamic polarization procedure, the polarity and magnitude of the current density between a material specimen and an inert counter electrode are measured as a function of electrochemical potential. For the anodic portions of the curve of such a plot, the current measured is equal to the corrosion rate of the specimen if two conditions are met: (1) the over potential (difference between the free-corrosion potential and polarized potential) is large enough such that the rate of the cathodic reaction is negligible, and (2) the rates of parasitic oxidation reactions are negligible.

Schematics of anodic polarization curves showing several types of behavior are given in Figure 3.1. For the active-corrosion case, the anodic curve is linear on a potential vs. logarithm of current (E-log i) plot, and the forward and reverse scans are coincident. The presence of a peak in the anodic portion of the curve, followed by decreasing current, generally indicates the onset of passivation. The occurrence of hysteresis between the forward and reverse scans indicates pitting. Where the hysteresis loop is very large, the protection potential may be very close to the open-circuit potential, indicating a high probability of pitting in service.

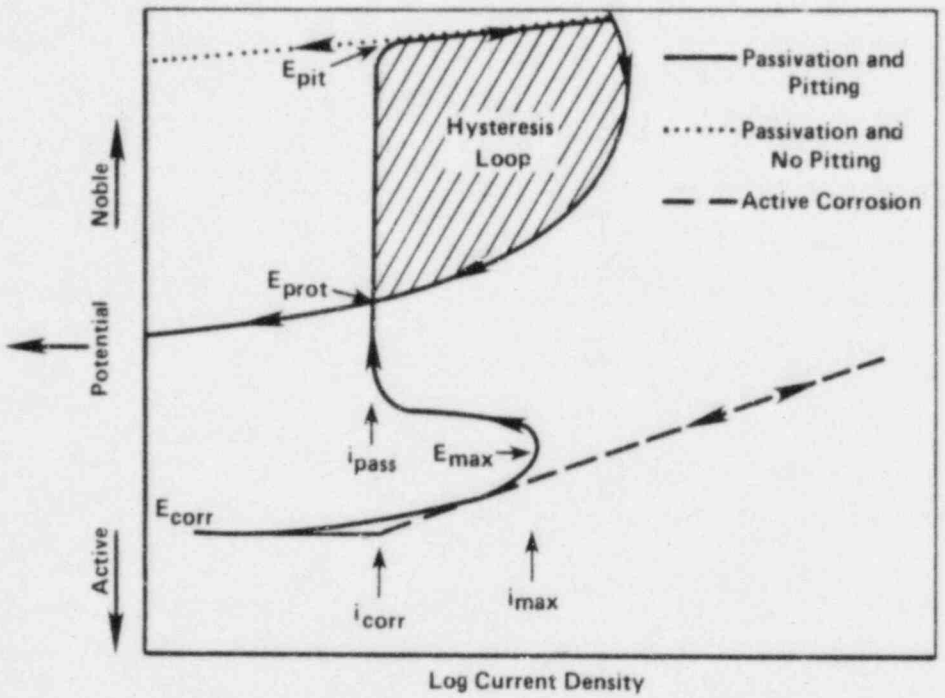

Figure 3.1. Schematic of typical anodic potentiodynamic polarization curves.

E_{cor} = corrosion potential; E_{pit} = potential at which pits initiate on forward scan; E_{prot} = potential at which pits repassivate on reverse scan; i_{cor} = current density at the free-corrosion potential; i_{max} = current density at active peak; i_{pas} = current density in passive range.

The potentiodynamic polarization technique also has been found to be useful in identifying possible SCC environments for carbon steels. It has been shown[3.1] that SCC is associated with environments that promote active-passive behavior and that the range of electrochemical potentials that promote SCC is near to and more noble (positive) than E_{max}. Moreover, it has been observed[3.1] that severe cracking occurs in environments where i_{max} on the fast scan is greater than about 1×10^{-3} A/cm^2 and where the fast scan exhibits currents at least an order of magnitude higher than those of the slow scan.

The polarization behavior of the candidate alloys is being determined using conventional polarization techniques. The equipment used for these experiments includes a PAR Model 173 potentiostat with an ECO Model 567 function generator, coupled to a computer data-acquisition system. A three-compartment electrochemical cell is used that utilizes a saturated calomel reference electrode (SCE) and a platinum counter electrode. The three-compartment electrochemical cell separates the working electrode from the counter electrode, thus preventing the solutions in the electrode compartments from mixing. The working-electrode specimens, made from hot-rolled 1020 carbon steel, are cylindrical rods drilled and tapped at both ends and then sealed using TEFLON* gaskets. The composition of the steel is given in Table 3.1. The specimens are 0.6 cm in diameter and 1.9 cm in length; the actual area of each specimen is measured prior to immersion in the electrochemical cell. The electrodes are polished with successively finer grades of silicon carbide paper, finishing with a 600-grit paper.

Prior to testing, the working electrode remains in the test solution overnight while the solution is sparged with the desired gas mixture. The polarization scans are then performed approximately 16 hours after the working electrode is immersed in the cell. Partial cathodic and full anodic polarization curves are obtained by scanning at a rate of 0.6 V/hr, beginning the scan approximately 100 mV more negative than the free-corrosion potential. The current for the anodic curve is then scanned until a current density of approximately 3×10^{-3} A/cm^2 is attained; the anodic scan is then reversed until repassivation occurs and the current changes polarity, becoming cathodic. When the polarization plot is completed, a new steel specimen is inserted into the polarization cell and immediately polarized to a potential of approximately -0.90 V (SCE). Within five minutes of immersion, a fast-anodic scan is performed using a scan rate of 18 V/hr. After the polarization scans are completed, the following polarization parameters are obtained from the polarization curves of potential (E) versus the logarithm of current density (log i) and versus i_{cor}, E_{cor}, i_{pas}, E_{pit}, E_{prot} and i_{max} (obtained from fast-scan curves).

---

*TEFLON is a registered trademark of the E. I. duPont de Nemours Company.

Table 3.1. Chemical compositions and other data on steels used in the corrosion studies.

SAE Number or Designation	Thermomechanical Treatment	Tests Used In	Dimensions	Composition (weight percent)										
				C	Mn	P	S	Si	Cu	Sn	Ni	Cr	Mo	Al
1018	Hot-Rolled	Pitting Exposures	7.6 cm x 15.2 cm strip	0.18	0.77	0.017	0.019	0.22	--	--	--	--	--	--
1020[a]	Hot-Rolled	Electrochemical Pitting Monitor, Potentiodynamic Polarization	1.27 cm rod	0.20	0.46	0.011	0.032	0.17	0.38	0.027	0.014	0.018	0.024	--
1020[a]	Hot-Rolled	Slow Strain Rate	0.635 cm dia. rod	0.22	0.55	0.01	0.037	--	--	--	--	--	--	--
Clean BCL Steel	Cast or Hot-Rolled	Potentiodynamic Polarization	Ingot	0.18	0.49	0.004	0.002	0.30	0.006	--	0.002	0.007	0.00	0.10
Doped BCL Steel	Cast or Hot-Rolled	Potentiodynamic Polarization	Ingot	0.17	0.55	0.029	0.036	0.35	0.007	--	0.004	0.011	0.00	0.14
Ferrovac E	Cast	Potentiodynamic Polarization	Ingot	0.003	Tr[b]	--	--	Tr	--	--	Nil[c]	Nil	Tr	Nil

(a) Hot-rolled 1018 carbon steel not available in rod form.
(b) Tr = Trace.
(c) Nil = None detected.

Several two-factor interaction effects were shown to be significant in describing the polarization behavior of carbon steel from research last quarter. Five of the most significant interactions were (1) pH-borate, (2) pH-chloride, (3) chloride-borate, (4) nitrate/nitrite-oxygen, and (5) chloride-carbonate/bicarbonate. To examine these interactions in more detail, the high-high, low-low, high-low, and low-high concentration matrices are being examined for each interaction separately using the standard basalt groundwater[3.2] as the base solution. Fast- and slow-scan potentiodynamic polarization experiments are being performed for each of the four combinations of the two species in the interaction.

During this reporting period, experiments were completed for the following interactions: pH-borate, pH-chloride, and chloride-borate. Figures 3.2, 3.3, and 3.4 show the slow-scan polarization behavior for all three interactions. The polarization behavior is presented here, but the statistical analysis and comparison to the previous work of Year Three will be completed next quarter.

The polarization curves representing the pH-borate interaction are shown in Figures 3.2a and 3.2b. A significant change is observed in the polarization behavior when going from conditions of low pH (6) and low borate (1 ppm B) to conditions of high pH (11.5) and high borate (1000 ppm B). For the high pH-high borate condition, the carbon steel is completely passive with no indication of pitting. This agrees with the predictions from the previous work which showed that both an increase in pH and borate tend to increase E_{pit} and E_{prot}. It is interesting to note that the low pH-high borate combination produced active behavior, that is, no passivity.

The polarization curves representing the pH-chloride interaction are shown in Figures 3.3a and 3.3b. pH and chloride have opposing main effects on the pitting behavior as determined in last year's work. The polarization curve for low pH (6.0) with low chloride (100 ppm) shows essentially active behavior (no passivation), and the curve for high pH (11.5) with high chloride (100,000 ppm) exhibits only very limited passivity (barely detectable). The polarization behavior for the high pH - low Cl condition exhibits the largest passive range, but the large hysteresis loop indicates pitting and/or crevice corrosion over a wide range in potential.

The polarization curves representing the chloride-borate interaction are shown in Figures 3.4a and 3.4b. Chloride and borate have opposing main effects on the pitting behavior of carbon steel as determined in last year's work. The pitting behavior of the low chloride-low borate and high chloride-high borate conditions are very similar, with the low-high combinations differing significantly. The polarization behavior for low chloride-high borate indicates a large (between -500 and +200 mV(SCE)) passive range, but the hysteresis loop indicates that pitting/crevice corrosion is likely over a very large range in potential as well.

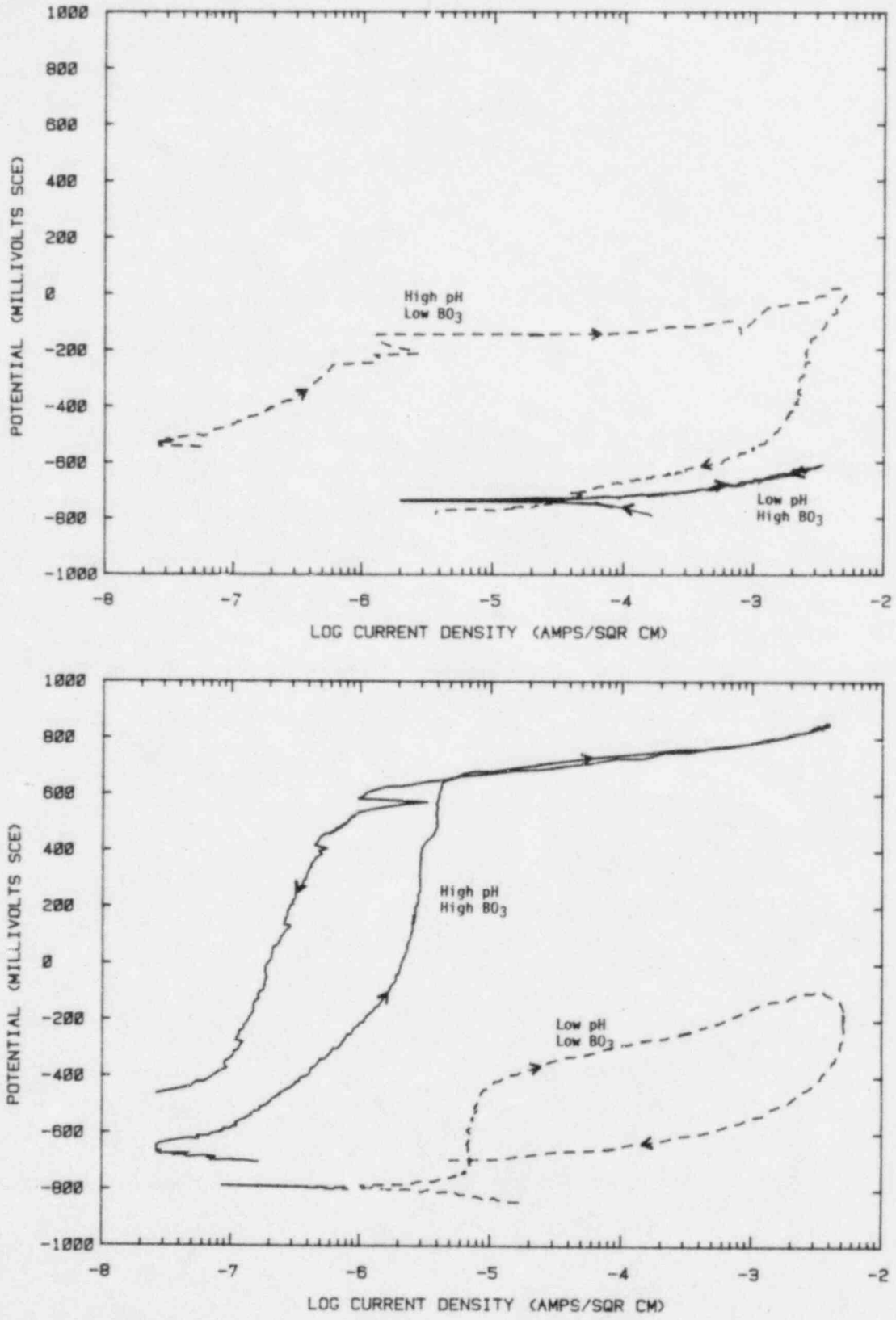

Figure 3.2. Slow-scan potentiodynamic polarization curves for two-level (high and low concentration) combinations of the pH-borate interaction.

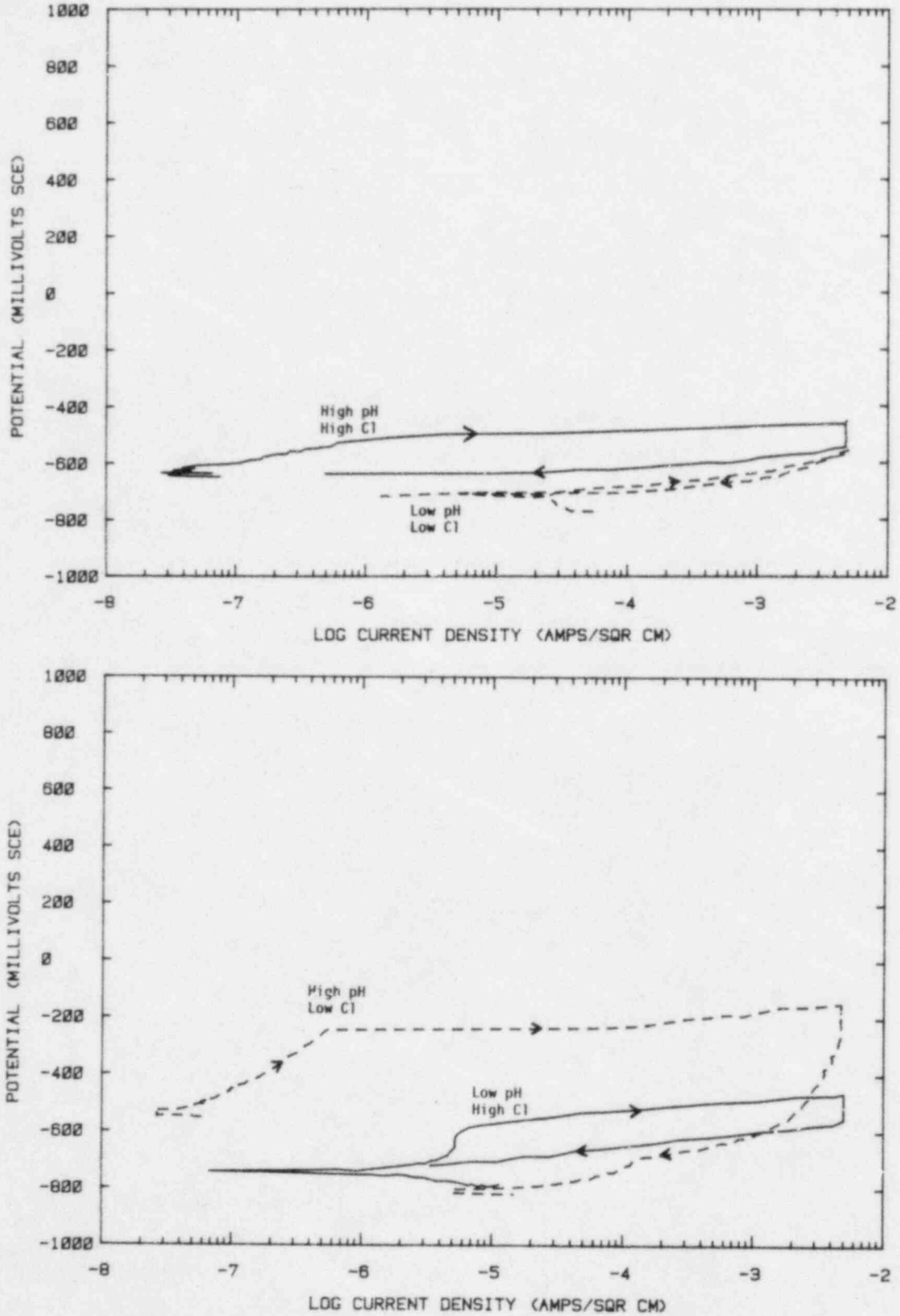

Figure 3.3. Slow-scan potentiodynamic polarization curves for two-level (high and low concentration) combinations of the pH-chloride interaction.

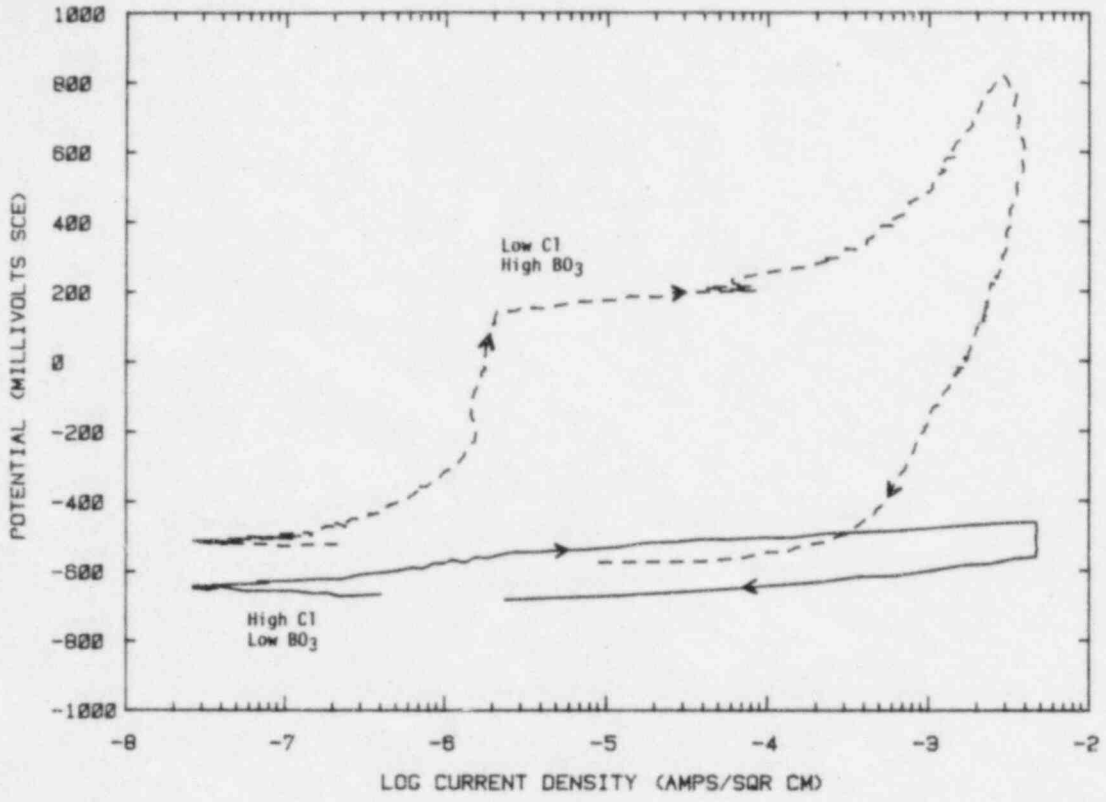

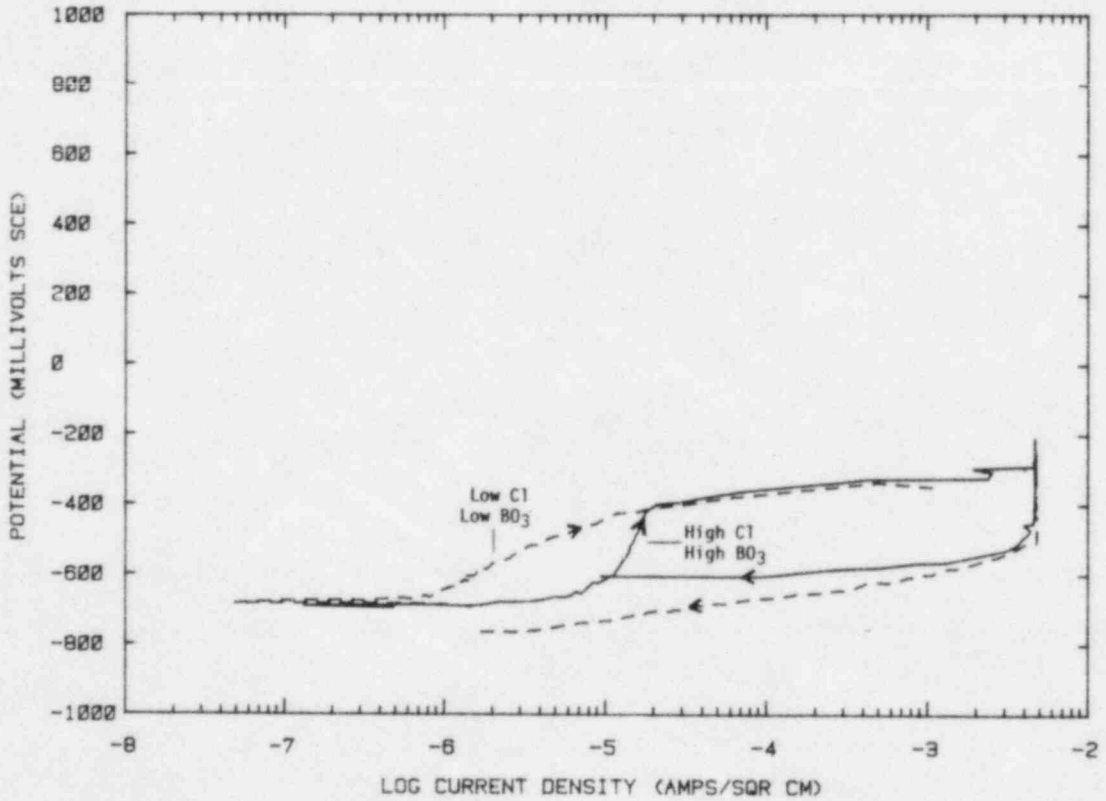

Figure 3.4. Slow-scan potentiodynamic polarization curves for two-level (high and low concentration) combinations of the chloride-borate interaction.

During the next quarter, the two remaining two-factor interactions will be examined and the data will be analyzed more completely.

3.2 Slow Strain Rate Studies

The objective of the slow strain rate (SSR) studies is to assess the stress-corrosion cracking susceptibility of carbon steels in candidate repository environments. Specific environmental conditions (solution composition and electrochemical potential) are being selected on the basis of the results of a literature survey and the electrochemical studies. During this program year, all of the tests have been performed on a commercially available hot-rolled 1020 carbon steel having the composition shown in Table 3.1.

During Year Three, results of the literature survey indicated that $FeCl_3$ is a potentially severe SCC agent for carbon steels and may be important in affecting overpack performance since ferric ions may be generated by radiolysis. Accordingly, SSR experiments were carried out to identify the optimum strain rate for subsequent testing and the solution concentration range over which SCC occurs in $FeCl_3$ solutions. It was found that a strain rate of about 1×10^{-7} sec^{-1} was the most practicable, and subsequent tests performed at this rate indicated that severe cracking occurred in solutions as dilute as 5×10^{-4} M $FeCl_3$.

Experiments also were started to evaluate the effect of temperature on SCC susceptibility of hot-rolled 1020 carbon steel in aqueous 5×10^{-4} M $FeCl_3$. These experiments were completed this past quarter. The results, given in Table 3.2 and Figure 3.5, indicate that susceptibility to SCC was at a maximum between 150 C and 200 C and decreased rapidly above or below this temperature range. The morphology of the cracking at 150 C is similar to that reported at higher temperatures with oxide-filled cracks and numerous pits in the gauge section of the specimen; see Figure 3.6. On the other hand, only shallow groove-like features were present in the gauge length of the specimen tested at 125 C, as shown in Figure 3.7.

During the next quarter, the effect of pH on SCC in aqueous $FeCl_3$ will be evaluated, and SSR experiments will be started in potential cracking environments identified from the potentiodynamic polarization studies.

3.3 Pitting-Kinetics Studies

Results of the potentiodynamic polarization experiments and autoclave exposures performed in Year Two suggest that pit initiation in low-carbon steels is likely in basalt groundwater. The polarization curves exhibit considerable hysteresis on the reverse scans, and protection potentials are very near the corrosion potentials, even for deaerated solutions. In the autoclave exposures, pits actually were found on specimens exposed for approximately 1000 hours in a deaerated simulated basalt groundwater at 250 C.

Table 3.2. Summary of results of slow strain rate experiments performed on hot-rolled 1020 carbon steel in aqueous 5×10^{-4} M $FeCl_3$ at a strain rate of 1×10^{-7} sec^{-1}.

Temperature (C)	Maximum Crack Depth (mm)	Time to Failure (hours)	Crack Velocity (mm/sec)
315	0.28	282	2.75×10^{-7}
275	0.12	165	2.05×10^{-7}
250	0.14	148	2.67×10^{-7}
225	0.52	164	8.80×10^{-7}
200	0.45	188	6.65×10^{-7}
175	0.59	211	9.37×10^{-7}
150	0.33	254	3.61×10^{-7}
125	0.07	366	5.3×10^{-8}

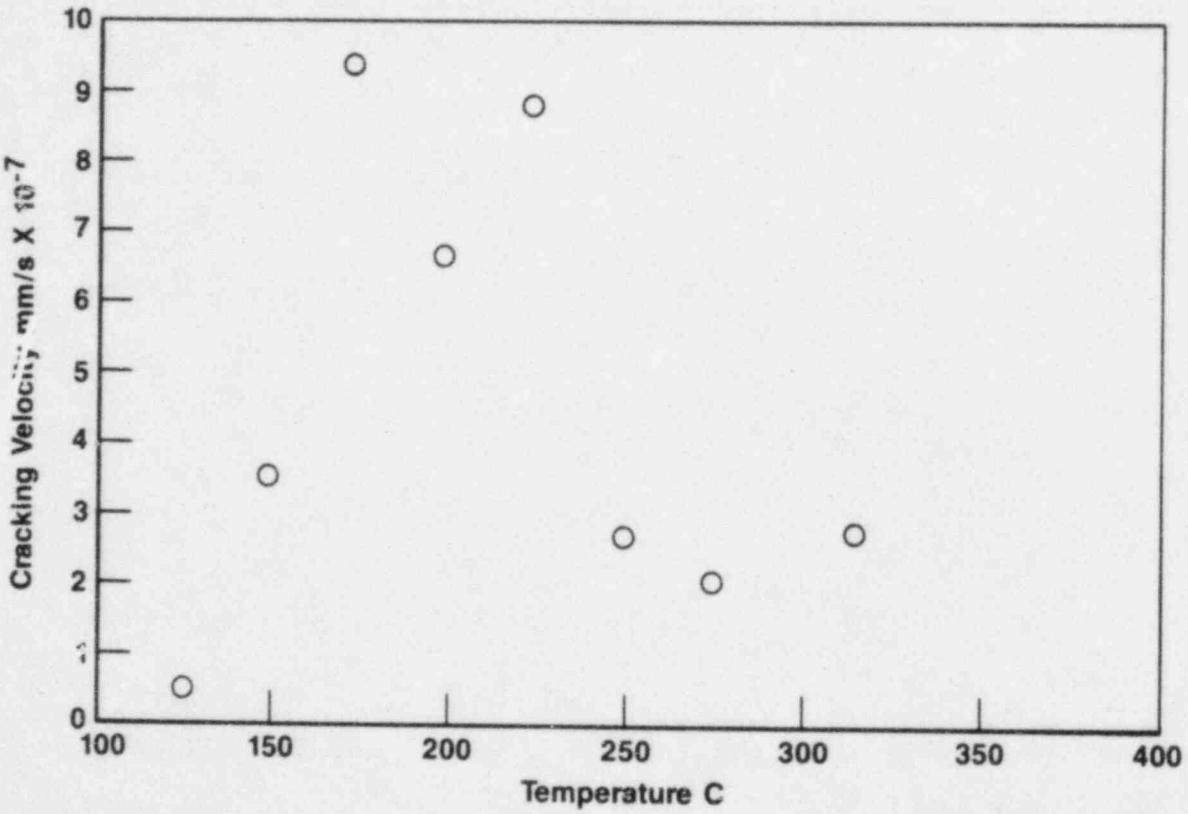

Figure 3.5. Crack depth as a function of temperature for hot-rolled 1020 carbon steel tested in 5×10^{-4} M $FeCl_3$ at a strain rate of 1×10^{-7}/sec.

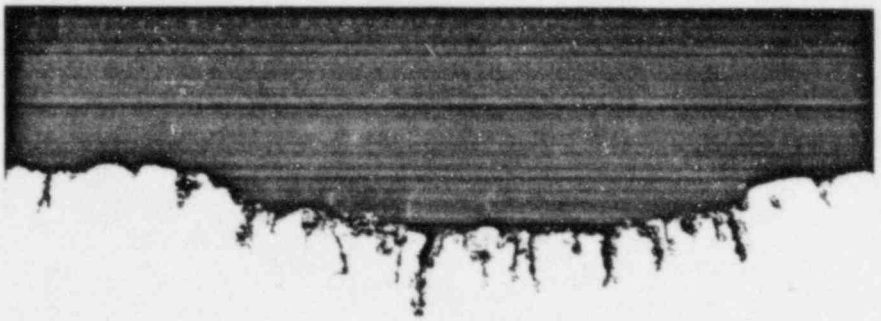

100X OM655

a. Photomicrograph of gauge section of specimen.

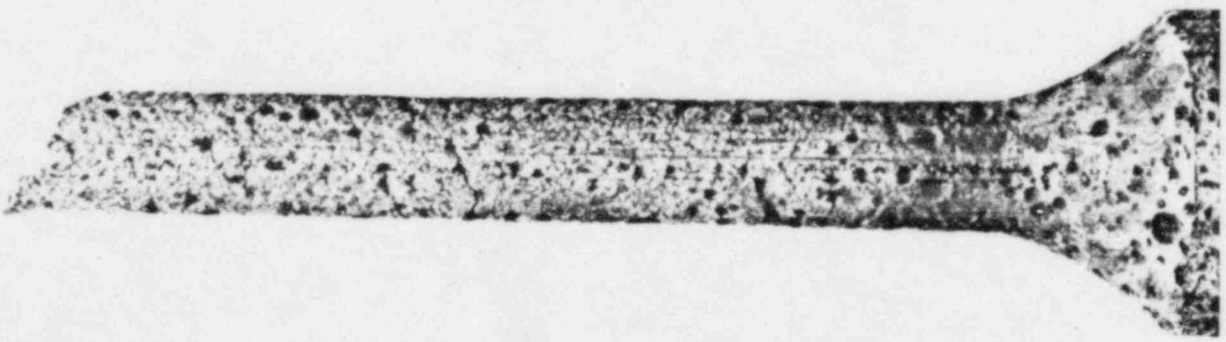

7X OM571

b. Low-power photograph of gauge section of specimen.

Figure 3.6. Optical photographs of hot-rolled 1020 carbon steel specimen following slow strain rate testing at 150 C in aqueous 5×10^{-4} M $FeCl_3$ at a strain rate of 1×10^{-7} sec^{-1}.

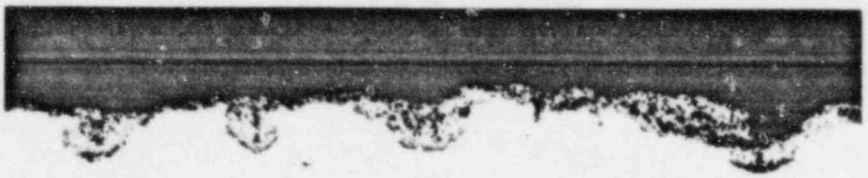

100X OM911

a. Photomicrograph of gauge section

10X OM908

b. Low-power photograph of gauge section of specimen.

Figure 3.7. Optical photographs of hot-rolled 1020 carbon steel specimen following slow strain rate testing at 125 C in aqueous 5×10^{-4} M $FeCl_3$ at a strain rate of 1×10^{-7} sec^{-1}.

Accordingly, experiments were undertaken to characterize the pit-propagation behavior of carbon steel in simulated basalt-repository environments. Two types of experiments are being performed: long-term exposures of "prepitted" specimens, and electrochemical pit-propagation experiments. The objective of these experiments is to characterize the pit-propagation behavior of carbon steel and to develop an understanding of the mechanism of pitting attack. Results of these experiments are discussed below.

3.3.1 Exposures of Prepitted Specimens

Simulated pits of various depths and aspect ratios (depth/diameter ratios) were drilled in specimens of hot-rolled 1018 carbon steel and are being exposed at 90 C in deaerated and in oxygenated basalt groundwater. The steel used in this study was commercially obtained, and its composition is given in Table 3.1. Prior to exposure, the depths of the pits were measured with a micrometer having a thin needle point. After exposure, the specimens are metallographically sectioned so that the morphology and depth of attack can be studied.

Four different pit diameters are being examined: 5.1 mm (0.2 inch), 2.54 mm (0.10 inch), 1.35 mm (0.05 inch), and 0.53 mm (0.021 inch). For each diameter, there are three aspect ratios: 2:1, 5:1, and 10:1. Thus, for a 5.1-mm-diameter pit, the initial pit depths were 10 mm, 25 mm, and 50 mm. The overall specimen dimensions are approximately 40 mm long x 20 mm wide x 75 mm thick (in the dimension of the pit), and the specimens were machined from 7.6 cm (3 inches) x 15.2 cm (6 inches) strip steel.

Prior to exposure, the specimens were cleaned with acetone, each pit was filled with the simulated basalt groundwater[3.2] using a syringe, and the specimens were placed in high-density polyethylene vessels containing one inch of crushed basalt. In each vessel, an electrical connection was attached to one specimen for subsequent potential measurements. The basalt-groundwater solution was added and the vessels were sealed. The vessels were then placed in oil baths, Luggin probes were connected, and the flow of nitrogen or oxygen was started (for deaerated or aerated solutions, respectively).

During the first 2000 hours of exposure, aliquots of solution were taken periodically and the pH was analyzed. As reported in the Annual Report for Year Three, the pH of the solution in the oxygenated vessels increased from 9.8 to about 11.5 during the first 1000 hours of exposure and stabilized at this value over the second 1000 hour period. On the other hand, the pH of the deoxygenated solutions decreased from 9.8 to about 6.5 over the first 2000 hours of exposure. Periodic solution-pH analyses were discontinued after 2000 hours to prevent depleting the test solutions.

Corrosion potentials also are being measured periodically during the experiments. As reported in the last Annual Report, the potential of

the specimens in the deoxygenated solutions have been stable during the experiments at values between -700 and -750 mV SCE. However, the potentials of the specimens in the oxygenated solution increased from -750 mV SCE to about -200 mV SCE after about 600 hours of exposure and have stabilized at approximately this value.

Specimens were removed from the oxygenated and deoxygenated solutions and examined following four months of exposure, and results of the examination were presented in the last Annual Report. During the past quarter, specimens were removed following approximately 8 months of exposure.

The specimens removed from the oxygenated solution were optically examined, metallographically sectioned, and then reexamined. The specimens were found to be covered with relatively thin, adherent black oxides with some evidence of red rust and patches on the surface where the corrosion product layer was somewhat thicker; see Figure 3.8.

Results of the metallographic examination of the specimens indicated that the simulated pits did not act as sites of initiation of localized corrosion. Based on surface profiles and oxide thicknesses, the attack within the pits did not appear to be significantly greater than on the free surfaces. Moreover, there was no evidence that the severity of attack could be correlated with pit depth or diameter. A photograph of simulated pits from one specimen are shown in Figure 3.9.

There was considerably more evidence of corrosion on these specimens than on the oxygenated specimens removed after 120 days. Patches of localized attack were evident on the boldly exposed surfaces of the specimens, and these patches were associated with the presence of the thicker deposits; see Figure 3.10. There was also evidence that this localized attack followed stringers or other microstructural features in the metal in some cases; see Figure 3.11. An approximate corrosion rate for these areas (245 μm/yr) was calculated based on the change in surface profile. Actual rates were somewhat higher since some uniform attack on the free surface had occurred.

3.3.2 Electrochemical Pit-Propagation Experiments

A schematic of the pit-propagation monitor is shown in Figure 3.12. Experimentally, the monitor is positioned vertically in a test cell containing an electrolyte, and the current flow between the base of the simulated pit and the boldly exposed surface is monitored as a function of exposure time. Current measurements provide an estimation of the rate of pit propagation, where shifts in the electrochemical potential of the pit base, as a result of the couple, are greater than about 50 mV. For potential shifts less than this value, the rate measured may be somewhat non-conservative since the reduction reactions occurring on the pit base will contribute to pit propagation but will not be detected.

1X 1M949

Figure 3.8. Low-power optical photograph of prepitted specimens of 1018 carbon steel following exposure in oxygenated basalt groundwater at 90 C for 238 days.

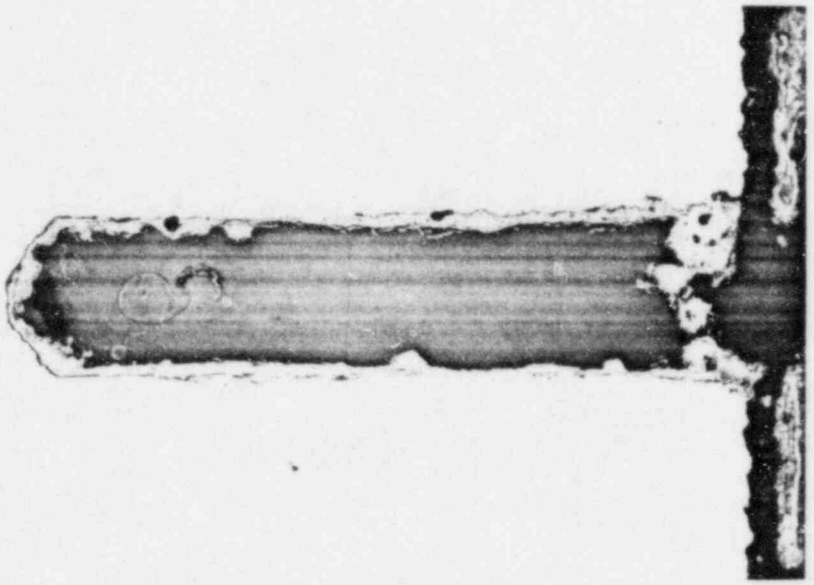

40X 2M063

a. 5:1-Aspect-Ratio Pit

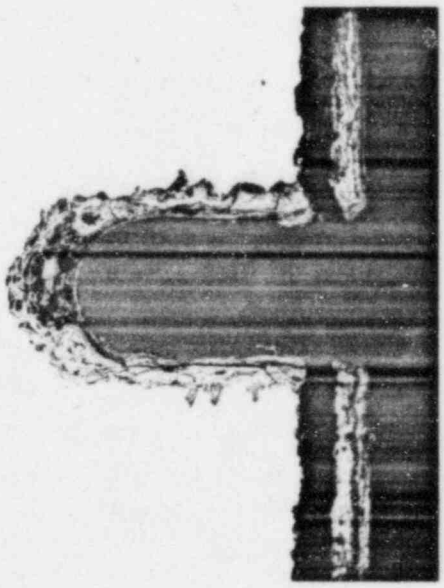

40X 2M062

b. 2:1-Aspect-Ratio Pit

Figure 3.9. Optical photographs of metallographic sections of prepitted specimen (0.53-mm diameter pits) of hot-rolled 1018 carbon steel following exposure in oxygenated simulated basalt groundwater containing crushed basalt for 238 days (5712 hours).

100X

2M060
2M061

Figure 3.10. Optical photographs of boldly exposed surface of specimen in Figure 3.9, showing evidence of localized attack.

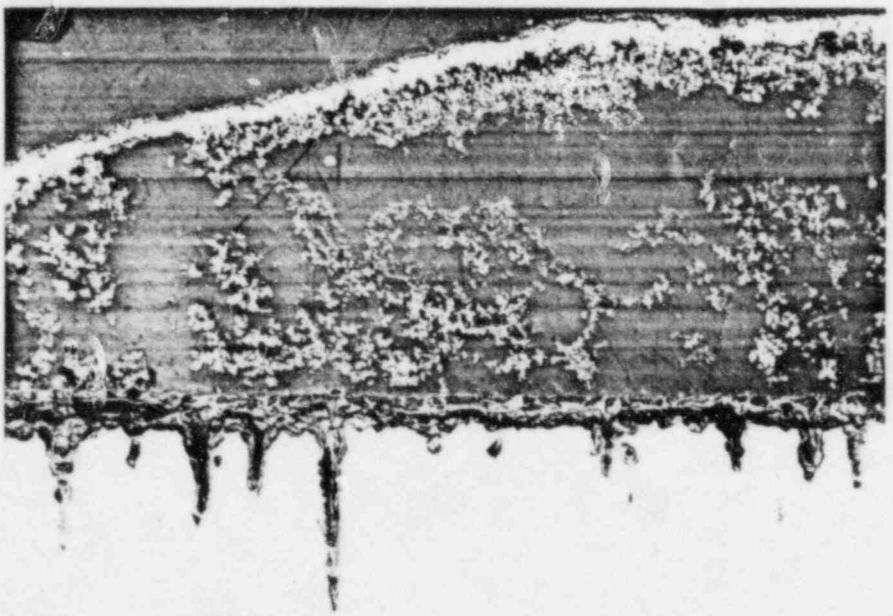

50X 1M938

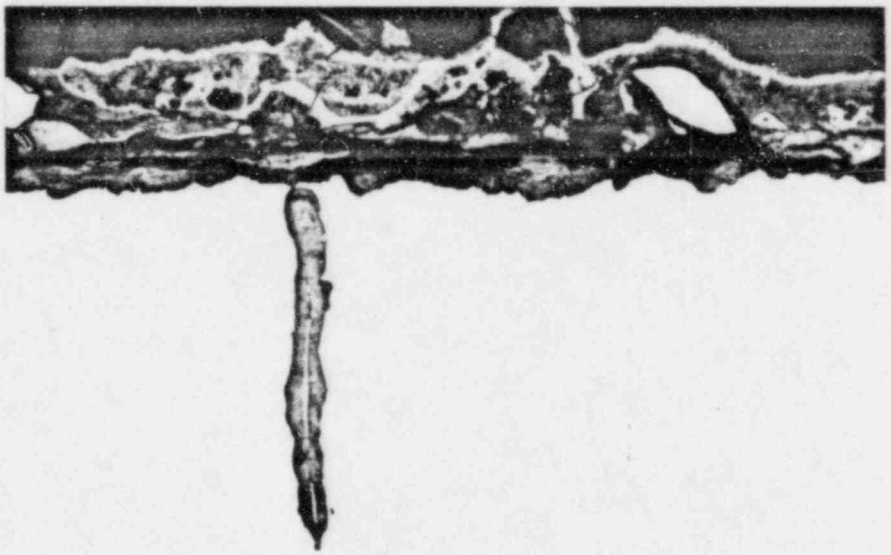

200X 1M944

Figure 3.11. Optical photographs of specimen in Figure 3.8, showing evidence of attack of stringers (elongated inclusions) beneath deposits on the boldly exposed surface.

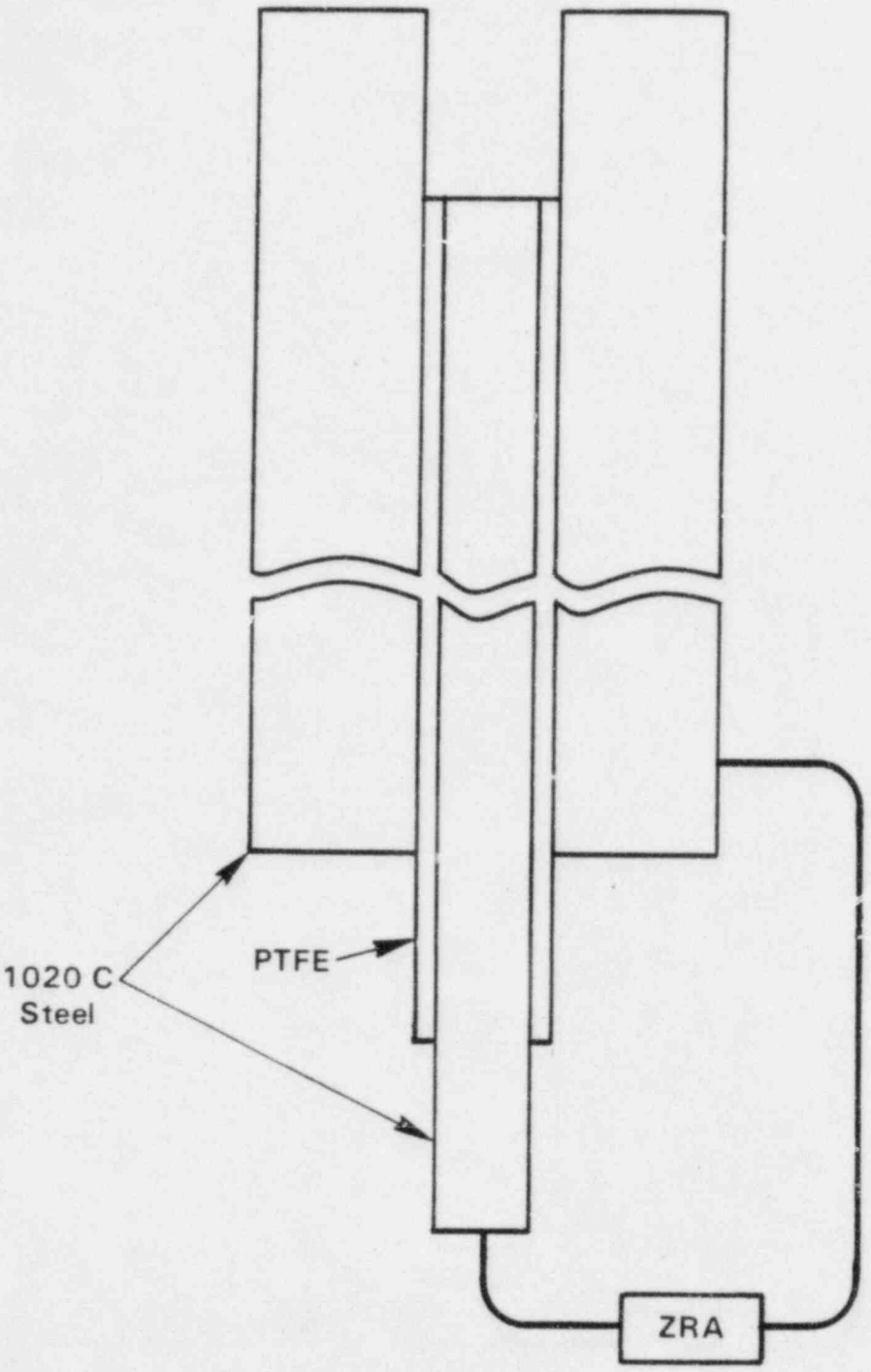

ZRA = Zero Resistance Ammeter

Figure 3.12. Schematic of pit-propagation monitor.

A standard procedure was developed last year to initiate pitting with the monitor. This procedure consisted of (1) pre-packing the simulated pit with a paste prepared with basalt groundwater and Fe_3O_4; (2) deaerating the test solution for 24 hours to fully deaerate the pit, during which time the simulated pit and boldly exposed surfaces are not coupled; and (3) aerating the test solution and coupling the simulated pit and boldly exposed surface through the zero-resistence ammeter (ZRA).

Double-walled PYREX* cells are used in the experiments so that the temperature can be controled by flowing a heat-transfer solution in the annular region between the inner and outer walls. The cells consist of (1) a counter-electrode cell containing a platinum electrode for potentiodynamic or potentiostatic measurements, (2) a reference-electrode cell containing standard calomel electrode (SCE) for electrochemical potential measurements, (3) a platinum wire for Eh measurements, (4) a frit bubble for deaeration or aeration of the solution, and (5) provisions for refreshing the solution continuously. Prior to the test, the specimens are cleaned with acetone and assembled, and the simulated pits are packed with a paste as previously described. The specimens are then inserted in the cell, the test solution is added, and the experiment is started. During the course of the experiment, couple potentials, Eh, temperature, and galvanic current flow are continuously monitored and recorded with a data acquisition system. Solution and gas flow rates are continuously monitored and maintained at 40 cc/hour and 10 cc/min, respectively.

During Year Three, it was found that the simulated pits passivated during the course of the experiments when they were packed with a basalt groundwater-Fe_3O_4 paste. It was thought that this passivation led to non-conservative estimates of the rate of pit propagation; accordingly, experiments were carried out this past quarter in an attempt to activate the pits.

Two experiments were conducted using 4.25-mm-diameter pits with an aspect ratio of 5:1 in simulated basalt groundwater at 75 C. In these experiments, one pit was packed with a paste of Fe_3O_4 and 0.1 N HCl, while the other was packed with a 0.01 N HCl-Fe_3O_4 paste. These tests were performed to simulate the low-pH conditions that are thought to develop within pits and, in so doing, to obtain active pitting and conservative estimates of pit-propagation rates.

Results of the current measurements for the two simulated pits are given in Figures 3.13 and 3.14; air flow and the current measurements were initiated simultaneously after 24 hours of nitrogen sparging. These data indicate that, as in the previous experiments, the pitting current values were very low and fluctuated considerably during the exposure

---

*PYREX is a registered trademark of Corning Glass Works.

period. In some cases, currents actually became negative. Results of the potential measurements are given in Figures 3.15 and 3.16. These data show that the coupled potentials for the two experiments were similar. Prior to aeration, the potentials were approximately -650 mV SCE, and a noble shift of 100 to 150 mV occurred when air sparging was started. Over the next few hours, the potentials for the two cells moved in the active (negative) direction and fluctuated between -550 mV and -600 mV SCE over the remainder of the test. A slight active shift occurred after 140 to 160 hours as a result of a decrease in the airflow rate, which occurred over a weekend when the air tank was depleted.

After one week of exposure, potentiodynamic polarization curves were obtained for the pits; the results are given in Figure 3.17 and 3.18. These data show that the pit packed with the 0.01 N HCl-Fe_3O_4 paste exhibited passive behavior with significant hysteresis on the reverse scan, indicating initiation of localized attack on the pit base. Similar behavior was observed and reported last quarter for the pits which were packed with a basalt groundwater-Fe_3O_4 paste. On the other hand, the pit that was packed with the 0.1 N HCl-Fe_3O_4 paste exhibited active behavior with no evidence of passivation. The latter behavior is similar to that expected for an actively corroding pit. The fact that the ZRA currents for the two pits were similar suggests that the absence of pit activation was not responsible for the low currents measured.

The free-corrosion potentials estimated from the potentiodynamic polarization curves were -575 mV SCE for the .01 N HCl-packed pit and -540 mV SCE for the 0.1 N HCl-packed pit. These values are nearly identical to the terminal values recorded for the coupled potentials, -572 and -542 mV SCE, respectively.

A standard procedure for determining the value of the corrosion rate at the free-corrosion potential is to extrapolate the linear Tafel region of the polarization curve to the free-corrosion potential. This analysis of the polarization curves indicates corrosion rates (currents) of about 3×10^{-4} A/cm^2 for the 0.1 N HCl-packed pit and 3×10^{-5} A/cm^2 for the 0.01 N HCl-packed pit. These values are two orders and one order of magnitude, respectively, higher than the corrosion currents estimated from the ZRA measurements. These observations, together with the electrochemical potential data which indicate that the coupled potentials were very close to the free-corrosion potentials for the pit bases, suggest that the reduction reactions occurring within the pit are the primary contributors to the corrosion attack of the pit base.

Next quarter, experiments will be performed to test the hypothesis that reduction reactions are responsible for pit-base corrosion. First of all, the last few tests will be repeated, with the addition of careful weight-loss measurements on the pit bases. These measurements were not performed in the previous experiments because the polarization experiments performed on the pits subsequently invalidated any weight loss data that could have been obtained. A matrix of long-term exposure tests also will be performed next quarter in which the relationship

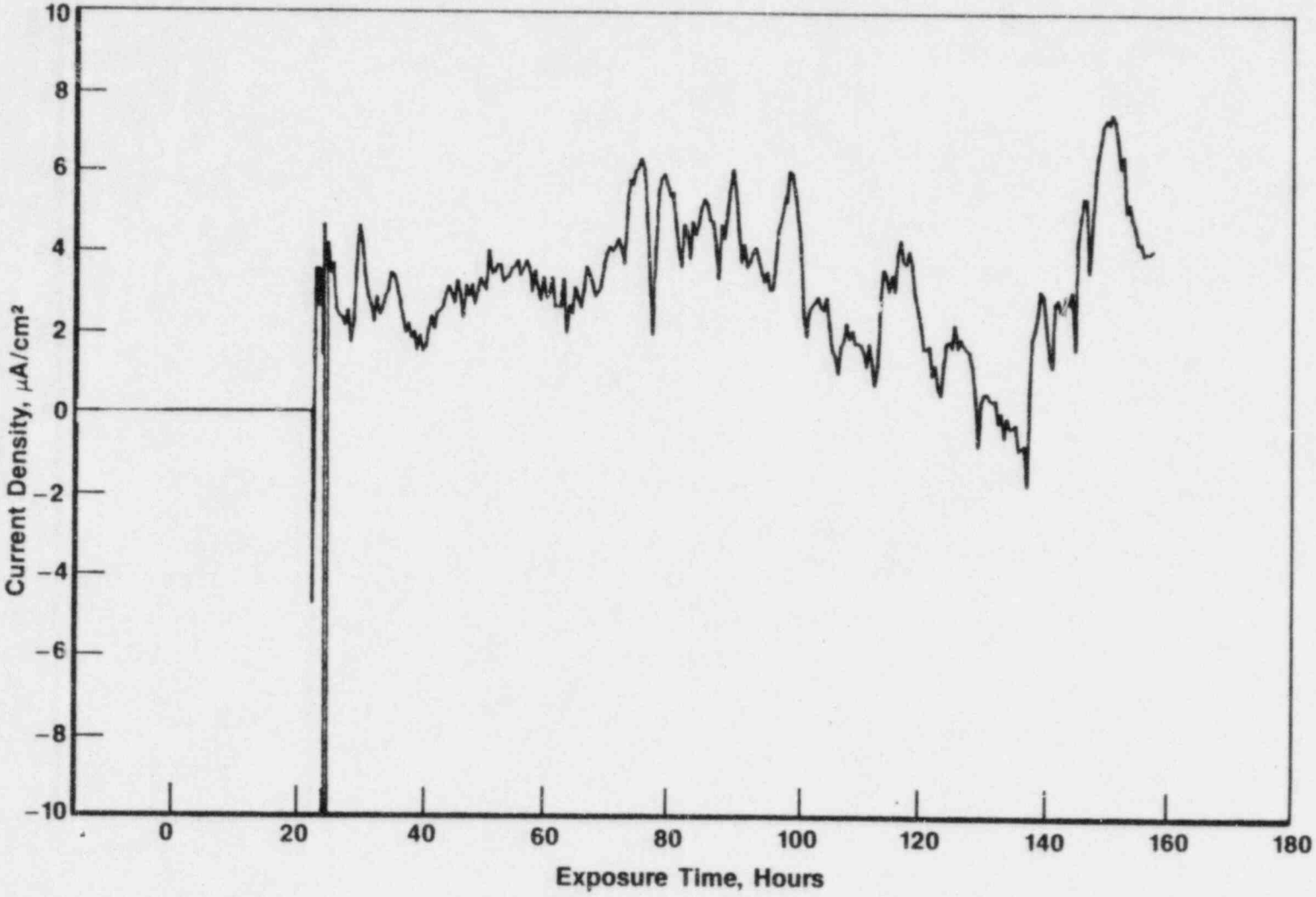

Figure 3.13. Current density as a function of exposure time for pit-propagation experiment performed at an aspect ratio of 1:5 in aerated basalt groundwater at 75 C with a 0.1 N HCl-Fe_3O_4 paste-packed pit.

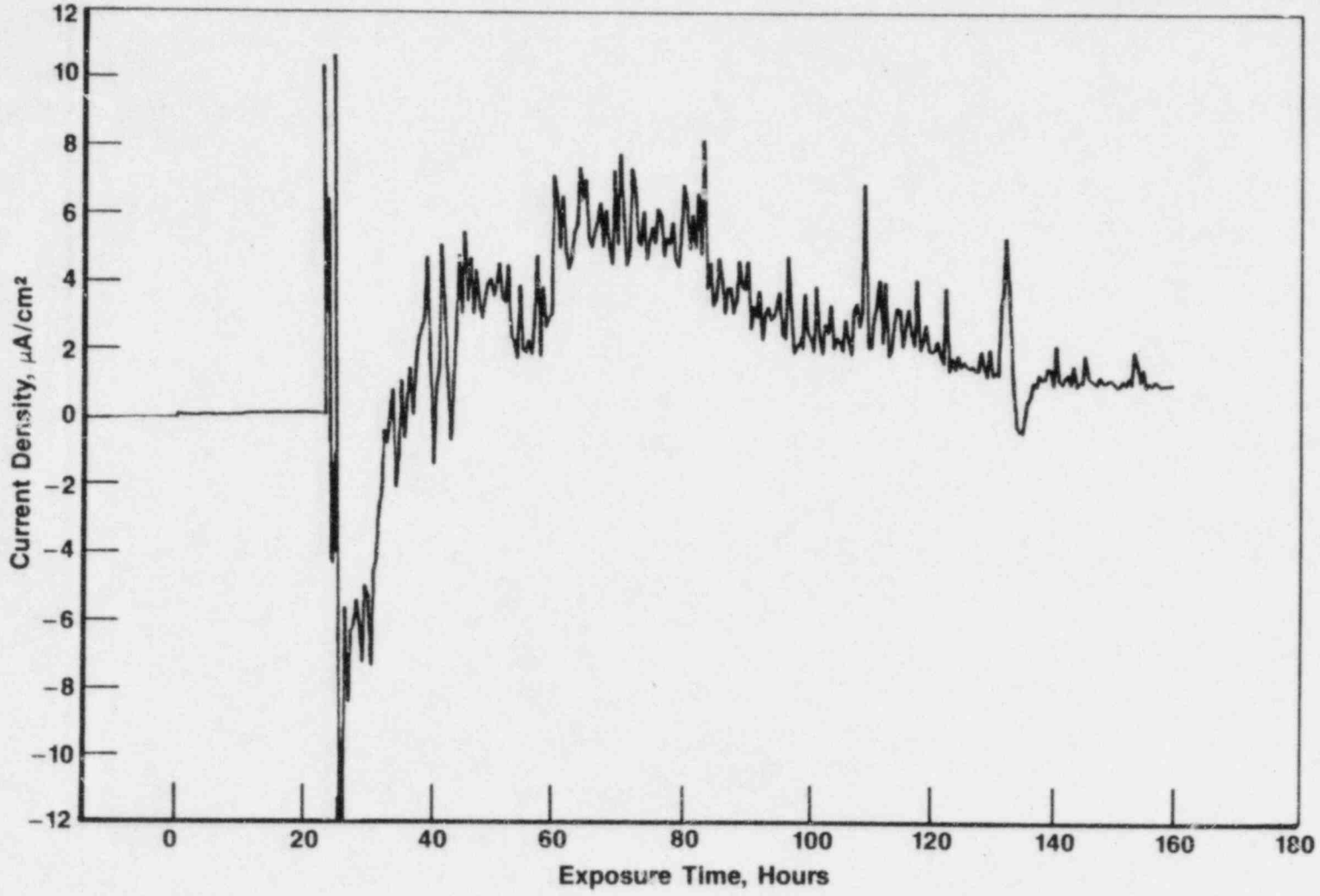

Figure 3.14. Current density as a function of exposure time for pit-propagation experiment performed at an aspect ratio of 1:5 in aerated basalt groundwater at 75 C with a 0.01 N HCl-FeO_4 paste-packed pit.

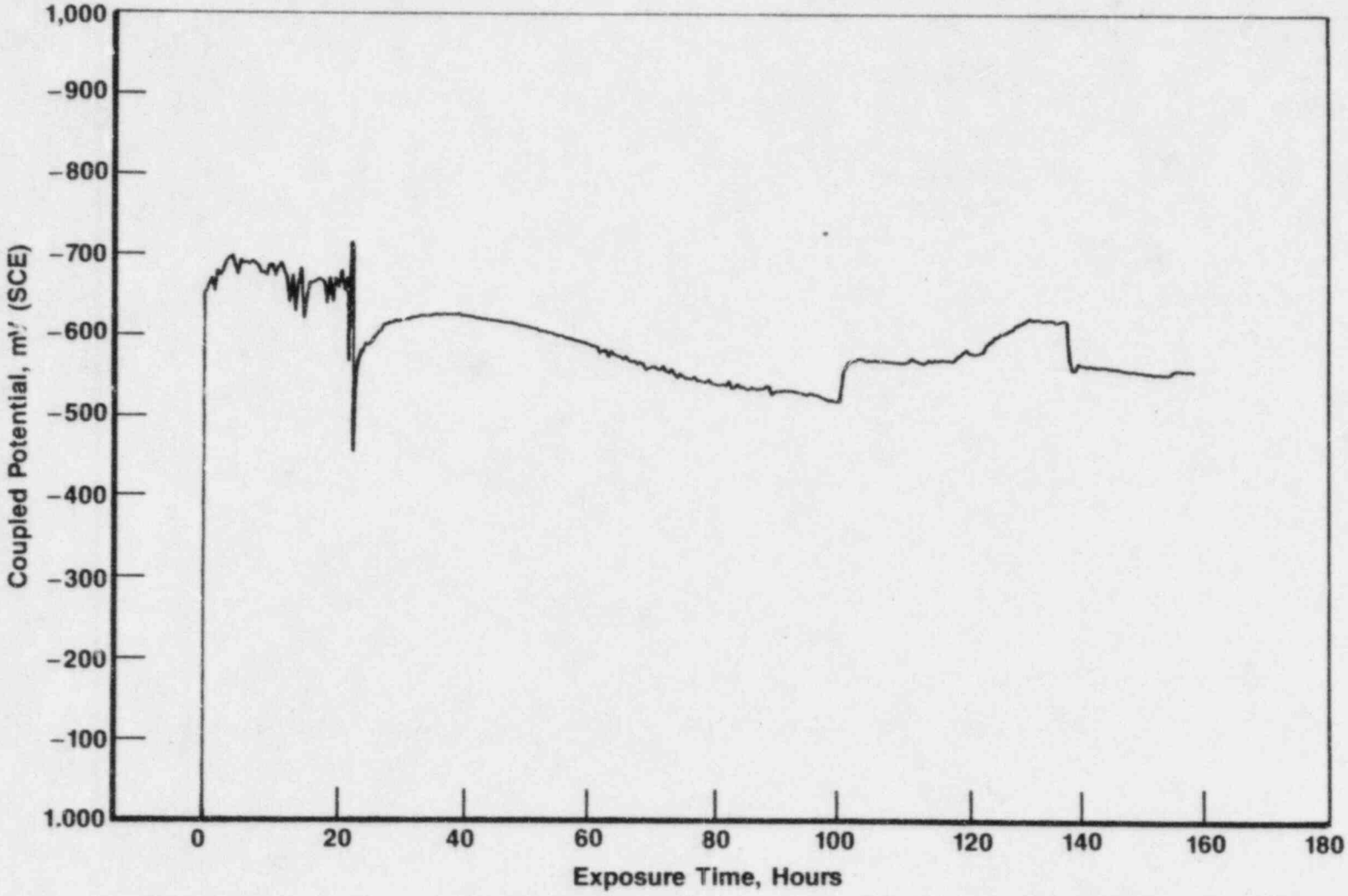

Figure 3.15. Electrochemical potential of the pit-boldly exposed surface couple as a function of exposure time for pit-propagation experiments performed at an aspect ratio of 1:5 in oxygenated basalt groundwater at 75 C with a 0.1 N HCl-Fe_3O_4 paste-packed pit.

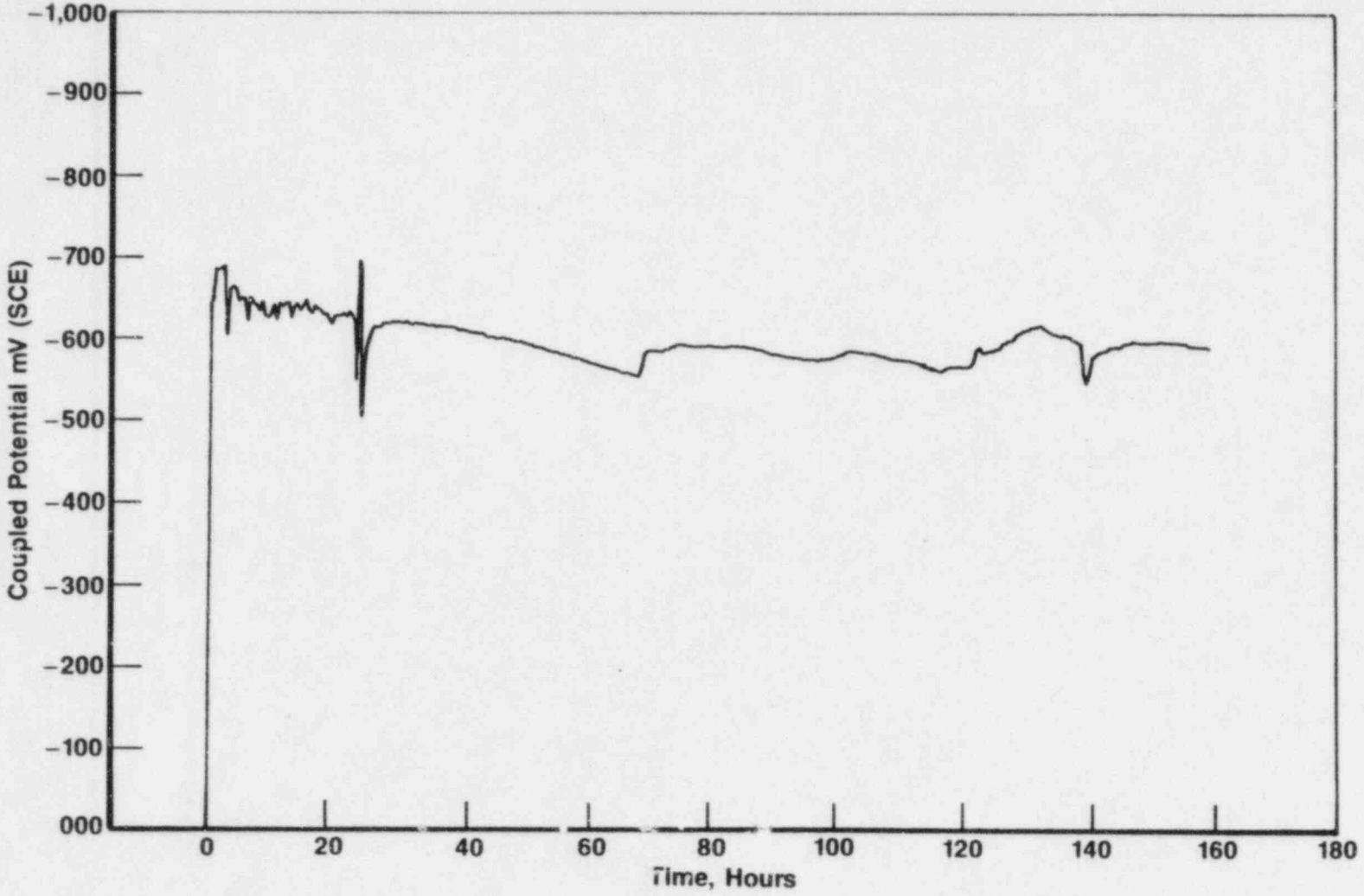

Figure 3.16. Electrochemical potential of the pit-boldly exposed surface couple as a function of exposure time for pit-propagation experiments performed at an aspect ratio of 1:5 in oxygenated basalt groundwater at 75 C with a 0.01 N HCl-Fe_3O_4 paste-packed pit.

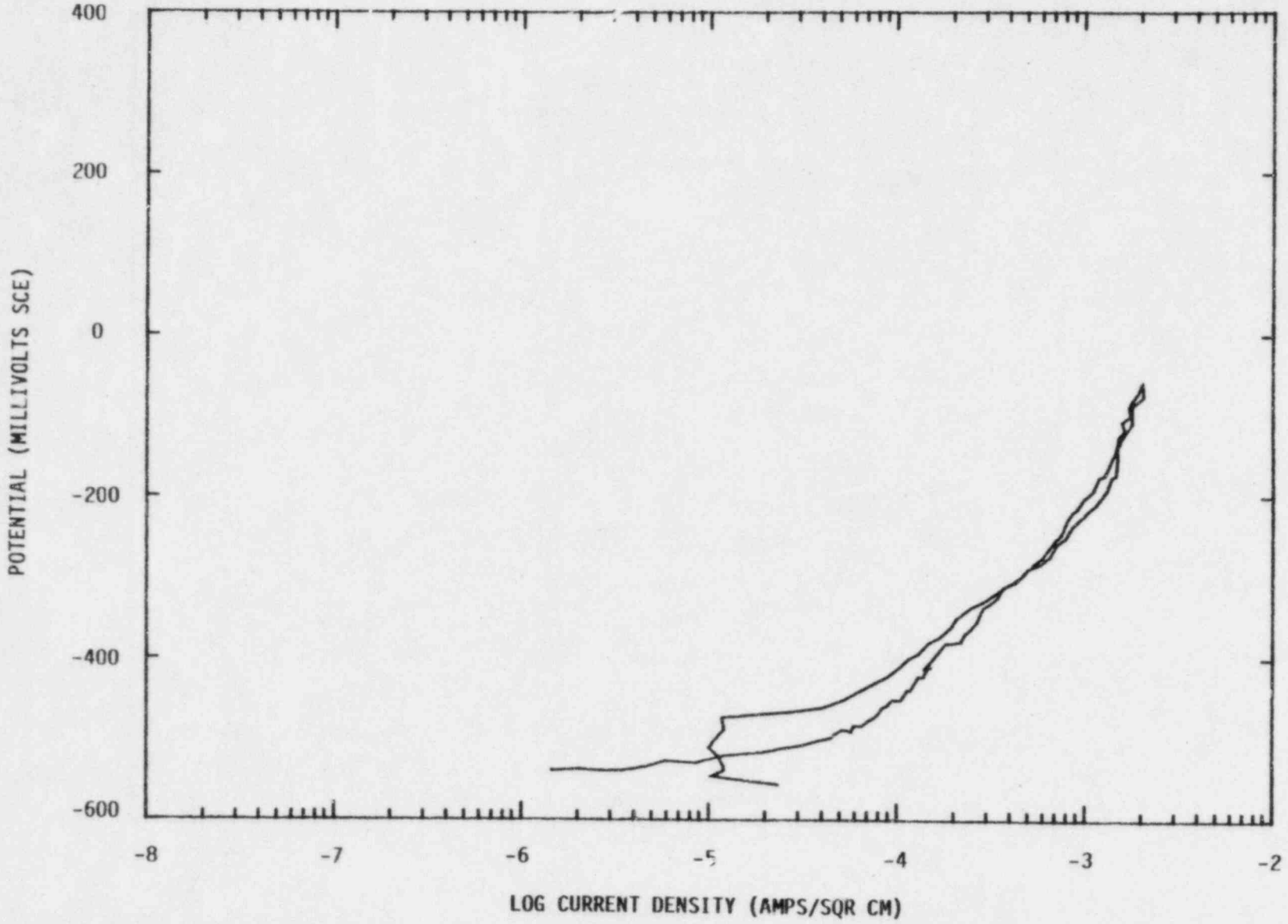

Figure 3.17. Potentiodynamic polarization curve for 1:5-aspect-ratio pit with 0.1 N HCl-Fe_3O_4 paste packing in aerated basalt groundwater at 75 C following one-week exposure; scan rate is 0.6V/hr.

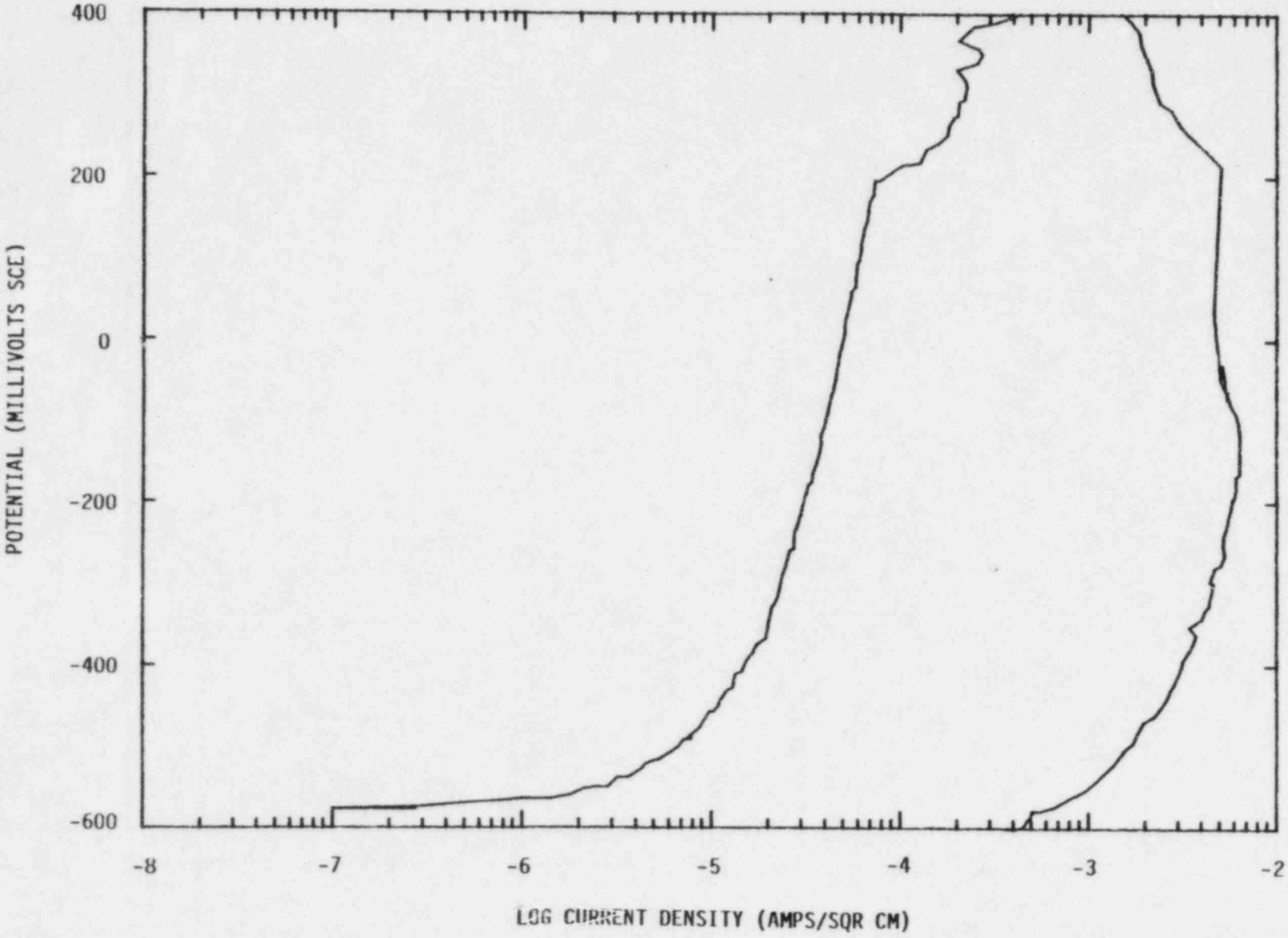

Figure 3.18. Potentiodynamic polarization curve for 1:5-aspect-ratio pit with 0.01 N HCl-Fe_3O_4 paste packing in aerated basalt groundwater at 75 C following one-week exposure; scan rate is 0.6V/hr.

between weight loss and parameters such as pit geometry, the pH of the paste used to pack the pits, and aeration are evaluated.

3.4 Corrosion Correlations

The objective of the corrosion-modeling effort is to provide information about corrosion processes that will affect overpack materials in a repository environment. Models under development deal with general corrosion, pitting corrosion, and mechanical degradation.

3.4.1 General Corrosion

By the end of Year Three, a comprehensive model for the kinetics of general corrosion of waste-package overpack materials had been developed[3.3]. The following major features were incorporated in this model:

- Transport of chemical species (assumed for the present to be electrically neutral) from the surrounding groundwater to the overpack surface by chemical diffusion
- Radiolytic production of chemical species within the groundwater, including such effects as temporal and spatial variations of the gamma-ray field, the latter being caused by geometric spreading of the gamma field and by gamma absorption within the groundwater
- Homogeneous chemical reactions between chemical species within the groundwater
- Kinetics of oxide-film growth on the metal surface.

To facilitate modeling, only very idealized groundwater compositions have been considered to date, e.g., groundwaters containing one oxidizing and one reducing species.

A major goal for Year Four is to expand the model to account for groundwater compositions that more realistically characterize the potential repository environment near the waste package. To this end, efforts were devoted during the past quarter to describing a groundwater-radiolysis model that would satisfy the requirements of (1) not being exceedingly complex but (2) providing a realistic description of the major features of the radiolysis process. The first requirement is important to keep the corrosion model as simple as practical. Such simplicity is desirable in order to interpret results from the model with relative ease, thereby minimizing the effort and expense in constructing and operating the numerical model and avoiding potential problems associated with obtaining reaction-rate data.

One radiolysis model that has been suggested* for use is as follows:

$$H_2O \xrightarrow{\gamma} H + OH$$

$$H + H \rightarrow H_2$$

$$OH + OH \rightarrow H_2O_2$$

$$H_2O_2 \rightarrow H_2O + 1/2\ O_2 \quad .$$

This model is being evaluated. If it is found to represent a physically reasonable summary of the radiolysis process, it will be incorporated into the corrosion model. Of course, subsequent extensions or alterations to the radiolysis description will be considered as required. The radiolysis model (including any modifications that may be required) will be included in the overall general-corrosion model during the next quarter.

3.4.2 Pitting Corrosion

3.4.2.1 Pit-Generation Kinetics

To describe the kinetics of pit generation on a waste-package overpack surface, it was suggested[3.4] that the most profitable approach would be to use an existing model[3.5] for the pitting induction time at an "average" site and then use essentially empirical techniques to account for a statistical distribution of induction times about that site. More recently, the problem of selecting a statistical distribution that would reasonably describe gross features of pit-generation kinetics was discussed[3.6]. It was suggested that the Weibull distribution, which has long been used to describe statistically based materials phenomena, would be adequate for this purpose.

The importance of knowing the time-dependent pit-generation rate has been shown[3.4,3.7] to result from the fact that the time-dependent pit-depth distribution function is intimately related to the pit-generation rate. The pit-depth distribution provides a direct measure of the pitting damage to a metal surface. Knowing the pit-generation rate and the growth kinetics of any given pit would be sufficient to predict the evolution of the pit-depth distribution with time. The general subject of extracting quantitative information regarding pit-generation rates from other measured properties of pit distribution was considered during the past quarter.

---

*Personal communication by Digby D. Macdonald (Consultant), Menlo Park, California.

Because of the relationship that exists between the pit-depth frequency distribution, f(h,t), and the pit-generation rate, G(t), the form of G(t) could be estimated by deriving G(t) information directly from f(h,t). Here f(h,t) is defined such that f(h,t) dh is the pit concentration on the metal surface at time t, having a depth within the interval h to h + dh. G(t) is then the rate at which pits are generated per unit area of surface.

The simplest way to deduce the relationships between f(h,t) and G(t) is to regard individual pits as being "points" in a one-dimensional "pit-depth" space. As a given pit grows, its characteristic "point" moves along the one-dimensional space in the direction of increasing h. The "flux", then, of such points crossing a given, fixed value of h at time t must be equal to the rate at which those particular pits were generated at the time they were generated. This statement can be expressed mathematically as follows, assuming that the rate, v, of increasing pit size with time is an explicit function of h only:

$$v(h)f(h,t) = G\,t - \int_0^h \frac{dh}{v(h)} \quad . \tag{3-1}$$

If pitting is assumed to begin at time t=0, then Equation 3-1 is valid only for those values of h for which the argument of the G function is greater than zero. For larger h values, f(h,t)=0 since no pits have yet grown to these larger sizes. Thus, if v(h) is known, e.g., by direct measurement of pit-growth kinetics for individual pits, and if f(h,t) is measured at a given time t, then G(t), for times up to the given value, t, can be estimated through appropriate application of Equation 3-1.

Deducing nucleation (or generation) rates from other measured properties of a system is actually more generic than just this application to pitting corrosion. Moreover, the subject has been of interest for many years and is still under investigation. For example, more than four decades ago Hull, et al,[3.8] described a method analogous to Equation 3-1 for calculating the nucleation rate of pearlite from austenite using size-distribution data. They considered the special case for which the growth rate of the pearlite species is independent of size.

These same authors[3.8] also reviewed another method which involved calculating the nucleation rate from measurements of the total concentration of pearlite species as a function of time. Indeed, an approach analogous to the latter has recently been suggested by Janik-Czachor and Ives[3.7] for determining pit-generation rates. With this method, the instantaneous pit concentration on a surface, n(t), is measured experimentally and related to G(t) through the expression

$$G(t) = dn(t)/dt \quad . \tag{3-2}$$

Equation 3-2 would have to be modified as the area fraction of the container surface covered by pits becomes appreciable. An analogous modification that was included in the treatment of Hull, et al,[3.8] applied to pearlite.

The general problem of estimating nucleation and species growth rates from measurements of more "global" properties continues to be a problem of interest, e.g., in the recent work of Gokhale and Dehof[3.9]. Regarding pitting kinetics, it appears that sufficient information relative to pit-generation kinetics can be obtained from measurements of related quantities to provide a satisfactory description of gross properties of pit-generation kinetics.

3.4.2.2 Pit-Growth Kinetics

Preliminary steps have been taken to extend the simple pit-growth model that was developed at an earlier stage of this program[3.10] based on the well-known binary-electrolyte theory. Two areas currently being investigated for incorporation into the model are (1) inclusion of film-growth kinetics at the pit base and (2) consideration of the effects of radiolytically produced species on pit-growth kinetics. Substantial progress in these areas is expected over the next quarter.

3.4.3 Mechanical Degradation

As a part of the corrosion studies, work is continuing toward identifying parameters that could influence the stress-corrosion cracking behavior of low-carbon steel overpack material to be used in nuclear waste disposal. Some environmental factors that have been identified[3.11] as having an important effect are water chemistry, temperature, water-flow rate, the Eh and pH of the solution, and radiolysis of the groundwater.

At present, activity is focused on identifying the mechanical stress that the overpack will be exposed to during its manufacture and subsequent service conditions. This study will aid in determining whether stress levels can be expected that, in combination with expected environmental conditions, would cause stress-corrosion cracking of the overpack.

Residual stresses from the fabrication process could play an important role in determining the stress state of the container. As such, the process used to manufacture the overpack should be optimized to minimize these stresses in the material. In addition, thermal stresses, hydrostatic and lithostatic stresses, and internal pressure due to gas generation inside the overpack are expected during service. The influence of these stresses on the stress-corrosion performance of the material is being evaluated. These studies of the mechanical stresses will be completed during the next quarter.

3.5 JAERI-NRC Program Support

A significant portion of the overpack-corrosion effort during the past quarter was devoted to providing support for the JAERI-NRC joint program. This support consisted of designing and preparing a proposed experimental matrix, participating in the 2nd JAERI (Japan Atomic Energy Research Institute)/NRC Technical Group meeting in Japan, and providing follow up to the meeting. Two staff members from Battelle attended this meeting during the week of June 17, 1985.

The proposed experimental matrix consists of SSR experiments to evaluate the influence of a radiation field on SCC of carbon steel in simulated basalt repository environments. The proposed SSR tests would be an extension of the work being performed at Battelle and would consist of tests in three environments with and without a radiation field: the standard basalt groundwater, an established cracking environment where the radiation field may move the electrochemical potential into the cracking range, and an environment where the radiation field may generate species that will promote SCC. The latter two environments will be selected on the basis of the results of the electrochemical task. As proposed, triplicate experiments would be run at 90 C in the environments under freely corroding conditions with no radiation field and in a radiation field of about 10^3 R/hour.

The objectives of the meeting in Japan were to finalize the experimental plan and identify the best location for carrying out the experiments. JAERI agreed to conduct experiments in a radiation field as part of the JAERI-NRC research agreement. They also agreed upon the matrix of experiments and a preliminary time schedule. However, the site location and the specific radiation source were not agreed upon, and the specific designs for the test rig, test cell, and specimens were not finalized. In addition, the type of carbon steel and environmental conditions for testing were not agreed upon. JAERI expressed interest in evaluating a Japanese steel and an appropriate simulated groundwater for a Japanese high-level waste repository. Inclusion of Japanese groundwaters or steels into the matrix is potentially problematic since this may require that electrochemical and SSR experiments be performed on these systems at Battelle.

Upon returning to Battelle, a report on the meetings was prepared and forwarded to NRC. In addition, meetings were held with Battelle personnel, and it was tentatively agreed that the ^{137}Cs source and facilities at the Tokai site will be adequate for performing the experiments. JAERI indicated that this is the most desirable site for them.

In the near future, Battelle will supply JAERI with information on the recommended test sample dimensions, cell dimensions, and cell design. During Fall, 1985, Battelle will supply JAERI with the desired test environment specifications and procedures for their preparation, test specimens, and detailed experimental procedures. It is anticipated that one or possibly two additional trips to Japan will be required to suc-

cessfully complete this task; one trip when the cold experiments start in January, 1986, and a second when the hot (irradiation) experiments start in mid-1986.

3.6 References for Section 3

(3.1) "Long-Term Performance of Materials Used for High-Level Waste Packaging", D. Stahl and N. E. Miller (Compilers), NUREG/CR-3900, Vol. 4, BMI-2127 (July 1985), pp. 3-14 ff.

(3.2) T. E. Jones, "Reference Material Chemistry--Synthetic Groundwater Formulation", RHO-BW-ST-37P (April, 1982).

(3.3) "Long-Term Performance of Materials Used for High-Level Waste Packaging", D. Stahl and N. E. Miller (Compilers), NUREG/CR-3900, Vol. 4, BMI-2127 (July 1985), pp. 3-79 ff.

(3.4) "Long-Term Performance of Materials Used for High-Level Waste Packaging", D. Stahl and N. E. Miller (Compilers), NUREG/CR-3427, Vol. 4, BMI-2113 (June 1984), Section 3.4.2.1, pp. 3-121 ff.

(3.5) L. F. Lin, C. Y. Chao, and D. D. Macdonald, J. Electrochem. Soc., 128 (1981) 1194.

(3.6) "Long-Term Performance of Materials Used for High-Level Waste Packaging", D. Stahl and N. E. Miller (Compiler), NUREG/CR-3900, Vol. 4, BMI-2127 (July, 1984), pp. 3-52 ff.

(3.7) M. Janik-Czachor and M. B. Ives, in Passivity of Metals, R. P. Frankenthal and J. Kruger (Editors), Electrochem. Soc. (Princeton, N. J., 1978), p. 369.

(3.8) F. C. Hull, R. A. Colton, and R. F. Mehl, Tans. Am. Inst. Mining Metall. Engrs., 150 (1942) 185.

(3.9) A. M. Gokhale and R. T. Dehoff, Metall Trans. A., 16A (1985) 559.

(3.10) "Long-Term Performance of Materials Used for High-Level Waste Packaging", D. Stahl and N. E. Miller (Compilers), NUREG/CR-3427, Vol. 4, BMI-2113 (June 1984), Section 3.4.2.2.2, pp. 3-126 ff.

(3.11) Long-Term Performance of Materials Used for High-Level Waste Packaging", D. Stahl and N. E. Miller (Compilers), NUREG/CR-3900, Vol. 4, BMI-2127 (July 1985), pp. 3-103 ff.

4. INTEGRATED SYSTEM PERFORMANCE

Studies in the integrated system performance task are designed to provide a better understanding of the phenomena that affect the long-term performance of waste packages at the system level. Knowledge gained in these studies will aid in assessing the adequacy of system-performance models for nuclear waste packages.

During the past quarter, emphasis has been placed on water-chemistry studies, the development of a mechanism for the radiolysis of solutions containing chloride and ferric species, analytical simulations of systems containing chloride species, assessments of simple models for groundwater radiolysis, and construction and further planning of the integral experiments.

The water-chemistry studies will improve our understanding of the local water chemistry in the vicinity of the waste package. This will provide information on how the corrosion of the metallic barriers and the dissolution of the waste form alters the local water chemistry. Such changes in the water chemistry in turn may affect these processes of corrosion and dissolution. The water-chemistry studies also will provide information on the chemical speciation of radionuclides released from the waste form. This information will be useful for assessing the transport rate of these radionuclides through the waste package.

The groundwater-radiolysis studies will provide information on the concentrations of the radiolytic species in the vicinity of the waste package. These species may affect both the corrosion of the metallic barriers and the chemical speciation of the radionuclides released from the waste form. Such phenomena can influence the expected containment period of for a waste package, as well as the release rate of radionuclides from the waste package to the repository environment after the containment is breached. These studies are also providing a means for assessing the adequacy of simplified groundwater-radiolysis models being considered for inclusion in the corrosion models under development in the container-materials task of the program.

The integral experiments are being assembled to provide a means of assessing the relative importance of various combined-effects processes that may affect the long-term performance of nuclear waste packages. These experiments will also provide information on the performance of spent-fuel waste forms in an environment approximating that of a potential repository. These experiments will also provide data which can be used to benchmark the radiolysis and water-chemistry models that are under development.

4.1 Water Chemistry

In addition to supporting work on waste-form dissolution, water-chemistry calculations during the past quarter demonstrated that the water-chemistry computer program does give results that are physically

reasonable. The results reported in this section were obtained with a 13-element water-chemistry program. The program is only slightly modified from the version used for calculating waste-form dissolution.

In Figures 4.1 and 4.2, pH is shown as a function of the molarity of KOH and HCl, respectively. As expected, the pH is constant at about 7.0 for very small concentrations of acid and base. For moderate concentrations, the pH varies linearly with the logarithm of the concentration, with a smooth transition to the constant value at low concentrations. For relatively high concentrations (about 0.01 M), close inspection of the pH curve shows that it deviates from linearity due to changes in the activity coefficients.

The calculations reported in Figures 4.3 and 4.4 are basically titration calculations. In Figure 4.3, pH is shown as a function of H_2SO_4 molarity in a solution of 0.01 M NaOH. This calculation differs from a standard titration only in that the NaOH does not become diluted as H_2SO_4 is added. The curve has the sigmoid shape characteristic of strong-acid/strong-base titrations. Since H_2SO_4 becomes doubly ionized in water, the endpoint is reached when the molarity of H_2SO_4 is one-half that of NaOH.

Figure 4.4 gives the results of a similar titration calculation, but here pH is a function of the NaOH molarity in a solution of 0.03 M H_2CO_3. The starting solution is near the solubility limit of CO_2 in water. The titration shows endpoints at 0.03 M and 0.06 M NaOH. The first endpoint corresponds to essentially complete consumption of H_2CO_3; the second corresponds to consumption of HCO_3^-.

4.2 Groundwater-Radiolysis Studies

Radiolysis of groundwater in the vicinity of the waste package can alter the local water chemistry, thereby affecting the long-term performance of waste packages. Effects on the local water chemistry can include changes in pH and oxygen potential, as well as the production of additional species which may have a deleterious effect on the waste-package materials. As reported previously, other investigators have observed that gamma radiation may adversely affect the time-to-failure performance measure for metal components exposed to water.(4.1)

One objective of these studies is to develop a generalized model for analyzing the radiolysis of unaltered groundwater systems and groundwater systems whose composition has been altered by the presence of other materials such as packing and corrosion products. This model will provide concentration estimates of radiolysis products near the metallic components of waste packages. This information will aid the container-materials task of the program in selecting appropriate solution compositions for the corrosion experiments. The model will also provide a means of assessing abbreviated groundwater-radiolysis models to be integrated into the general-corrosion model described in Section 3.4.

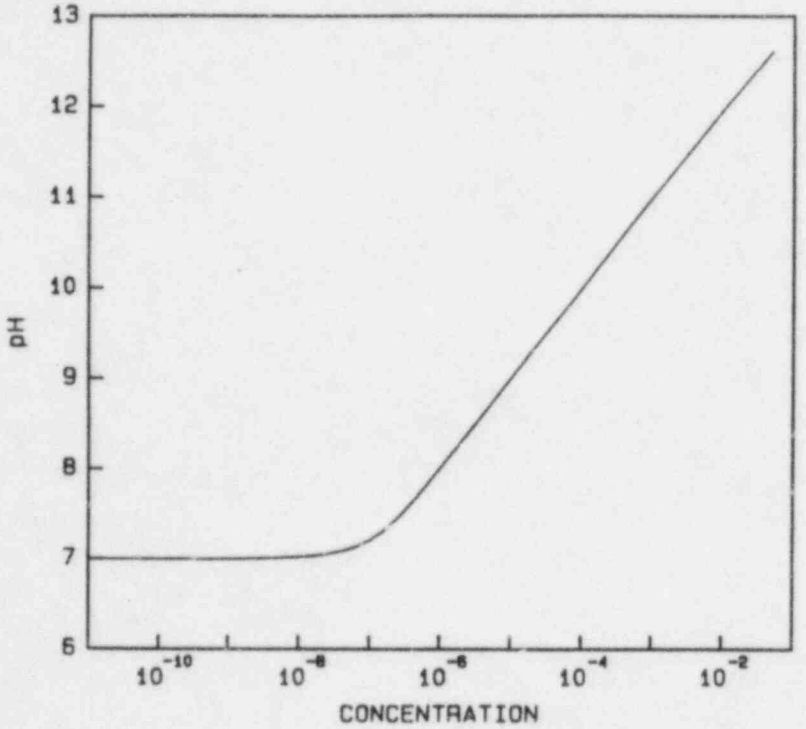

Figure 4.1. pH as a function of KOH molarity.

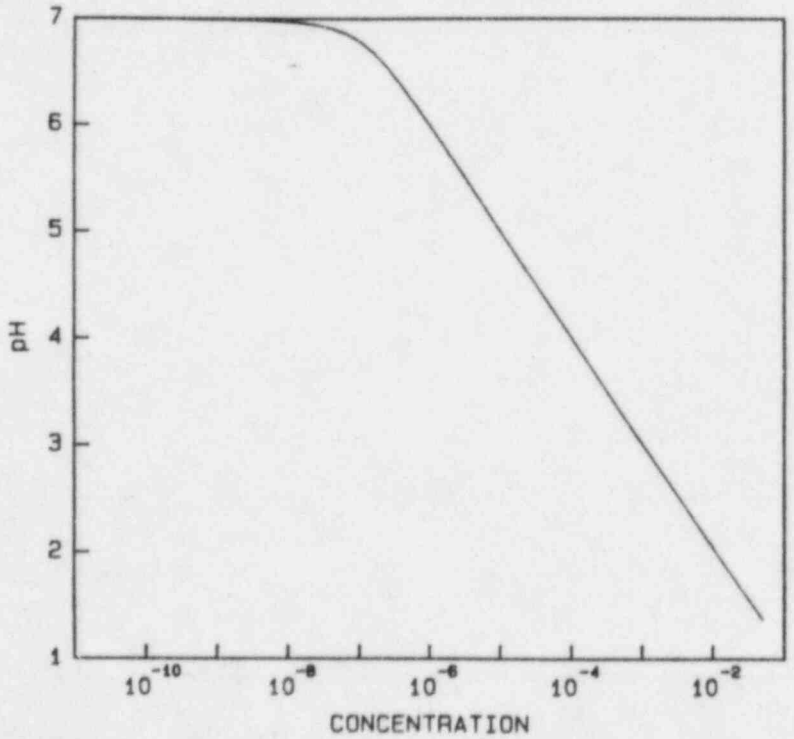

Figure 4.2. pH as a function of HCl molarity.

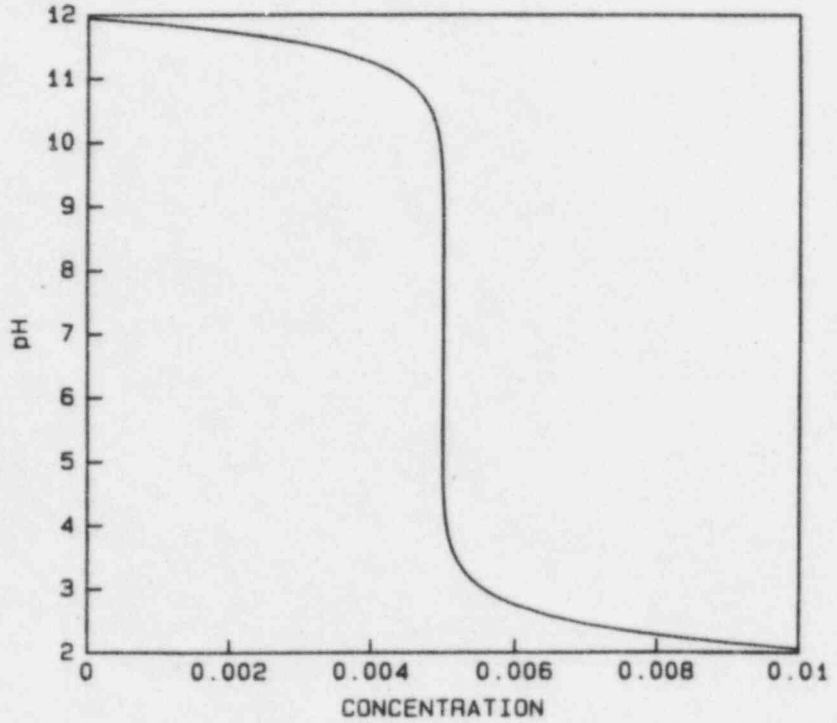

Figure 4.3. pH as a function of H_2SO_4 molarity in a solution of 0.01 M NaOH.

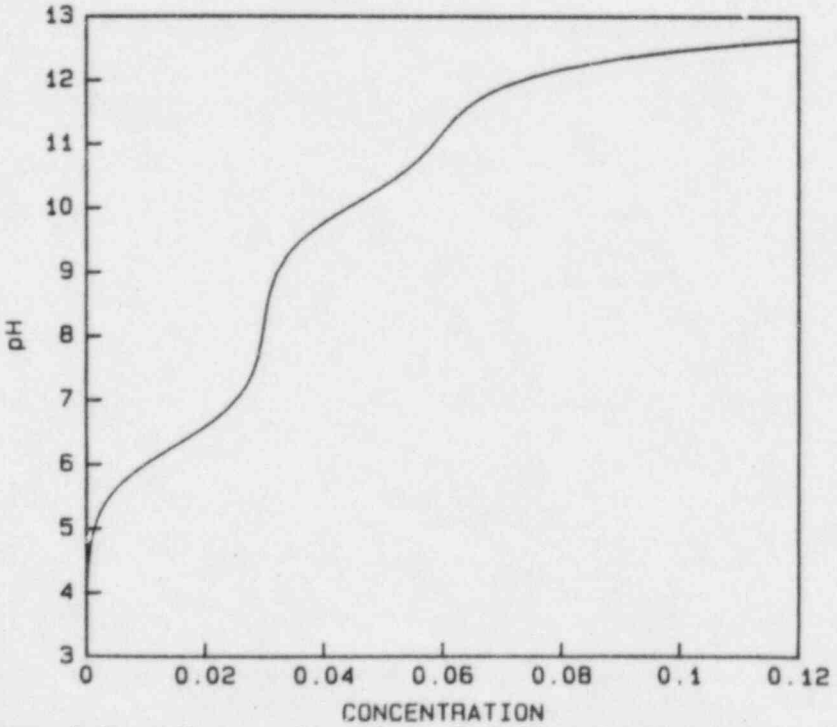

Figure 4.4. pH as a function of NaOH molarity in a solution of 0.03 M H_2CO_3.

In addition, the model will provide a vehicle for determining effective rate constants for reactions included in the water-radiolysis component of the corrosion model.

The approach taken in these studies was to first develop a description for the radiolysis of pure water which might contain hydrogen and/or oxygen. This description is being extended to account for anions and cations which may be present in significant amounts in groundwaters of interest. As the description of groundwater radiolysis is developed, it is being benchmarked against experimental data available from the literature. As part of this effort, gamma-energy deposition calculations were used to determine energy-deposition rates to groundwater and the materials surrounding the spent fuel and commercial high-level waste packages. Results of these calculations have been reported previously.(4.1) In these earlier studies, several mechanisms for the radiolysis of water were evaluated on the basis of their ability to predict the behavior of water-radiolysis experiments described in the literature. Of these, the mechanism presented by Rosinger and Dixon(4.2) was chosen as the basis for developing a generalized description of groundwater radiolysis.

Work this past quarter has been directed toward further developing the mechanism for the radiolysis of solution containing chloride species. Also, a simplified model for the radiolysis of groundwater was assessed. This model may become integrated into the general-corrosion model discussed in Section 3.4.

4.2.1 Radiolysis of Chloride Solutions

Last quarter, a mechanism for the radiolysis of aqueous chloride solutions was described. This mechanism consisted of ten elementary reactions which augment the mechanism for the radiolysis of groundwaters developed earlier in the program.(4.3) Although the mechanism accounted for the production of HOCl, it did not account for the reactivity of HOCl with other species. This past quarter, the mechanism for the radiolysis of aqueous solutions containing chlorides was extended to account for sources and sinks of HOCl and other species. The subset of reactions for describing the behavior of chloride species in the groundwater-radiolysis mechanism is shown in Table 4.1. In this table, Reactions 1 to 10 were reported last quarter.(4.3) Reactions 11 to 16 were added this past quarter and were taken from the literature. The rate constants for these reactions were reported in the literature and are shown in Table 4.2, along with their literature sources. The rate constant for Reaction 15 was assumed to be the same as that for the related bromine species shown in Reference 4.9. Reaction 11, which contains OCl^-, was added for completeness to allow for future expansion of the model. At present, this reaction has no effect on the calculated result since the model does not account for sources of OCl^-. Reactions 12 and 13 describe reaction pathways for HOCl, and Reaction 15 is an additional source reaction for HOCl. Reactions 14 to 16 describe the production and depletion of H_2OCl_2.

Table 4.1. Reactions to account for interactions between radiolytic and chloride species.

Reaction Identification Number	Reaction	Reference
1	$H + Cl^- \rightarrow HCl + e^-$	4.4
2	$e^- + HCl \rightarrow H + Cl^-$	4.4
3	$H + HCl \rightarrow Cl + H_2$	4.5
4	$OH + HCl \rightarrow H_2O + Cl$	4.6
5	$H_2 + Cl \rightarrow HCl + H$	4.7
6	$Cl + Cl \rightarrow Cl_2$	4.3
7	$H + Cl_2 \rightarrow Cl + HCl$	4.5
8	$OH + Cl_2 \rightarrow Cl + HOCl$	4.5
9	$OH + Cl_2 \rightarrow ClO + HCl$	4.5
10	$O + ClO \rightarrow Cl + O_2$	4.5
11	$H_2O_2 + OCl^- \rightarrow H_2O + Cl^- + O_2$	4.8
12	$HO_2^- + HOCl \rightarrow H_2O + Cl^- + O_2$	4.8
13	$HOCl + H^+ + Cl^- \rightarrow Cl_2 + H_2O$	4.8
14	$Cl_2 + H_2O \rightarrow H_2OCl_2$	4.8
15	$H_2OCl_2 \rightarrow HOCl + H^+ + Cl^-$	4.8
16	$H_2OCl_2 \rightarrow Cl_2 + H_2O$	4.8

Table 4.2. Rate constants for the reactions shown in Table 4.1.

Reaction	Rate Constant*	Reference
1	3.9×10^{8}	4.4
2	2.1×10^{9}	4.4
3	2.65×10^{7}	4.5
4	4.86×10^{8}	4.6
5	1.59×10^{3}	4.8
6	1×10^{10}	(estimated in Ref. 4.3)
7	1.2×10^{10}	4.5
8	4.04×10^{7}	4.5
9	1.04×10^{5}	4.5
10	3×10^{10}	4.5
11	3.4×10^{3}	4.8
12	4.4×10^{7}	4.8
13	1.8×10^{4}	4.8
14	11.0	4.9
15	5×10^{9}	(estimated from data in Ref. 4.9)
16	2×10^{9}	4.9

*Units are liter/mole-sec, except Reaction 13 which has units of $1^2/m^2$-sec and Reactions 15 and 16 which have units of sec^{-1}.

4.2.2 Simple Groundwater-Radiolysis Model

The general-corrosion modeling effort in the container-materials task requires a simple model describing the effects of radiation on water chemistry. A subroutine-type model (which can be programmed into a larger code) for water radiolysis is necessary to develop a tractable general-corrosion model. One possible water-radiolysis model is shown in Table 4.3. The first three reactions in this model are known elementary reactions with measured rate constants. The fourth reaction, however, is complex in that it proceeds in several steps. In exercising this model, the fourth reaction was used with a rate constant for a different H_2O_2 decomposition reaction which is used in the Battelle groundwater-radiolysis model. The model was first exercised using the set of four reactions shown in Table 4.3 and the rate constants taken from the Battelle model. This is referred to as Mechanism "A". Then, the fourth reaction was replaced with the reaction

$$H_2O_2 \rightarrow H^+ + HO_2^-$$

for the H_2O_2 decomposition taken from the Battelle model. This is referred to as Mechanism "B".

Table 4.3. Groundwater-radiolysis model under consideration for inclusion in the Battelle general-corrosion model.

No.	Reaction
1	$H + OH \rightarrow H_2O$
2	$H + H \rightarrow H_2$
3	$OH + OH \rightarrow H_2O_2$
4	$H_2O_2 \rightarrow H_2O + 1/2\ O_2$

To assess Mechanisms A and B, simulations were performed using the Battelle water-radiolysis model with and without the reactions describing the behavior of iron species. Since these mechanisms do not account for reactions with dissolved oxygen, a single simulation was performed with each mechanism.

Predicted concentrations from Mechanisms A and B are compared with the concentrations of species calculated using the more complete Battelle model for water and groundwater radiolysis at 3000 seconds in Table 4.4. As can be seen in this table, the concentrations calculated with Mechanisms A and B are identical for OH, H and H_2O_2. Also, the concentrations of H^+ and H_2 are within two orders of magnitude. Mechanism A accounts for the formation of HO_2^- but not O_2, and Mechanism B accounts for the formation of O_2 but not HO_2^-. Mechanism A does not account for any reaction that removes O_2 from solutions. Therefore, the O_2 concentration calculated using this mechanism is the initial amount of O_2 present in the solution plus the amount generated as a result of H_2O_2 decomposition.

When comparing the concentrations of species calculated with Mechanisms A and B to those calculated with the Battelle models, the agreement is variable. The amount of O_2 in solution is in fair agreement with that predicted by the Battelle model for Cases 1, 3, and 5. However, the simulations in Cases 2 and 4 depart from agreement because the reactions of the ferrous ion help remove O_2 from solution over the long term. The H_2 concentrations calculated with Mechanisms A and B are within about one order of magnitude of all the Battelle simulations shown in Table 4.4 at 3000 seconds. The H^+, H, and H_2O_2 concentrations calculated with Mechanisms A and B are within about two orders of magnitude of those for the other simulations shown, and the HO_2^- concentration calculated with Mechanism B is within about three orders of magnitude of the other HO_2^- concentrations.

In summary, Mechanism A is able to predict the concentrations of H_2 and O_2 on an order-of-magnitude basis for the trial simulations with initial oxygen concentrations of 6×10^{-8} and 6×10^{-4} mol/l. Mechanisms A and B underpredict the H_2O_2 concentrations calculated with the more complete groundwater-radiolysis model by about two to three orders of magnitude. Similar shortcomings were seen for some of the other species. The adequacy of these simplified mechanisms thus depend upon which species are important for the application, the initial water chemistry, and the simulation time required for the model. A review and comparison of all of the data are necessary to show when the user's applications are met by Mechanisms A and B for the particular system and conditions simulated.

4.2.3 Near-Term Plans

In the second quarter, the MAKSIMA-CHEMIST code will be modified to handle more than 99 elementary reactions. This will allow radiolysis simulations of groundwater containing iron, chloride and other species.

4.3 Integral Experiments

The selection of combined effects to be targeted for detailed study is often based upon engineering judgment. When applying the knowledge from

Table 4.4. Comparison of species concentrations calculated using Mechanisms A and B with the Battelle-model simulations at 3000 seconds[a].

Model	Case	Fe^{2+}/Cl^- Reactions	Initial Dissolved O_2 (mol/l)	Species Concentrations (mol/liter)						
				H^+	OH	H	H_2	H_2O_2	HO_2^-	O_2
Mech. A				1.446×10^{-7}	5.848×10^{-11}	6.164×10^{-12}	2.395×10^{-8}	3.043×10^{-10}	(b)	(b)
Mech. B				2.356×10^{-7}	5.848×10^{-11}	6.164×10^{-12}	2.395×10^{-8}	3.043×10^{-10}	9.096×10^{-8}	(b)
Battelle[c]	1	No	6×10^{-11}	1.668×10^{-10}	2.137×10^{-11}	7.251×10^{-13}	8.839×10^{-9}	1.434×10^{-9}	1.628×10^{-11}	1.308×10^{-9}
"	2	Yes	6×10^{-11}	1.611×10^{-10}	1.792×10^{-14}	2.288×10^{-14}	2.300×10^{-8}	1.046×10^{-8}	1.181×10^{-10}	1.173×10^{-12}
"	3	No	6×10^{-8}	1.897×10^{-10}	3.742×10^{-12}	2.368×10^{-14}	1.879×10^{-8}	2.345×10^{-8}	2.661×10^{-10}	3.955×10^{-8}
"	4	Yes	6×10^{-8}	1.613×10^{-10}	2.229×10^{-14}	1.764×10^{-14}	2.289×10^{-8}	2.500×10^{-8}	2.819×10^{-10}	6.447×10^{-9}
"	5	No	6×10^{-4}	2.002×10^{-10}	3.169×10^{-15}	6.648×10^{-19}	2.281×10^{-8}	1.151×10^{-7}	1.303×10^{-9}	4.998×10^{-4}
"	6	Yes	6×10^{-4}	1.616×10^{-10}	5.779×10^{-15}	6.651×10^{-19}	2.281×10^{-8}	9.328×10^{-8}	1.049×10^{-9}	5.996×10^{-4}

(a) For groundwater containing 4×10^{-10} mol/l dissolved hydrogen at a pH of 9.82.

(b) Value not predicted by model.

(c) Battelle Water-Radiolysis Model.

these studies in formulating a system description or in assessing licensing applications, one must have some basis for determining whether any important combined-effects processes have been omitted from the process. Thus, there is a need for a test to provide investigators with a reasonably realistic view of the processes contributing to the degradation of waste packages containing spent fuel. Such a test would help to confirm the importance of processes believed to be important, and may serve to identify others not previously considered. The result would establish a technical basis for identifying the level of detail necessary in a system model as well as in a licensing application.

The primary purpose of the integral experiments is to provide scoping information that will help to identify potentially important combined effects. The secondary purpose of these experiments is to provide qualitative information on corrosion phenomena, release rates, and water chemistry for spent-fuel packages.

4.3.1 Apparatus

The apparatus used in the experiments will consist of 29 parallel test chambers placed in a hot cell. The radiation field about these chambers will be approximately 1,000 R/hr. Fluid will flow through these chambers in a once-through fashion, allowing the chemistry and radiochemistry samples to be collected without recirculating any fluids. A basic diagram of the apparatus is shown in Figure 4.5. Simulated groundwater will be stored at room temperature in a stainless steel drum. The storage drum for the simulated basalt groundwater will flow from the storage containers, through a peristaltic pump, through a test chamber, and finally to a sample-collection reservoir. Each test section will be fed with fluid supplied by a separate channel of a peristaltic pump to control the flow through each test section.

4.3.2 Matrix of Experiments

Table 4.5 shows a matrix of 29 test sections which will contain samples for the spent fuel integral tests. Test Sections 1 through 15 contain spent-fuel samples with various amounts of cladding removed to simulate cladding-failure openings. The purpose of these test sections is to explore the effects of cladding failure on the release rates of radionuclides from spent-fuel waste forms. Test Section 1 contains an intact spent-fuel rod segment which has been capped at the ends with press-fit plugs. This sample has been included to establish a baseline for the concentration levels to be expected from cladding contamination and possible end-cap leakage. Sections 2 through 7 contain pressurized water reactor (PWR) spent-fuel rod segments with press-fit end caps. These samples have 1/16-inch holes drilled through the cladding to simulate pitting perforations. The fractional area of the removed cladding varies from 0.5 to 10 percent as indicated. Sections 8 through 11 have bare spent-fuel fragments which have been removed from spent-fuel rods. Two of these sections will have a flow rate ten times that of the other test sections in this series. Test Sections 14 and 15 have 1/32-inch

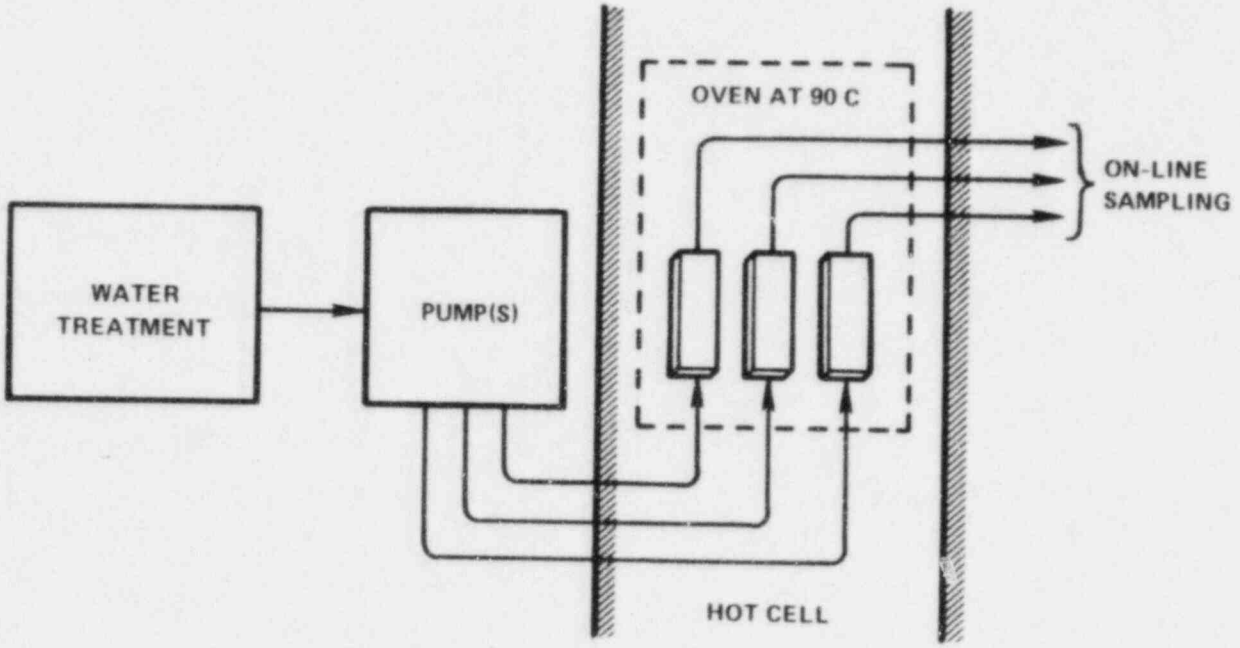

Figure 4.5. Schematic of apparatus to be used in integral experiments.

Table 4.5. Matrix of Integral Experiment

Test Section	Description	Cladding Failure Area (%)	Flow Rate 1=1 ml/day 2=10. ml/day	Water B=Basalt T=Tuff
1	PWR intact fuel rod segment	0	1	B
2	PWR degraded fuel rod segment (1/16-inch perforations)	0.5	1	B
3	PWR degraded fuel rod segment (1/16-inch perforations)	0.5	1	B
4	PWR degraded fuel rod segment (1/16-inch perforations)	3	1	B
5	PWR degraded fuel rod segment (1/16-inch perforations)	3	1	B
6	PWR degraded fuel rod segment (1/16-inch perforations)	10	1	B
7	PWR degraded fuel rod segment (1/16-inch perforations)	10	1	B
8	PWR spent fuel fragments	100	1	B
9	PWR spent fuel fragments	100	1	B
10	PWR spent fuel fragments	100	2	B
11	PWR spent fuel fragments	100	2	B
12	BWR spent fuel fragments	100	1	B
13	BWR spent fuel fragments	100	1	B
14	PWR degraded fuel rod segment (1/32-inch perforations)	3	1	B
15	PWR degraded fuel rod segment (1/32-inch perforations)	3	1	B
16	BWR fuel rod section with in-service failure	-	1	B
17	BWR fuel rod section with in-service failure	-	1	B
18	BWR fuel rod section with in-service failure	-	1	B
19	BWR fuel rod section with in-service failure	-	1	B
20	PWR sections embedded in packing (2 prepared and 2 as-removed; 1/16-inch perforations)	-	1	B
21	Defueled PWR cladding with perforation and slit embedded in packing	-	1	B
22	Defueled PWR cladding with perforation and slit embedded in simulated corrosion products	-	1	B
23	PWR spent fuel rod section with 1/16-inch perforation	-	1	B
24	PWR spent fuel rod section with slit machined in cladding	-	1	B
25	PWR fuel fragments	-	1	T (sat.)
26	PWR fuel fragments	-	1	T (sat.)
27	PWR fuel fragments	-	1	T (cyclic)
28	PWR fuel fragments	-	1	T (cyclic)
29	Blank (control)	-	1	B

holes comprising a 3 percent failure area to examine the effects of perforation size on release rates. Test sections 16 through 19 contain boiling water reactor (BWR) fuel rod segments with in-service failures. These samples will provide information on release rates of radionuclides from disposed fuel with existing failures.

Section 20 contains four PWR spent-fuel rod segments embedded in packing material. Each sample will have a 1/16-inch drilled hole. Two samples will be cleaned to remove surface films, and two will be emplaced with existing cladding-surface films. Section 21 will contain defueled PWR cladding with a perforation and a slit embedded in packing material. Section 22 will contain defueled PWR cladding embedded in simulated corrosion products. Sections 20 to 22 will provide information on the combined-effects processes. The relatively low activity of samples in Sections 21 and 22 will facilitate surface analyses, and samples in Section 20 will provide information on the influence of defueling on the study of these effects. Sections 23 and 24 will provide information on the effect of the geometry of machined openings on the measured release rates of radionuclides from defected spent fuel rod samples. Section 23 contains a PWR spent-fuel rod section with a 1/16-inch circular opening, and Section 24 contains a spent-fuel rod section with a machined slit opening. Sections 25 to 28 will provide information on the performance of spent fuel in tuff environments. Sections 25 and 26 contain PWR spent-fuel fragments exposed to flowing simulated tuff groundwater. Sections 27 and 28 contain PWR spent-fuel fragments exposed to alternating conditions of flowing simulated tuff groundwater and flowing air. Section 29 is a control blank that will contain flowing simulated basalt groundwater.

4.3.3 Analysis

On-line and post-test analyses will be performed. The on-line analyses will be performed on fluid effluents taken from individual test trains. These specimens will be analyzed for radionuclides by gamma spectroscopy. General elemental analyses will be performed using inductively coupled argon-plasma (ICAP) spectroscopy and low-energy photon spectroscopy. Uranium will be analyzed using laser-excited fluorescence. If solid-phase reaction products are observed, the fluid can be filtered with membrane filters and the residue examined by techniques such as X-ray fluorescence and scanning electron microscopy (SEM). On selected samples, total alpha activity will be measured, and some specific alpha-emitting nuclides will be identified. The radionuclide-release data based on the fluid effluent will be presented as total releases for each test section and as releases normalized to the exposed surface area of waste form in each test section. These data will be presented as current concentrations and estimated cumulative releases. At the conclusion of the experiments, attempts will be made to integrate the total release from waste forms for selected test sections by summing the inventories of radionuclides in the lines and adsorbed on materials. The current concentrations will be presented as a direct function of time, and the cumulative releases will be presented as a function of time and the square root of time.

Following the experiments, post-test analyses will be performed on samples of components, surfaces, and interfaces removed from the test sections. These analyses will include gamma spectroscopy and a variety of surface techniques including secondary ion mass spectrometry, Auger electron spectroscopy, electron spectroscopy for chemical analysis, SEM, and electron microprobe analysis.

4.3.4 Status of Experiments

The apparatus has been constructed and is ready for installation in the hot cell and for sample loading. Sample selection and preparation is under way, and the deionized water to be used in the simulated groundwater solutions has been analyzed. The basalt used in these experiments was acquired from the Cohassett Flow at the Hanford Site by collecting rotary drilling chips during a well-drilling operation.

After construction, the apparatus was degreased by filling it with water containing a low-metal, low-organic, and low-phosphate detergent for 48 hours at room temperature. This was followed by flushing with deionized water for 30 minutes. After flushing, water was left in the system so that all internal surfaces would remain wet. This procedure eliminates the need to add a wetting agent to facilitate flow when operation of the apparatus is started.

All of the PWR fuel-rod samples have been sectioned from two Turkey Point* spent-fuel rods. Burnup analyses have been completed for selected locations in the rod as part of the characterization of the spent-fuel rod samples. Determination of the radionuclide composition of the samples chosen for burnup analysis is under way.

Spent fuel-rod specimens for test Section 2 to 7 and 14 to 15 require drilling a number of 1/16- and 1/32-inch holes to attain an exposed surface area of 0.5 to 10 percent of the cladding geometric surface area. A jig is being constructed to aid in drilling the holes through the cladding while the fuel-rod sections are in the hot cell.

BWR spent fuel-rod samples with existing failures are being selected. Eddy-current testing was performed on such rods to locate possible sites of existing cladding failures. An example of an eddy-current trace showing a possible failure site is given in Figure 4.6. The abscissa in each trace represents the axial location along the rod. The presence of a peak on each trace is an indication of the position of a possible cladding defect.

The deionized water to be used in the simulated groundwater solutions was analyzed for cations and anions. The cation analysis was performed using ICAP spectroscopy. Cation concentrations determined from these

---

*Turkey Point Plant, Florida Power and Light Co.

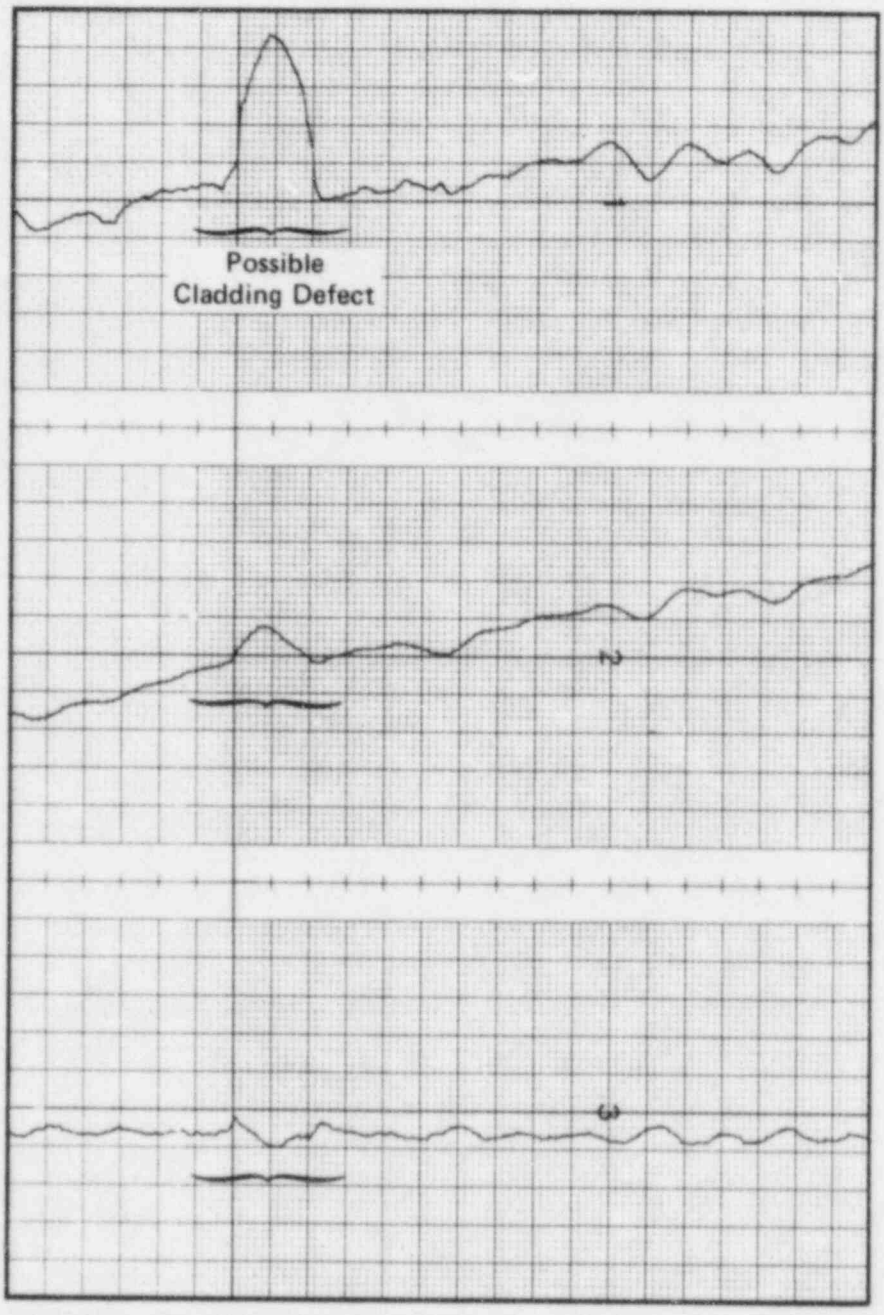

Figure 4.6. Eddy-current scan of BWR fuel-rod segment showing location of a possible cladding defect.

analyses are shown in Table 4.6 for two water samples. The anion composition was determined by the ICAP spectroscopy, atomic absorption, and ion chromotography methods. Measured anion concentrations are shown in Table 4.7, and a basalt-groundwater composition reported in the literature is given in Table 4.8. The concentrations of most of the cations and anions is lower in the source deionized water than the concentrations shown in Table 4.8. The exceptions were magnesium and bicarbonate, where the basalt groundwater compositions reported in the literature were 0.032 mg/l and 1.82 meq/l, respectively. The concentrations of these species measured in the deionized water samples were 0.08 mg/l and 3.4 meq/l, respectively.

Basalt chips were obtained from four depth ranges of the Cohassett Flow at the Hanford site. These depth ranges are 3054 to 3118 ft, 3182 to 3246 ft, 3118 to 3182 ft, and 2990 to 3054 ft. A small sample from each range was removed for X-ray diffraction and energy dispersive X-ray (EDX) analyses. Analyses of the X-ray diffractometer data are presented in Tables 4.9 to 4.12. The tables list the possible chemical compositions and corresponding analysis reliability factors for the various basalt samples. An EDX spectrum of a typical sample is shown in Figure 4.7, and results of the semiquantitative elemental analyses of the EDX data are given in Tables 4.13 to 4.16. These data are currently being evaluated.

4.3.5 Near-Term Plans

In the second quarter, samples will be prepared and loaded into the apparatus. Following this, the apparatus will be moved into the hot cell for final assembly, and the tests will be started. X-ray diffraction data will also be interpreted.

4.4 References for Section 4

(4.1) "Long-Term Performance of Materials Used for High-Level Waste Packaging", D. Stahl and N. E. Miller (Compilers), NUREG/CR-3427, Vol. 4, BMI-2113 (June 1984), Section 4.

(4.2) E.L.J. Rosinger and R. S. Dixon, "Mathematical Modeling of Water Radiolysis: A Discussion of Various Methods", AECL-5958 (1977).

(4.3) "Long-Term Performance of Materials Used for High-Level Waste Packaging", D. Stahl and N. E. Miller (Compilers), NUREG/CR-3900, Vol. 4, BMI-2127 (July 1985), Section 4.

(4.4) H. F. Calcote and D. E. Jensen, "Reactions in Flames", in Ion Molecule Reactions, R. F. Gould, Ed., American Chemical Society, pp. 311-2 (1966)

(4.5) L. M. Lowenstein and J. G. Anderson, "Rate and Product Measurements for the Reactions of OH with Cl_2, Br_2, and BrCl at 298 K. Trend Interpretations", J. Phys. Chem. 88, 6277-86 (1984).

Table 4.6. Concentrations of cations in the deionized water that will be used to prepare the simulated groundwater.

Species	Concentrations (mg/liter) Sample 1	Sample 2
Tl	< 0.01	< 0.01
As	< 0.01	< 0.01
Se	< 0.01	< 0.01
Cr	< 0.001	< 0.001
Sb	< 0.01	< 0.01
B	< 0.01	< 0.01
Zr	0.14	0.16
Pb	0.005	0.005
Cd	< 0.01	< 0.01
Ni	0.01	0.01
Ba	< 0.01	< 0.01
Co	< 0.01	< 0.01
Mn	< 0.01	< 0.01
Fe	0.03	0.03
Mg	0.08	0.08
Al	< 0.01	< 0.01
V	< 0.01	< 0.01
Be	< 0.001	< 0.001
Ca	0.4	0.4
Cu	0.008	0.008
As	< 0.001	< 0.001
Ti	< 0.01	< 0.01
Na	< 0.5	< 0.5
K	< 0.5	< 0.5

Table 4.7. Concentration of anions in the deionized water that will be used to prepare the simulated groundwater.[10]

Species	Concentration (ppmv)
F^-	< 0.01
Cl^-	0.10
SO_4^{2-}	2.6
Br^-	< 0.1
NO_3^-	< 0.25
NO_2^-	< 0.20
CO_3^{2-}	nil
HCO_3^-	61

Table 4.8. Composition of basalt groundwater reported in the literature.[10]

Species	Concentration (mg/liter)	Concentration (meq/liter)
Na^+	363	15.8
K^+	3.43	0.0877
Ca^{2+}	2.76	0.138
Mg^{2+}	0.032	3.1×10^{-4}
Total Cations		16.00
Cl^-	310	8.75
SO_4^{2-}	173	3.604
F^-	33.4	1.76
Alkalinity (HCO_3^-)		1.82 (9.03×10^{-4} mol/l inorganic carbon)
Total Anions		16.06

Table 4.9. Composition analysis of basalt sample from 3054 to 3118 feet depth range comparing X-ray diffractometer scans with JCPDS* chemical file data.

JCPDS Card No.	Unknown Peaks	Standard Peaks	Chemical Formula	Reliability Factor**
310261	15	18	$Ca_7Si_6O_{18}(CO_3)_2H_2$	160
290712	4	6	$Fe_5O_7(OH)_4H_2O$	148
210920	6	11	Fe_2O_3	113
240030	8	12	$CaCO_3$	102
310038	14	17	$(NH_4)_2Al(ClO_4)_5$	98
120286	9	12	$K_{10}Ca_5Al_6Si_{32}O_{80}Cl_6 \cdot 18H_2O$	97
100447	11	18	$Ca_2(AlFe)_3Si_3O_{11}(OH)_2$	89
180988	12	18	$K_2Al_2Si_2O_8 \cdot 3.8H_2O$	89
230124	11	18	$Ca_3Si_2O_7$	87

*Joint Committee on Powder Diffraction Standards.

**Reliability factor is an indication of how closely JCPDS file data matches sample scans. Perfect match equals a reliability factor of 500.

Table 4.10. Composition analysis of basalt sample from 3182 to 3246 feet depth range comparing X-ray diffractometer scans with JCPDS* chemical file data.

JCPDS Card No.	Unknown Peaks	Standard Peaks	Chemical Formula	Reliability Factor**
290042	17	18	$Al_{13}Fe_4$	286
200867	14	18	$K_2Ca_2(SO_4)_3$	171
200847	15	18	$KAlCl_4$	164
310249	14	18	$CaAl_2SiO_6$	141
221117	4	7	$Fe_2O_3 \cdot 1.2H_2O$	133
310247	11	18	$CaAl_2Si_2O_8$	115
110658	15	18	$K_2S_2O_5$	100
251202	12	18	$(CaK)_4(Si,Al)_5O_{11}(SO_4)_2(CO_3)_2$	97
10563	4	6	$Al_2(SiF_6)_3$	97

*Joint Committee on Powder Diffraction Standards.

**Reliability factor is an indication of how closely JCPDS file data matches sample scans. Perfect match equals a reliability factor of 500.

Table 4.11. Composition analysis of basalt sample from 3118 to 3182 feet depth range comparing X-ray diffractometer scans with JCPDS* chemical file data.

JCPDS Card No.	Unknown Peaks	Standard Peaks	Chemical Formula	Reliability Factor**
10962	9	9	CaC_2	485
50678	9	13	AlTi	169
30498	7	8	$Ca(ClO_4)_2 \cdot 3H_2O$	168
20344	13	18	(K,Al,C)·(N,Si,O)***	163
80231	12	15	$Al(SO_4)_3 \cdot H_2SO_4$	163
30713	9	15	$Ca(OCl)_2 \cdot 2Ca(OH)_2$	120
30378	9	13	$Ca(ClO_4)_2$	119
20802	8	12	$K_2Fe_2O_4$	112
10864	16	18	$KHSO_3$	108
10726	14	18	Al_2S_3	107

*Joint Committee on Powder Diffraction Standards.

**Reliability factor is an indication of how closely JCPDS file data matches sample scans. Perfect match equals a reliability factor of 500.

***Composition could not be exactly determined.

Table 4.12. Composition analysis of basalt sample from 2990 to 3054 feet depth range comparing X-ray diffractometer scans with JCPDS* chemical file data.

JCPDS Card No.	Unknown Peaks	Standard Peaks	Chemical Formula	Reliability Factor**
330988	15	18	$KAlSiO_4$	213
10917	16	18	CaC_2	205
310300	16	18	$CaSiO_3$	204
100416	5	7	$Ca_5H_2Si_6O_{18}\cdot 6H_2O$	196
120708	9	11	SiO_2	195
150615	16	18	Fe_2O_3	184
190207	15	18	$CaAl_2SiO_6$	184

*Joint Committee on Powder Diffraction Standards.

**Reliability factor is an indication of how closely JCPDS file data matches sample scans. Perfect match equals a reliability factor of 500.

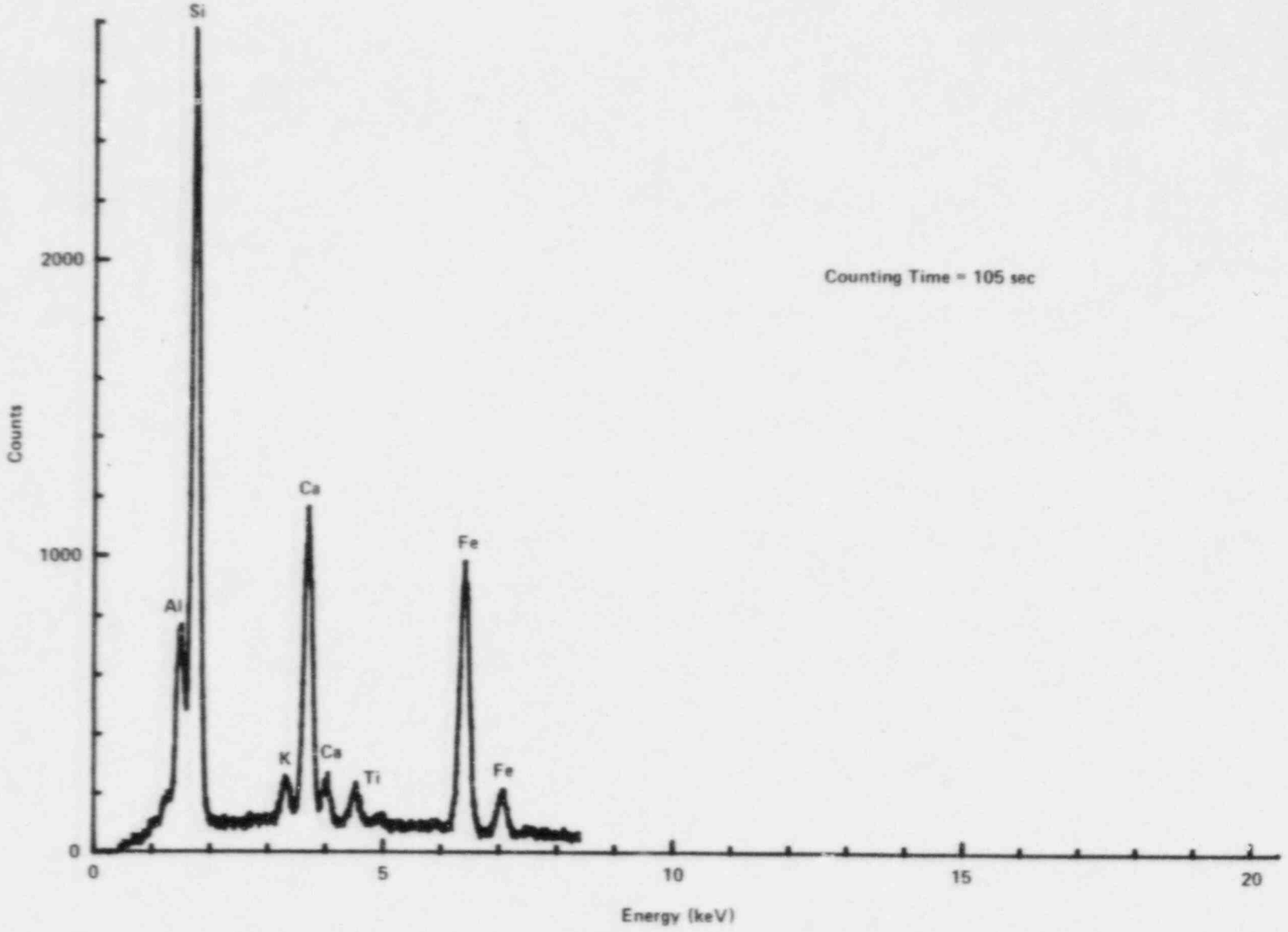

Figure 4.7. EDX analysis of basalt rotary drilling chips; depth range 3054 to 3118 feet.

Table 4.13. Element concentration analysis of basalt sample from 3054 to 3115 feet depth range.

Element	K	Z	A	F	ZAF	Atom Percent	Weight Percent
Al	0.107	0.955	2.067	0.983	1.942	17.98	13.90
Si	0.291	0.931	2.086	0.997	1.939	46.72	37.46
K	0.040	1.009	1.321	0.971	1.295	3.13	3.49
Ca	0.175	0.993	1.252	0.986	1.227	12.50	14.32
Ti	0.048	1.100	1.208	0.976	1.299	3.03	4.17
Fe	0.335	1.126	1.063	1.000	1.197	16.63	26.67

K = Specimen counts
Z = Atomic number
A = Absorption
F = Fluorescence
ZAF = Combined correction factor

Table 4.14. Element concentration analysis of basalt sample from 3182 to 3246 feet depth range.

Element	K	Z	A	F	ZAF	Atom Percent	Weight Percent
Al	0.095	0.957	2.091	0.980	1.964	15.75	12.32
Si	0.348	0.933	2.047	0.998	1.909	54.11	43.88
K	0.003	1.009	1.349	0.975	1.327	0.29	0.33
Ca	0.148	0.995	1.245	0.987	1.224	10.35	11.99
Ti	0.009	1.103	1.189	0.970	1.273	0.60	0.84
Fe	0.393	1.128	1.046	1.000	1.181	18.90	30.65

K = Specimen counts
Z = Atomic number
A = Absorption
F = Fluorescence
ZAF = Combined correction factor

Table 4.15. Element concentration analysis of basalt sample from 3118 to 3182 feet depth range.

Element	K	Z	A	F	ZAF	Atom Percent	Weight Percent
Al	0.122	0.961	1.975	0.981	1.864	18.83	14.91
Si	0.325	0.937	2.059	0.997	1.927	49.87	40.95
K	0.027	1.015	1.338	0.972	1.322	2.08	2.38
Ca	0.178	0.999	1.254	0.988	1.239	12.30	14.42
Ti	0.031	1.107	1.210	0.977	1.311	1.89	2.66
Fe	0.314	1.133	1.059	1.000	1.200	15.02	24.67

K = Specimen counts
Z = Atomic number
A = Absorption
F = Fluorescence
ZAF = Combined correction factor

Table 4.16. Element concentration analysis of basalt sample from 2930 to 3054 feet depth range.

Element	K	Z	A	F	ZAF	Atom Percent	Weight Percent
Al	0.093	0.955	2.123	0.982	1.992	16.16	12.47
Si	0.314	0.931	2.075	0.997	1.929	50.38	40.33
K	0.009	1.006	1.332	0.971	1.302	0.74	0.83
Ca	0.181	0.993	1.237	0.987	1.214	12.80	14.64
Ti	0.012	1.100	1.202	0.971	1.285	0.78	1.07
Fe	0.388	1.126	1.051	1.000	1.184	19.14	30.65

K = Specimen counts
Z = Atomic number
A = Absorption
F = Fluorescence
ZAF = Combined correction factor

(4.6) Leon F. Keyser, "High Pressure Flow Kinetics. A Study of the OH + HCl Reaction from 2 to 100 Torr", J. Phys. Chem 88, 4750-8 (1984).

(4.7) Richard W. Ramette, "Photon Initiated Hydrogen-Chlorine Reaction", J. Chem. Ed. 61(8) 722-3 (1984).

(4.8) A. M. Held, D. J. Halko, and J. K. Hurst, "Mechanism of Chloride Oxidation of Hydrogen Peroxide", J. Amer. Chem. Soc. 100, pp. 5732-40.

(4.9) M. Eigen and K. Kustin, "The Kinetics of Halogen Hydrolysis", J. Amer. Chem. Soc. 84, 1355 (1952).

(4.10) "Engineered Waste Package System Design Specification," Westinghouse Electric Corporation, ONWI-423.

5. QUALITY ASSURANCE

Quality assurance surveillance of the various program activities continues. No new procedures were prepared during this past quarter, leaving a total of 36 approved QA procedures and 2 approved work instructions for the program.

A summary of the procedures which are being used to conduct the experimental program is given in Table 5.1. Included is the procedure number, the current revision number, the title, and the status.

Quality assurance surveillance activities will continue this quarter. Procedures will be revised and new ones prepared as necessary to meet program requirements.

Table 5.1. Status of NRC waste packaging program QA procedures.

Procedure No.	Title	Status
WF-PP-1 Revision 0	Procedures for Record Keeping and Documentation for NRC Waste Form System Model Development	Approved
WF-PP-5 Revision 0	Procedures for Record Keeping and Documentation for Separate Effects Model Development	Approved
WF-PP-10 Revision 0	Laboratory Procedure for Preparation of Glasses for NRC Waste Form Project	Approved
WF-PP-11 Revision 1	Laboratory Procedures for Preparation of Teflon-Leach Containers	Approved
WF-PP-14 Revision 1	Laboratory Procedure for Leaching Glass Samples	Approved
WF-PP-16 Revision 0	Laboratory Procedure for Operating the Orton Dilatometer	Approved
WF-PP-20 Revision 0	Procedure for Determining the Corrosion Rates of Alloys at High Temperatures	Approved
WF-PP-25 Revision 0	Procedure for Preparation of Carbon-Steel Casting	Approved
WF-PP-26 Revision 0	Procedure for Preparation of Steel Hydrogen-Embrittlement Test Specimens	Approved
WF-PP-26.1 Revision 0	Procedure for Preparation of Hydrogen-Embrittlement Test Specimens from Steel or Iron Samples	Approved

Table 5.1. Continued.

Procedure No.	Title	Status
WF-PP-27 Revision 4	Procedure for J-Testing Compact Tension Specimens	Approved
WF-PP-27.1 Revision 1	Procedures for Performing Subcritical-Crack-Growth Tests with Compact Tension Specimens	Approved
WF-PP-28 Revision 1	Procedure for Performing Tension Tests of Steel Specimens	Approved
WF-PP-29 Revision 0	Procedure for Conducting Hydrogen-Absorption Experiments	Approved
WF-PP-30 Revision 0	Laboratory Procedure for Preparation, Cleaning, and Evaluation of Titanium Grade-12 Specimens for Corrosion Studies of the Overpack Performance for the NRC Waste Packaging Program	Approved
WF-PP-31 Revision 0	Laboratory Procedure for Preparation, Cleaning, and Evaluation of Cast and Wrought Carbon Steel Specimens for Corrosion Studies of the Overpack Performance for the NRC Waste Packaging Program	Approved
WF-PP-32 Revision 0	Procedure for Preparation of Brine A for Corrosion Testing Under Simulated Repository Conditions	Approved
WF-PP-33 Revision 0	Procedure for Preparation of Simulated Basalt Groundwater Solution	Approved
WF-PP-33.1 Revision 0	Procedure for Preparation of Basalt Rock for Use in Corrosion Studies for the NRC Waste Packaging Program	Approved

Table 5.1. Continued.

Procedure No.	Title	Status
WF-PP-34 Revision 0	Procedure for Preparation of Simulated Tuff Groundwater Solutions	To be Written
WF-PP-35 Revision 1	Procedure for Performing Autoclave Exposures for Corrosion Tests in Simulated Brines	Approved
WF-PP-35.1 Revision 0	Procedure for Performing Autoclave Exposures for Corrosion Tests in Simulated Brines Using Sealed Internal Canister	Approved
WF-PP-36 Revision 0	Procedure for Performing Stagnant Autoclave Exposures for Corrosion Tests in Simulated Basalt or Tuff Groundwaters	Approved
WF-PP-37 Revision 0	Laboratory Procedure for Preparing Polarization Resistance Specimens, Performing Polarization Resistance Measurements and Evaluating Polarization Resistance Data	Approved
WF-PP-37.1 Revision 0	Laboratory Procedure for Performing Eh and Corrosion Potential Measurements in Autoclave Exposures in Simulated Basalt and Tuff Groundwater	Approved
WF-PP-37.2 Revision 0	Laboratory Procedure for Determination of the Polarization Behavior of Metal Specimens at Ambient Pressure	Approved
WF-PP-38 Revision 0	Procedure for Preparing and Evaluation of U-Bend Specimens for Stress Corrosion Studies of Overpack Materials for the NRC Waste Packaging Project	Approved
WF-PP-38.1 Revision 0	Procedure for Performing and Evaluating 3 Point Bend Beam Specimens for Stress Corrosion Studies of Overpack Materials for NRC Waste Package Program	Approved
WF-PP-39 Revision 0	Procedure for Preparing, Testing and Evaluating Crevice Corrosion Specimens of Titanium Grade-12 and Cast Steel	Approved

Table 5.1. Continued.

Procedure No.	Title	Status
WF-PP-40 Revision 0	Laboratory Procedures for Preparation, Cleaning, and Evaluation of Thermogalvanic and Heat-Transfer Specimens	Approved
WF-PP-41 Revision 0	Laboratory Procedures for Determination of Corrosion Rates Under Heat-Transfer Conditions	Approved
WF-PP-42 Revision 0	Laboratory Procedure for Determination of Thermogalvanic Corrosion Rates	Approved
WF-PP-43 Revision 0	Procedure for Welding Titanium Grade-12 Plate for Use in Corrosion Studies of Overpack Materials for NRC Waste Isolation Project	Approved
WF-PP-44 Revision 0	Procedure for Welding Cast and Wrought Steel Specimens	To be Written
WF-PP-45 Revision 0	Laboratory Procedure for Preparing and Evaluating Slow Strain-Rate Specimens and for Performing Slow Strain-Rate Tests	Approved
WF-PP-45.1 Revision 0	Laboratory Procedures for Performing Slow Strain-Rate Tests Under Potentiostated Conditions	Approved
WF-PP-46 Revision 0	Procedure for Preparation of Titanium Grade-12 Corrosion Specimens with Metallic Iron Embedded in the Surface	Approved
WF-PP-47 Revision 0	Procedure for Preparing Specimens and Performing Electrochemical Pit Propogation Experiments on Carbon Steel	Approved

DISTRIBUTION LIST

Office of Regulatory Research
Division of Radiation Programs and Earth Sciences
Mail Stop 1130 SS
U.S. Nuclear Regulatory Commission, Washington, D.C. 20555

Attn: Division Director/Deputy Director
E. F. Conti, Chief, Waste Management Branch
F. A. Costanzi
J. R. Randall
M. B. McNeil
K. S. Kim, Project Manager (15)

Division of Waste Management, NMSS
Mail Stop 623 SS
U.S. Nuclear Regulatory Commission, Washington, D.C. 20555

Attn: Division Director/Deputy Director
Chief, Engineering Branch
E. A. Wick
M. Tokar
K. C. Chang
Document Control Center

Division of Waste Management, NMSS
U.S. Nuclear Regulatory Commission
1955 Jadwin Ave - Suite 310A
Richland, WA 99352

Attn: R. Cook, BWIP Site Rep.

Advisory Committee on Reactor Safeguards
Mail Stop H-1016
U.S. Nuclear Regulatory Commission, Washington, D.C. 20555

Attn: Waste Management Subcommittee
R. C. Tang

Battelle's Columbus Laboratories
505 King Avenue
Columbus, Ohio 43201-2693

Attn: D. Stahl, Program Manager (50)

DISTRIBUTION LIST (Continued)

Martin J. Steinuler
Argonne National Lab.
Argonne, IL 60439

Donald G. Schweitzer
Brookhaven National Lab.
Upton, NY 11973

Peter Soo
Brookhaven National Lab.
Upton, NY 11973

David Martin
Iowa State University
Ames, IA 50011

Harold Wollenberg
Lawrence Berkeley Lab.
Berkeley, CA 94720

Nestor Ortiz
Sandia National Lab.
Albuquerque, NM 87185

Pedro B. Macedo
Catholic University of America
Washington, D.C. 20064

Robert Williams
Electric Power Research Institute
P.O. Box 10412
Palo Alto, CA 94301

William P. Reed
U.S. Department of Commerce
National Bureau of Standards
Washington, D.C. 20234

Ray Walton
U.S. Department of Energy
Washington, D.C. 20545

John E. Mendel
Materials Characterization Center
Pacific Northwest Lab.
Richland, WA 99352

Larry Hench
University of Florida
Gainesville, FL 32611

David E. Clark
University of Florida
Gainesville, FL 32611

Joseph Mascara
MS 5650 NL
U.S. Nuclear Reg. Comm.
Washington, DC 20555

Ken W. Stephens
The Aerospace Corp., Suite 400
955 L'Enfant Plaza, S.W.
Washington, DC 20024

Robert S. Dyer
Office of Radiation Programs (ANR-461)
U.S. Environmental Protection Agency
401 M Street, S.W.
Washington, DC 20460

Lorenzo Ricks
Office of Energy Research
U.S. Department of Energy
Washington, D.C. 20545

Larry Evans
Armco Research Center
703 Curtis Avenue
Middletown, OH 45043

Woody Swope
Armco Stainless Steel Division
P.O. Box 1697
Baltimore, MD 21203

M. John Plodinec
Savannah River Laboratory
Aiken, SC 29808

Alan L. Liby
Manufacturing Sciences Corp.
711 Walnut Street
Boulder, CO 80302

DISTRIBUTION LIST (Continued)

Martin A. Molecke
Sandia National Lab.
Albuquerque, NM 87185

Neville Pugh
National Bureau of Standards
Washington, D.C. 20234

Nicholas Grant
Department of Metallurgy
Massachusetts Institute
of Technology
Cambridge, MA 02139

Jerome Kruger
Corrosion Section
National Bureau of Standards
Washington, D.C. 20234

Don J. Bradley
Waste Package Programs
Battelle Pacific Northwest Labs
Richland, WA 99352

Allen G. Croff
Oak Ridge National Laboratory
P.O. Box X
Oak Ridge, TN 37830

Lynn Hobbs
Department of Materials Science
Massachusetts Institute of
Technology
77 Massachusetts Avenue
Cambridge, MA 02139

Richard E. Westerman
Pacific Northwest Lab.
P.O. Box 999
Richland, WA 99352

Thomas D. Chikalla
Pacific Northwest Lab.
P.O. Box 999
Richland, WA 99352

John Crandall
Savannah River Lab.
Aiken, SC 29808

Edward J. Hennelly
Savannah River Lab.
Aiken, SC 29808

Arthur A. Bauer
Office of Crystalline Rock Development
Battelle Memorial Institute
505 King Avenue
Columbus, OH 43201

Michael Smith
Basalt Waste Isolation Projects
Rockwell Hanford Operation
Richland, WA 99352

Kenneth Russell
Department of Materials Science
and Engineering
Massachusetts Institute of
Technology
Cambridge, MA 02139

Robert H. Doremus
Materials Engineering Department
Rensselaer Polytechnic Institute
Troy, NY 12181

David C. Kocher
Oak Ridge National Lab.
P.O. Box X
Oak Ridge, TN 37830

Stanley Wolf
DOE/BES
Washington, D.C. 20585

Neville Moody
Sandia Livermore Lab.
Livermore, CA 94550

Donald E. Clark
ONWI
Battelle Memorial Institute
505 King Avenue
Columbus, OH 43201

Martin Seitz
Argonne National Lab.
Argonne, IL 60439

NRC FORM 335 (11-81)

U.S. NUCLEAR REGULATORY COMMISSION

BIBLIOGRAPHIC DATA SHEET

1. REPORT NUMBER (Assigned by DDC)
NUREG/CR-4379, Vol. 1

4. TITLE AND SUBTITLE (Add Volume No., if appropriate)
Long-Term Performance of Materials Used for High-Level Waste Packaging, First Quarterly Report, Year Four April - June 1985

2. (Leave blank)

3. RECIPIENT'S ACCESSION NO.

7. AUTHOR(S)
Compiled by D. Stahl and N. E. Miller

5. DATE REPORT COMPLETED
MONTH: August YEAR: 1985

9. PERFORMING ORGANIZATION NAME AND MAILING ADDRESS (Include Zip Code)
Battelle's Columbus Laboratories
505 King Avenue
Columbus, Ohio 43201-2693

DATE REPORT ISSUED
MONTH: September YEAR: 1985

6. (Leave blank)

8. (Leave blank)

12. SPONSORING ORGANIZATION NAME AND MAILING ADDRESS (Include Zip Code)
Division of Radiation Programs and Earth Sciences
Office of Nuclear Regulatory Research
U.S. Nuclear Regulatory Commission
Washington, D.C. 20555

10. PROJECT/TASK/WORK UNIT NO.

11. FIN NO.
B6764

13. TYPE OF REPORT
Quarterly

PERIOD COVERED (Inclusive dates)
April - June 1985

15. SUPPLEMENTARY NOTES

14. (Leave blank)

16. ABSTRACT (200 words or less)

High-level waste glass studies are being concluded and efforts are being directed toward studying spent-fuel performance. The effects of devitrification on glass leach rates are being investigated, and silica dissolution was studied to provide data for the glass dissolution model. Preliminary data support this model. A leach test using organic acids was conducted and leaching trends were observed. Real and simulated spent fuels are being incorporated in integral tests using simulated groundwater in a prototypic repository environment. The reactions of groundwater species with steels are being analyzed to evaluate susceptability to pitting and stress-corrosion cracking. Potential cracking agents are being investigated by slow strain rate experiments. General and pitting corrosion models were further developed, based on known principles of mass transport and radiolytic production. A simplified groundwater-radiolysis model, developed for use with the corrosion models, was compared with other mechanisms for species concentration predictions.

17. KEY WORDS AND DOCUMENT ANALYSIS

17a. DESCRIPTORS

High-level waste
Waste package
Waste form/container/overpack

17b. IDENTIFIERS/OPEN-ENDED TERMS

18. AVAILABILITY STATEMENT
Unlimited

19. SECURITY CLASS (This report)
Unclassified

21. NO. OF PAGES

20. SECURITY CLASS (This page)
Unclassified

22. PRICE
$

UNITED STATES
NUCLEAR REGULATORY COMMISSION
WASHINGTON, D.C. 20555

cover 4